University of Calabria

PhD Course in Chemical Engineering and Materials

DOCTORAL SCHOOL "PITAGORA"

Thesis

GOLD BASED PHOTOCATALYSTS USED IN THE OVERALL WATER SPLITTING IN A MEMBRANE REACTOR AND IN ORGANIC SYNTHESIS

Settore Scientifico Disciplinare **CHIM07** – Fondamenti chimici delle tecnologie

Thesis in Co-Tutela with Universidad Politécnica de Valencia

Supervisors

Ch.mo Prof. Raffaele Molinari

Ch.mo Prof. Hermenegildo Garcìa

PhD Coordinator

Ch.mo Prof. Raffaele Molinari

PhD Student

Tiziana Marino

Ciclo XXIV

A.Y. 2010-2011

Alla mia famiglia

Index

Summary

Heterogeneous photocatalysis based on supported gold catalysts is a promising technique for the conversion of solar energy into chemical energy. It can also be applied to organic syntheses given that visible light can be used as radiation source for environmental friendly processes.

In this work, several supported gold catalysts prepared by the deposition-precipitation method were tested for the reactions of water splitting and the partial oxidation of benzene to phenol.

Initially, the photocatalytic efficiency of several Au/TiO_2 and Au/CeO_2 samples was tested for the hydrogen or oxygen evolution from water, respectively. The influence of parameters such as gold particles dimensions and loading, catalyst (either TiO_2 or CeO_2) concentration and radiation source was studied in order to gain insights in the photocatalyzed water splitting process. Data collected so far suggest that gold could have an additional role as light harvester besides hydrogen evolution center. Moreover, it seems that small gold loadings (up to 0.25% in weight) coupled with particles dimensions of the order of 2-3 nm could enhance the photocatalytic activity of the Au/TiO_2 samples. By using a radiation with wavelenght near to the gold surface plasmon band, gold nanoparticles are able to absorb photons allowing for electrons to move into the titania

conductive band, with simultaneous creation of holes in the gold nanoparticle itself.

We also investigated an innovative method for the synthesis of CeO_2, utilized as support for oxygen evolution from water, and obtained catalyst particles with dimensions of the order of ca. 5 nm. Experimental data suggest in this case the photocatalytic properties of the system are strongly affected by the particle dimensions. Again, the presence of gold seems to positively affect the photocatalytic activity of Au/CeO_2 samples, as observed for Au/TiO_2 catalysts. Both the Au/TiO_2 and Au/CeO_2 samples were successively tested for the reaction of water splitting in a membrane system, in order to evolve both hydrogen and oxygen at the same time. The process, which required a modified nafion membrane and Iron(III) sulfate, afforded quantitative amounts of the two gases under irradiation with visible light.

The reaction of hydrogen evolution through water splitting was also investigated testing various sample of Au/TiO_2 supported on active carbon, prepared via different activation methods, to analyze the effect of functionalization on the overall photocatalytic process. Active carbons in basic pHs seem to positively influence the photocatalytic activity of Au/TiO_2 under irradiation with visible light.

Lastly, Au/TiO_2 catalysts were also investigated for the reaction of benzene partial oxidation to phenol in a batch reactor.

Preliminary data suggest the presence of gold is positive in such a way that the percentage of conversion to phenol is higher with respect to unmodified TiO_2, although secondary products form as well, i. e. benzoquinone, which represents a mayor inconvenience of the process.

Riassunto

La fotocatalisi eterogenea basata sull'utilizzo di catalizzatori di oro supportati si sta rivelando una tecnica promettente sia per la conversione di energia solare in energia chimica che per reazioni di sintesi organica, grazie alla possibilità di sfruttare la luce visibile come fonte di irradiazione e di ottenere processi ambientalmente sostenibili.

Nel corso di questo lavoro di Dottorato è stata studiata l'attività fotocatalitica di diversi catalizzatori oro supportati, preparati secondo la procedura di deposizione-precipitazione, per la reazione di water splitting e per l'ossidazione parziale del benzene a fenolo.

Nella prima parte del lavoro sperimentale, è stata investigata l'efficienza fotocatalitica di diversi campioni di Au/TiO_2 e Au/CeO_2 nelle reazioni di generazione di idrogeno e di ossigeno dall'acqua, rispettivamente. Gli effetti di parametri quali la quantità di oro, le dimensioni delle sue particelle, la concentrazione del catalizzatore ed il tipo di irradiazione luminosa, sono stati investigati al fine da evindenziare quali siano i principali fattori che influenzano il processo di water splitting. I risultati ottenuti lasciano supporre che l'oro svolga un duplice ruolo, ovvero che agisca come centro di raccolta di irradiazioni luminose oltre che come sito per la formazione di idrogeno ed ossigeno. Dai dati ottenuti sembrerebbe che la

combinazione di quantità molto basse di oro (0.25% in peso) e dimensioni dell'ordine di 2-3 nm delle sue nanoparticelle favoriscano l'attività fotocatalitica dei sistemi Au/TiO_2. Utilizzando radiazioni luminose con lunghezza d'onda vicine alla banda di assorbimento plasmonica dell'oro, le nanoparticelle assorbirebbero fotoni consentendo il trasferimento di elettroni nella banda di conduzione del supporto, con la contemporanea formazione di deficienze ellettroniche nelle particelle dell'oro.

E' stato studiato inoltre un metodo innovativo per la sintesi di CeO_2, utilizzato come supporto per la generazione di ossigeno dall'acqua e che ha consentito l'ottenimento di particelle di catalizzatore di circa 5 nm. I risultati sperimentali hanno messo in evidenza come le proprietà fotocatalitiche del semiconduttore siano strettamente correlate alle dimensioni delle sue particelle. La presenza dell'oro sembra influenzare positivamente la sua attività fotocatalitica sotto irradiazione con luce visibile. Successivamente, i catalizzatori Au/TiO_2 e Au/CeO_2, sono stati sperimentati nel processo di water splitting utilizzando un sistema a membrana, al fine di ottenere la generazione simultanea di idrogeno ed ossigeno. Il processo, che ha previsto l'utilizzo di una membrana di nafion modificata e di solfato ferrico, ha portato allo sviluppo dei due gas in quantità stechiometriche sotto irradiazione con luce visibile.

Il processo di water splitting per la generazione di idrogeno è stato inoltre studiato sperimentando Au/TiO_2 supportato su carboni attivi preparati attraverso differenti metodi di attivazione, al fine di analizzare l'influenza della funzionalizzazione sul processo fotocatalitico di generazione di idrogeno dall'acqua. Carboni attivi con pH basico sembrano svolgere un'influenza positiva sull'efficienza fotocatalitica di Au/TiO_2 sotto irradiazione con luce visibile.

Infine, nell'ultima parte del lavoro di tesi, catalizzatori Au/TiO_2 sono stati testati nella reazione di ossidazione parziale del benzene a fenolo in un reattore batch. L'utilizzo di campioni oro supportati ha consentito il miglioramento delle rese di fenolo rispetto a quelle registrate per il TiO_2 non modificato, sebbene la formazione di prodotti secondari, quali il benzochinone, rappresenti il principale incoveniente del processo.

Resumen

Fotocatalizadores heterogéneos basados en nanopartículas de oro suportadas es una técnica prometedora para la conversión de la luz solar en energía química. Los mismos materiales pueden ser igualmente aplicados a la síntesis orgánica empleando luz visible a fin de desarollar un proceso medioambientalmente benign.

En la presente Tesis Doctoral se han preparado varios catalizadores de oro soportado siguiendo el procedimiento conocido como "deposición-precipitación" y los materiales resultantes fueron empleados en la ruptura fotocatalítica del agua y para la oxidación parcial del benceno a fenol.

Inicialmente, se determinó la eficiencia de varias muestras de Au/TiO_2 y Au/CeO_2 en la generación de hidrógeno y oxígeno del agua, respectivamente. Se estudió la influencia de varios parámetros como el tamaño de las nanopartículas de oro, su carga, el rango de longitudes de onda de la radiación a fin de obtener información sobre el proceso fototacalítico. Los resultados obtenidos sugieren que el oro puede desempeñar varios papeles absorbiendo la luz, inyectando electrones en la banda de conducción del semiconductor y actuando como centro para la evolución de hidrógeno. Más aún, la máxima actividad se consigue cone una pequeña cantidad de oro (alrededor del 0.25 % en peso) junto con una dimensión entre 2 y 3 nm.

Empleando radiación en las longitudes de onda de la banda del plasmón del oro, los fotones absorbidos producen la inyección de electrones del oro al semiconductor dando lugar a la creación de un estado de separación de cargas.

También hemos descrito un método innovador para la síntesis del CeO_2 nanoparticulado y hemos utilizado el material resultante de unos 5 nm de diámetro como semiconductor en la generación fotocatalítica de oxígeno del agua. Los resultados experimentales sugieren que en el caso del CeO_2, las propiedades fotocatalíticas del material son afectadas por las dimensiones de las partículas. También en este caso, la presencia de oro aumenta notablemente la actividad fiotocatalítica de la muestra Au/CeO_2, tal y como se observó en el fotocatalizador a base de Au/TiO_2.

Ambos materiales Au/TiO_2 y Au/CeO_2 fueron evaluados para la reacción de la rupture fotocatalítica del agua en un reactor de membrane a find de conseguir la evolución simultánea de oxígeno e hidrógeno. El proceso requiere una membran de Nafion intercambiada con Fe^{3+}. En estas condiciones se observa la evolución de los dos gas cuando ambas celdas se iluminan con luz visible.

La reacción de evolución de hidrógeno mediante el empleo de Au/TiO_2 se investigó también soportando este material en carbón activo preparado siguiendo diferentes procesos químicos. Se observe que los carbones preparados a valores de pH básicos

ejercen un efecto cooperativo aumentando la actividad fotocatalítica del Au/TiO_2 en el proceso bajo irradiación con luz visible.

Finalmente, el material Au/TiO_2 fue empleado también para llevar a cabo la oxidación fotocatalíca parcial de benceno a fenol. Los datos preliminares sugieren que la presencia de oro aumenta la selectividad hacia el producto, disminuyendo la conversión de benceno. Sin embargo, también para el fotocatalizador Au/TiO_2 se observa la aparición de productos secundarios tales como la benzofenona, por lo que es aún necesario mejorar la selectividad de la reacción fotocatalítica.

Introduction

Photocatalysis is a rapidly expanding technology for environmental application. It implies the acceleration of a photoinduced reaction by the presence of a catalyst.

Initial interest in the heterogeneous photocatalysis started when Fujishima and Honda discovered in 1972 the photochemical water splitting into hydrogen and oxygen with TiO_2 [1]. Subsequently, extensive work started growing rapidly in many areas of water and air technologies [2-4], in addition to hydrogen production from water as a means of solar energy conversion. Semiconductors can act as promoters for light reduction-oxidation processes due to their electronic structure, which is characterized by a filled valence band and an empty conduction band. TiO_2 generally exhibits the highest photocatalytic activity among all the photocatalysts. The use of titanium dioxide as a photocatalyst has been of great interest due to its high activity, photochemical inertness, non-toxicity, biocompatibility, efficiency and low cost. The only disadvantage of TiO_2 is the inability to be activated by visible light, but only ultraviolet (UV).

How to improve the photocatalytic activity of TiO_2 in the visible region represents the main focus of the recent photocatalytic research. For the design of solar-driven treatment technologies, many efforts have been made to achieve highly efficient visible

light-activated semiconductors, such as noble metal doping, non-metal doping, dye sensitization. Nanoparticles of noble metals exhibit unique optical properties that arise from the collective oscillation of the conduction electrons upon interaction with electromagnetic radiation, namely, the localized surface plasmon resonance. This phenomenon can amplify the absorption of visible light and is therefore important in developing efficient visible light photocatalysts. In this context, due to its unique properties and in view of potential commercial applications, gold has attracted many interest in the last years, and represents an highly effective catalysts for many reactions.

Aim of this PhD thesis is the study of the water splitting reaction and the photo-oxidation of benzene to phenol using gold loading photocatalysts.

In the following an overiew of the contents of every chapter is reported.

Chapter 1 gives a presentation on the basic fundamentals of photocatalysis, with a wide overview on the current progresses and drawbacks present in literature. Then, an overview of recent developments of semiconductors, photocatalysis applications and photoreactors modelling is presented.

Chapter 2 reports the catalytic behaviour of a series of various types of gold supported on TiO_2 P25 samples with gold loadings ranging from 0-2.2 wt% in order to investigate which are the

characteristics of the gold deposited on the titania surface that can control and influence the water splitting reaction.

Chapter 3 reports a novel synthetic method of ceria that leads to the formation of very small nanoparticles. The water splitting reaction to generate oxygen using gold loaded on the novel CeO_2 was studied and the experimental data were compared with that obtained for a commercial ceria.

Chapter 4 presents the study of overall water splitting for separate hydrogen and oxygen generation using a membrane photoreactor in the absence of sacrificial agents and using a Fe^{3+}/Fe^{2+} as electrolyte. The effect of different parameters such as the presence of the iron species, the gold loading, the influence of irradiation type, was studied.

Chapter 5 reports the study of a new type of Au/TiO_2 activated carbon (Au/TiO_2-AC) prepared by different activation methods on the photocatalytic hydrogen generation from water. Photocatalytic tests using UV and visible light were performed and the results obtained for the Au/TiO_2-AC samples were compared to that obtained using unmodified TiO_2.

Finally, in Chapter 6, the one-step photo-oxidation of benzene to phenol using TiO_2 gold based photocatalysts is presented as a promising alternative to phenol synthesis.

1

Photocatalysis

1.1 Photocatalysis as clean technology

Since the first energy crisis in the early 1970s and the necessity of a search for new alternative sources of energy, much research has been devoted to the development of efficient systems that would enable the use of renewable resources. In this context, heterogeneous photocatalysis represents a promising way to convert solar into chemical energy at ambient temperature and pressure. Photocatalysis could be applied in the next future to decomposition of water with the production of molecular hydrogen as high-energy and ecologically clean fuel, in addition to a variety of problems of environmental interest. It has been shown to be useful for water and air purification [1-4], for the destruction of microganisms such as bacteria [5] and viruses [6], for the nitrogen fixation [7], for the inactivation of cancer cells [8], for odor control [9] and for the clean up of oil spills [10]. Semiconductors can carry out substrate oxidation and reductions

simultaneously under light irradiation, unchanging during the process. A wide range of inorganic semiconductors can be used for photocatalytic applications, such as TiO_2, CeO_2, ZnO, WO_3, CdS. The ideal photocatalyst should process the following properties [11]:

- High photoactivity
- Biological and chemical inertness
- Stability toward corrosion
- Suitability toward visible or near UV light
- Low cost
- Lack of toxicity.

To enhance the catalytic performance and the response to the visible light, semiconductors are often modified with different methods [12]. The possibility to use solar light for catalyzing many degradation and synthetic processes opens new perspectives for the sustainable chemistry.

1.2 Basic of heterogeneous photocatalysis

Heterogeneous photocatalysis was defined by Palmisano and Sclafani [13] in 1997 as “a catalytic process during which one or more reaction steps occur by means of electron–hole pairs photogenerated on the surface of semiconducting materials illuminated by light of suitable energy”. As a direct consequence

of this definition, both catalyst and light are necessary to induce a chemical process. In fact, upon irradiation excited states of the photocatalyst are generated and initiate subsequent processes like reduction-oxidation reactions and molecular transformations.

1.2.1 Mechanism

The basic mechanism of heterogeneous photocatalysis have been investigated by many research groups [14,15] and can be summarized by the scheme 1.

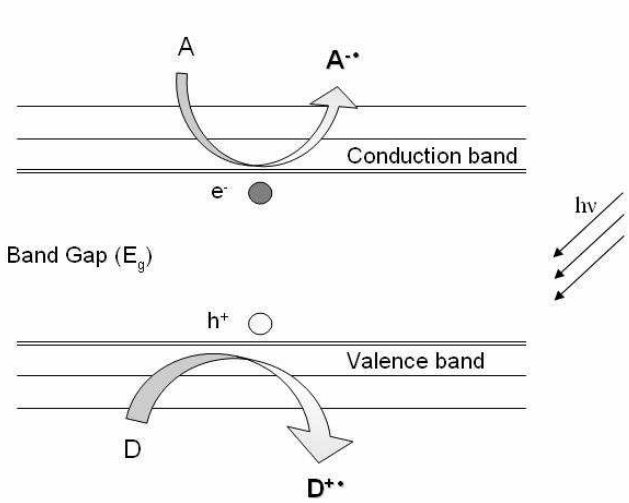

Scheme 1. Simplified reaction scheme of photocatalysis.

The irradiation of a semiconductor with light of energy equal or higher than its band-gap energy (E_g) gives rise to promotion of electrons (e^-) from the valence band to the conduction band, leaving at the same time positive holes (h^+) in the valence band. The photogenerated electron-hole pairs can induce redox reactions with electron donor (D in scheme 1) and electron acceptor (A in scheme 1) adsorbed on the semiconductor surface or located within the electrical double layer surrounding the charged particles. The oxidation-reduction process competes with a possible electrons-holes recombination (within a few nanoseconds), with a consequent input energy dissipation as heat. A thermodynamic condition necessary to the occurrence of such a process is a more negative potential for the electrons photogenerated in the conduction band compared with the reduction potential of the electron acceptor and a more positive potential for the holes of the valence band compared with the oxidation potential of the donor.

Fig. 1 reports the redox potentials and the band-gap value of several photocatalysts.

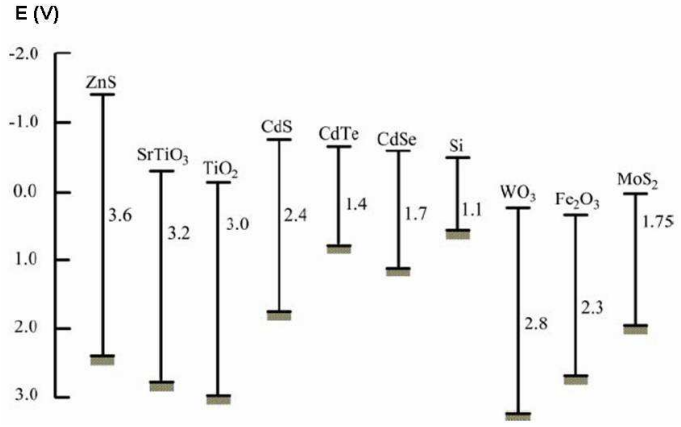

Figure 1. Band positions (top of the valence band and bottom of the conduction band) of the most common semiconductors (adapted from [16]).

The potential of both conduction and valence bands are pH dependent. The increase of pH in a electrolyte solution causes a shift of conduction and valence band potential towards more cathodic values (59 mV per pH unit) [17]. Among all investigated semiconductors (generally metal oxides and chalcogenides) TiO_2 is by far the most largely used [18]. The mechanism of the photocatalytic process using this semiconductor was proposed by several researchers [15,19,20] following the reactions:

$$TiO_2 \xrightarrow{h\nu} TiO_2\ (e^-_{CB}, h^+_{VB}) \qquad (1)$$

$$TiO_2(h^+_{VB}) + H_2O_{ads} \rightarrow TiO_2 + H^+ + HO^{\bullet}_{ads} \qquad (2)$$

$$TiO_2(h^+_{VB}) + HO^-_{ads} \rightarrow TiO_2 + HO^{\bullet}_{ads} \quad (3)$$

In general, donor (*D*) molecules will adsorb and react with a hole in the valence-band and an acceptor (*A*) will also be adsorbed and react with the electron in the conduction band, according to equations:

$$TiO_2(h^+_{VB}) + D_{ads} \rightarrow TiO_2 + D^+_{ads} \quad (4)$$

$$TiO_2(e^-_{CB}) + A_{ads} \rightarrow TiO_2 + A^-_{ads} \quad (5)$$

Oxygen can trap conduction-band electrons to form superoxide ion ($O_2^{\bullet -}$) that can react with hydrogen ions formed from water, forming $HO_2^{\bullet}$ and H_2O_2. Cleavage of H_2O_2 may yield an OH radical.

$$TiO_2(e^-_{CB}) + O_{2\,ads} + H^+ \rightarrow TiO_2 + HO_2^{\bullet} \rightarrow O_2^{\bullet -} + H^+ \quad (6)$$

$$H\,O^{\bullet}_2 + TiO_2(e^-_{CB}) + H^+ \rightarrow H_2O_2 \quad (7)$$

$$2\,H\,O^{\bullet}_2 \rightarrow H_2O_2 + O_2 \quad (8)$$

$$H_2O_2 + h\nu \rightarrow 2HO^{\bullet} \quad (9)$$

$$H_2O_2 + O_2^{\bullet -} \rightarrow HO^{\bullet} + O_2 + HO^- \quad (10)$$

$$H_2O_2 + TiO_2(e^-_{CB}) \rightarrow HO^{\bullet} + HO^- + TiO_2 \quad (11)$$

A could also be a metal ion (*M*) with a suitable redox potential to undergo a change of its oxidation state.

$$M^{n+} + TiO_2(ze^-_{CB}) \rightarrow M^{(n-z)+} \qquad (12)$$

1.2.2 Photocatalytic reaction parameters

A photocatalytic process can be affected by many factors, such as pH, substrate concentration, light intensity and presence of metal ions or inorganic species in solution and temperature.

- pH

One of the most important parameters affecting a photocatalytic process is the solution pH that influences the surface charge on the photocatalyst, the ionization state of the substrate and its adsorption on the catalyst particles. The role of initial solution pH on the photocatalytic reactions was studied by several authors [21-24]. For TiO_2, the point zero charge (PZC) is approximately at pH 6.0 [25,26]. Therefore at pH value lower than pH_{PZC} the TiO_2 surface results positively charged, whereas at pH higher than pH_{PZC} the catalyst surface is negatively charged. Sreethawong et al. [27] investigated the photocatalytic hydrogen evolution from water under various pH conditions over 0.6 wt% Pt/TiO_2. Experimental data showed that the optimum initial solution pH is around 6. The efficiency of

hydrogen evolution activity increases with an increase of pH in solution from 2 to 5-6 while further increase in pH value leads to a lower hydrogen evolution. The authors suggest that at acidic pH (pH< 5) an electrostatic repulsion between the positively charged particles of TiO_2 and the hydronium cations (H^+) present in solution retards the adsorption of H^+ ions reducing the photocatalytic hydrogen evolution. At alkaline pH values (pH> 7) another type of repulsion, between the negatively charged surface of the photocatalyst and the molecules of sacrificial agent (methanol) can occur. This limits the adsorption of the sacrificial agent molecules on the photocatalyst particles and as direct consequence, also the probability to scavenge the photogenerated holes by the methanol molecules is reducted while the electron-hole recombination results favoured. When the pH solution is near to the zero point charge of the catalyst, the species can probably react more easily with the semiconductor surface allowing to obtain higher hydrogen production [28,29].

- Catalyst concentration

It was observed that the reaction rate in a photocatalytic process increases with increasing catalyst concentration and becomes constant above a certain level [30]. This is essentially due to the aggregation of photocatalyst particles and consequently to the decrease in the number of surface active sites, and at the same

time to increase in opacity due to an higher light scattering photocatalyst particles. Nikazar et al. [31] investigated the photocatalytic degradation of the azo dye Acid Red 114 in water, using TiO_2 supported on the zeolite clinoptilolite as photocatalyst. The photodegradation efficiency increases with an increase in the amount of catalyst (10 wt% TiO_2/ zeolite) up to a value of 40 ppm. Then it decreases with an increase of catalyst concentration. The authors explain this result considering that an higher quantity of photocatalyst probably does not influence the photocatalytic efficiency and an excess of its particles in suspension causes an increase in opacity. In another study [32] the influence of several parameters on the photocatalytic decolorization of the azo dye AR27 under UV irradiation, using TiO_2 as photocatalyst, was reported. From experimental data, an enhancement of dye photodegradation using the catalyst in the range 0-300 mg L^{-1} was observed. Further increasing in TiO_2 loading may cause the aggregation of free catalyst and a decreasing of UV-light penetration.

- Light intensity and wavelength

The minimum level required to promote the excited state depends on the band-gap energy. For example, TiO_2 anatase with large band-gap energy (3.2), absorbs light only in the UV region of the solar spectrum ($\lambda < 400$ nm). It was extensively reported that the increase of light intensity can enhance the rate

of photocatalytic process [33,34]. Hermann et al. [35] in a study of photocatalytic oxidation of halide ions by oxygen in titania suspension, reported that only photons with wavelength shorter than the TiO_2 absorption edge can activate the photocatalyst and this phenomenon is predominant at low light intensity [36], whereas a electron-hole recombination seems to be favoured for higher intensity light. Molinari et al. [37] investigated the influence of light intensity on the photocatalytic oxidation of benzene to phenol in a membrane reactor. To decrease its reactivity before extraction, the authors carried out a photocatalytic experiment using a lower light intensity (4.7 mW cm^{-2}) respect that of the others photocatalytic runs (6.0 mW cm^{-2}). The obtained data showed that an intensity of 4.7 mW cm^{-2} is too low to promote an efficient photocatalytic process.

- Dissolved ions

New developments of photocatalysis technology have focused on searching for suitable compounds to promote the photocatalyst activity by quenching the conduction band electrons (in oxidation processes) or the valence band holes (in reduction processes). Several authors report the use of metal ions like Fe^{3+} [38,39] to enhance the photocatalytic reaction rate. The presence of small amount of Fe^{3+} (0-10 mg L^{-1}) increases the reaction rate of the organophosphourous insecticide Diazinon photodegradation [40], NO_2^- oxidation [41] and

oxygen generation from water [42]. Positively charged Fe^{3+} adsorbed on the photocatalyst surface is easily reduced by trapping electrons of the conduction band and the electron-hole recombination thus decreases. When the Fe^{3+} concentration is higher the $Fe(OH)^{2+}$ ions likely exhist as the predominant monomeric ion (III)-hydroxyl complex which is also the major light absorbing species, so the photocatalytic efficiency of the system decreases [43]. In addition to iron, the influence of other metals common in naturals waters such as Cu^{2+}[44] and Mn^{2+} [45] was investigated and also in this case the positive influence is closely correlated with their concentration in solution and the adsorption on the photocatalyst surface. Inorganic ions, such as S^{2-}/S_3^{2-} [46], Ce^{4+}/Ce^{3+} [47], IO^{3-}/I^- [48-50], Fe^{3+}/Fe^{2+} [51] working as redox mediators, were used as sacrificial agent for hydrogen or oxygen production from water. Two photocatalysts were employed to produce hydrogen and oxygen under the mediation of oxidated and reduced state of the metal, respectively. Photooxidation reaction rates were found to markely increase also upon addition of inorganic species, like IO_4^-, $S_2O_8^-$, BrO_3^- and ClO_3^- [52] either by inhibiting electron-hole pair recombination through scavenging conduction band electrons at the photocatalyst surface:

$$IO_4^- + 8e^-_{CB} + 8\ H^+ \rightarrow 4H_2O + I^-$$

or producing high reactive intermediate radicals such as IO_3^-, $HO^{\cdot}$, $IO_4^{\cdot}$, that assisted the oxidation process by free radicals pathway.

- Temperature

The overall reaction of photocatalytic processes is not too sensitive to the temperature. Due to photonic activation, the photocatalytic systems does not require heating and can operate at room temperature. This is very attractive for processes that can be carried out in aqueous medium because there is no need to waste energy in heating water.

1.3 Catalysts for photocatalytic processes

Heterogeneous photocatalysts are solids able to promote reactions in the presence of light without being consumed in the overall reaction. Catalysts used in photocatalytic reactions are invariably semiconductor materials. Chalcogenide include several metal oxides such as TiO_2, CeO_2, ZnO, WO_3, Fe_2O_3 or even sulfides like CdS, ZnS, MoS_2. Sensitized photoreactions are activated by absorption of a photon with sufficient energy, i.e., equal or higher than the bandgap energy of the catalyst. Bandgap energies of the most common semiconductors are show in Table 1.

Table 1. Band gap energies of semiconductors used in photocatalytic processes.

Photoatalyst	Band gap energy (eV)
Si	1.1
WSe_2	1.2
WO_3	2.8
α-Fe_2O_3	2.2
V_2O_5	2.7
SiC	3.0
$BaTiO_3$	3.3
CdO	2.1
CdS	2.4
CdSe	1.7
Fe_2O_3	3.1
TiO_2 rutile	3.0
TiO_2 anatase	3.2
$SrTiO_3$	3.4
SnO_2	3.5
GaAs	1.4
$SrTiO_3$	3.4
ZnS	3.7
ZnO	3.2

Nevertheless, some of the photocatalysts do not show a long-term activity during the irradiation process. Binary metal

sulfides such as CdS, CdSe or PbS are regarded as insufficiently stable for catalysis in aqueous media as they rapidly undergo photoanodic corrosion [53,54]. To overcame this drawback several works suggest the addition of sulfide and sulfite to the contacting solution [55]. These materials are also known to be toxic. Hematite (α-Fe_2O_3), for example, is absorptive in the visible region, but shows much lower photocatalytic activity than TiO_2 or ZnO, probably because of corrosion or the formation of short-lived metal-to-ligand or ligand-to-metal charge transfer states [56]. Although ZnO and TiO_2 (anatase) have similar bandgap energies (3.2 eV) and higher reactivity than TiO_2 [57], zinc oxide is more instable in illuminated aqueous solutions, with $Zn(OH)_2$ being formed on the particle surface leading to the deactivation of the catalyst [58]. Wu [59] also observed higher photocatalytic activity for TiO_2 compared to SnO_2. WO_3 has also been investigated as photocatalyst and it shows a remarkable photostability in acidic media, making it a powerful semiconductor for many tipes of photocatalytic processes [60]. It has a band-gap of ~2.8 eV, that is ~ 0.4 eV narrower than that of TiO_2, so it can absorb more visible light from sunlight [61]. However, it is generally less effective than TiO_2 and unsuitable for achieving an efficient oxidative reaction, probably due to the inability of photogenerated electrons of the conduction band to directly reduce molecular oxygen [62]. As one kind of important rare earth materials CeO_2 in the last years

has attracted great interest for its potential photocatalytic applications [63]. Furthermore, nanocrystalline cerium dioxide has some singular properties like as transition from boundary diffusion to lattice diffusion [64] and lattice expansion [65]. In the next section, a detailed description about TiO_2 and CeO_2 photocatalysts is presented.

1.3.1 Titanium dioxide

Having high photocatalytic activity and chemical stability, non-toxicity and low cost, titanium dioxide has become the most widely used photocatalyst. It has been widely used as white pigment in paints, plastic, paper, cosmetics and foodstuffs. Three crystalline forms exists in nature: anatase (tetragonal), rutile (tetragonal) and brookite (orthorhombic). Among them, anatase form has been found to be the most photocatalytically reactive form [66] even if the more stable form is rutile, whereas anatase and brookite are metastable and are readily transformed to rutile when heated [67]. TiO_2 can be prepared in the form of powders, crystals or thin films, by either liquid or gas phase methods. It can also be synthesized in special nanostructured morphologies like nanorods [68], nanowires [69], nanotubes [70], nanoribbons [68] and whiskers [71]. Gas phase methods are generally used for the preparation of thin films. The main techniques are vapour deposition [72], physical vapour

deposition [73] and spray pyrolisis deposition [74]. Liquid phase preparation procedures include sol-gel method [75], precipitation and co-precipitation [76, 77], solvothermal and hydrothermal methods [78, 79], microemulsion [80], combustion and electrochemical synthesis [81, 82]. The sol-gel procedure is the most popular technique to synthesize TiO_2 because it offers many advantages over the other production method, such as the formation of very pure and homogeneous materials. Typically sol–gel synthesis of TiO_2 leads to the amorphous phase which can be transformed into anatase by calcination at moderate temperatures. Temperatures around 500 °C initiate a phase change from anatase to rutile that is transformed into brookite at much higher temperatures. TiO_2 has a band-gap energy of ~3.2 eV, hence its photoactivation requires radiation with light of wavelength less than or equal to ~380 nm, with a maximum at approximately 340 nm. One of the most used commercial TiO_2 materials for photocatalytic oxidation applications is TiO_2 Degussa P25. It is composed by a mixture of 80% of anatase and 20% of rutile, with a surface area of 50 $m^2\ g^{-1}$ and an average particle size of 21 nm (manufacturer data).

1.3.2 Cerium dioxide

Cerium dioxide has attracted great interest during the last years [83] for its potential applications as fast conductor, catalyst, oxygen storage capacitors, polishing materials [84]. Ceria is also widely used as electrolyte for solid oxide fuel cells (SOFC) [85]. This material possess high ionic-electronic conductivity at relatively low temperatures. Up to now, many efforts have been devoted to the chemical synthesis of CeO_2 nanomaterials with various morphology and size, such as porous structures, films and nanoparticles [86]. The development of efficient methods to synthesize nanostructures with well-defined size and shape is one of the key trends in material chemistry because of their size/shape-dependent properties and potential applications [87]. Therefore, for the synthesis of CeO_2, reaction conditions are crucially important for controlling the growth of the crystal, as well as the crystal shape and the monodispersity of CeO_2.

In the past few years, some effective methods have been developed to prepare CeO_2. For example, by two-step precipitation using oleic acid as a capping agent [88], via the decanoic acid assisted supercritical hydrothermal process at 400 ◦C [89] and thermolysis reaction of cerium benzoyl acetonate complex in oleic acid/oleyl amine solvents under vacuum condition at 310–330 ◦C [90]. However, these above methods required complicated procedure, special equipments or

organometallic precursor. Hence, fabrication of ceria nanocrystals with uniform size and well-defined crystal shape by a simple and economical method represent a target of great interest. Ceria nanoparticles show a strong absorption below 400 nm with a maximum absorbance peak around 305 nm. The band-gap energy varies in the range 3.03-3.7 eV depending on the preparation method [91].

1.3.3 Modified photocatalysts

The efficiency of the classical photocatalysts is often reduced by some drawbacks, such as:

• quickly recombination of the photogenerated electron-hole pairs (within 10-100 ns) which releases thermal energy or unproductive photons;

• high reactivity that leads to fast backward or secondary reactions with the formation of undesirable by-products;

• a low absorption in the visible region which determines their inability to use solar light (less than 5% is used in the case of TiO_2 anatase).

In recent years, therefore, the development of photocatalysts able to overcome these problems represents one of the main topic in the photocatalytic research. The major practices involve catalyst modification by noble metal loading, ion doping into the

semiconductor lattice, dye photosensitization, mixing with other semiconductors.

1.3.3.1 Noble metal loading

Noble metals like Pt, Pd, Au, Rh, Ni, Cu and Ag have been reported to be very effective to enhance catalytic activity of several semiconductors and the visible light absorption [18].

As the Fermi levels of these noble metals are lower than that of catalysts like TiO_2, photo-excited electrons can be transferred from the conduction band to metal particles deposited on semiconductor surface, while photogenerated valence band holes remain on the photocatalyst [18]. Hence, migration of electrons to the metal particles results in a formation of a Schottky barrier at each metal-semiconductor contacting region. The Schottky barrier can serve as an efficient electron trap to avoid the electron-hole recombination in a photocatalytic process enhancing the efficiency of the photocatalytic process [92, 93]. Moreover, surface plasmon resonances of noble metal particles, which can be excited by visible light, increases the electric field around metal particles and thus it enhances the surface electron excitation and electron–hole separation on noble metal-deposited semiconductor particles.

Noble metals doped or deposited on a photocatalyst are expected to show various effects on its photocatalytic activity by different mechanisms. It follows that may act separately or simultaneously depending on the photoreaction conditions: noble metals (i) enhance the electron–hole separation by acting as electron traps, (ii) extend the light absorption into the visible range and enhance surface electron excitation by plasmon resonances excited by visible light, and (iii) modify the surface properties of photocatalyst [94]. The dosage level is an important factor that influences the enhancement effect of noble metals. Below an optimum dosage level noble metals can act as electron-hole separation centers, improve the charge separation, and thus enhance the photocatalytic efficiency of modified semiconductor. However, as dosage levels exceed optimum loading, noble metals can act as electron-hole recombination centres which are detrimental to the photocatalytic activity.

As one of the noble metals, Pt has been widely used as the cocatalyst in photocatalytic water splitting over many different kinds of semiconductors: oxides [95], (oxy)sulfides [96] and (oxy)nitrides [97]. All have been shown to greatly enhance the photocatalytic activity for hydrogen evolution. Mizoguchi et al. [98] reported that platinized $CaTiO_3$ powder, with band gap of 3.5 eV estimated from optical absorption edge, exhibited a high photocatalytic activity under UV irradiation for hydrogen generation from water splitting. Iwase et al. [99] found that fine

gold nanoparticles played an important role in the creation of active sites for hydrogen evolution and the enhancement of charge separation. In addition, the back-reaction between hydrogen and oxygen to produce water on the Au cocatalyst was negligible in comparison to that on a Pt cocatalyst. This ultimately led to improved photocatalytic activities of some titanate, niobate, and tantalate photocatalysts for overall water splitting. Wu et al. [100] investigated hydrogen production with low CO selectivity from the photocatalytic reforming of glucose in water on metal/TiO_2 catalysts (metal) Pt, Rh, Ru, Ir, Au, Ni, and Cu. The loaded metals, in particular Rh, were found to greatly enhance the rate of hydrogen production. This was attributed to the fact that the Schottky barrier formed at the metal and TiO_2 interface could serve as an efficient electron trap, thus preventing photogenerated electron-hole recombination. The effect of the nature of the metal cocatalyst was interpreted in terms of different electronic interactions between the metal nanoparticles and the TiO_2 surface. It has also reported that the smaller the Schottky barrier height at the metal/semiconductor junction, the greater was the electron flow from semiconductor to metal, thus leading to higher photocatalytic activity for hydrogen production [101]. When cocatalysts consisting of Au/Pd bimetallic nanoparticles with core/shell structures were loaded onto the TiO_2 surface, Pd shell permits selective hydrogen permeability and contribute to

reduce the protons with photogenerated electrons. As result the photocatalytic production of hydrogen from aqueous ethanol solutions was greatly enhanced [102].

1.3.3.1.1 Gold

Gold has been considered catalitically inactive for a long time. However in 1973 Bond et al. reported for the first time the activity of a gold catalyst for the hydrogenation of olefins [103]. In 1987 Haruta et al. discovered that Au supported on reducible oxide supports exhibited novel catalytic activity for low temperature oxidation of CO [104]. Later on, again Haruta demonstrated that high selectivity in the heterogeneous oxidation of propylene to propylene oxide could be achieved with gold on titania [105]. The regio-selective oxidation of alcohols and even carbohy-drates with molecular oxygen, developed by Rossi and coworkers, represents another surprising discovery of gold catalysis [106]. Furthermore, Hutchings and coworkers showed gold to be effective for the production of hydrogen peroxide [107].

The unique catalytic properties of supported nanosized-Au particles depend strongly on different factors, such as the support, shape and particles size. In particular, size of the Au nanoparticles and the properties of the support have been

showed to be critical for the Au catalytic activity. Thus, due to its unique properties and in view of potential commercial applications, gold has been intensively studied in material science, especially in the context of emerging nanotechnology, as also confirmed from the large number of papers reviewing the topic [108-111].

Methods of preparation of the semiconductor-metal catalyst play an important role in the photocatalytic activity of the overall system. The size of the gold nanoparticles is key in obtaining active catalysts for several reactions. In most cases, such as carbon monoxide oxidation, only small gold nanoparticles (< 5 nm) exhibit high catalytic activity. Most gold precursors used in preparing supported gold catalysts are salt complexes where the oxidation state of gold is typically +3 since the latter is more stable than the +1 oxidation state. Moreover, the size of the gold nanoparticles highly depend on the the gold ion concentration, the pH and the temperature of the solution used. The Au^{3+} atoms are easily reduced by performing thermal treatment since gold oxides are typically unstable in air. Gold nanoparticles can be synthesized by vacuum evaporation that involves the deposition of thin films of metals on a substrate by evaporation in a vacuum chamber, or as colloids, prepared through the use of various reducing agents that generate nanoparticles with size between 20 and 100 nm[112]. Unlike the colloidal technique, smaller gold nanoparticles with sizes of less than 10 nm can be

obtained by depositing gold onto a solid support. Different methods for the synthesis of supported gold nanoparticles have been reported in the literature to obtain well-dispersed particles with nanometer sizes. Among these methods, the most widely used are impregnation [108], coprecipitation [113] and deposition-precipitation [114]. The impregnation method is less preferable as it tends to produce large gold particles [115]. Coprecipitation, however, is often used to prepare supported base metal nanoparticles. Preparation involves the addition of chloroauric acid solution and a metal nitrate to a solution of sodium carbonate. The most commonly used procedure to synthesize gold nanoparticles is the deposition-precipitation (DP) method, suggested by Haruta [109]. This technique involves the deposition of gold hydroxide on the surface of the metal oxide support by raising the pH of the gold chloride precursors. The deposition-precipitation method has an advantage over other methods because the active component, the gold chloride precursor, remains on the surface of the support and not buried in it. Moreover, chloride ions, which are known to poison the activity of gold nanoparticles in many types of reactions, can be minimized by repetitive washing [116]. In addition, gold particles prepared by DP are associated with small particle sizes with a uniform particle distribution and a closed interaction between the gold particles and the support.

The pH value plays a key role for gold deposition in aqueous media permitting the distribution of gold (III) species and the charge of the solid support surface. The pH of aqueous $HAuCl_4$ solution is adjusted at a fixed point in the range of 6 to 10, and is selected primarily based on the isoelectric points of the metal oxide supports [109]. Careful control of the solution pH enables selective deposition of $Au(OH)_3$ only on the surfaces of the support metal oxides without precipitation in the liquid phase. The choice of the support was also considered as critical; transition metal oxides such as ferric oxide and titania worked well, whereas the more commonly used supports, such as silica (isoeletric point ~2) and tungsten oxide (isoeletric point ~1) worked with less efficiency.

1.3.3.2 Ion doping

Rare earth metal ion and transitional metal ion doping have found to be able for enhancing the photocatalytic activity of several semicondutors [117, 118]. Over the past decades, there have been numerous reports on the modification of wide band gap photocatalysts using metal ion doping to make them visible-light active. These include doped TiO_2[119], $SrTiO_3$ [120], ZnO [121] and doped ZnS [122] among others. The main objective of doping is to induce a batho-chromic shift, i.e., a decrease of the

bandgap or introduction of intra-bandgap states, which results in more visible light absorption. The dopant ions can work as hole and electron traps or they can mediate interfacial charge transfer. Dopant ions may be adsorbed on the semiconductor catalyst, incorporated into the interior of the semiconductor particle, or they may form separate oxide phases [53]. Once incorporated into the interior of the photocatalyst, the dopant ions may occupy either lattice (substitutional) or interstitial sites.

Choi et al. [123] carried out a systematic study of the effects of 21 different metal ion dopants on nanocrystalline TiO_2. Chloroform oxidation and carbon tetrachloride reductions were used as photoreactivity tests. It was found that doping with metal ions could expand the photo-response of TiO_2 into visible spectrum. The obtained data showed that some doped TiO_2 samples had much greater photocatalytic activity than the correspondent undoped samples, even if exists an optimum concentration of doped metal ion, above which the photocatalytic activity decreases due to the increase in electron-hole recombination. Metal ions such as Fe, Mo, Ru, Os, Re, V and Rh can enhance TiO_2 photoactivity, while others ions like Co and Al cause detrimental effects. Chae et al. [124] reported that, whereas Ga doped TiO_2 powder could split pure water stoichiometrically under UV irradiation, pure TiO_2 did not show any activity. The Ni^{2+} doping enhanced the photoactivity of the TiO_2 for hydrogen production from an aqueous methanol

solution [125]. Kudo and Kato [126] investigated the effects of doping lanthanide like La, Pr, Nd, Sm, Gd, Tb and Dy and alkaline earth metal ions such as Ca, Sr, and Ba into $NaTaO_3$ photocatalysts for efficient water splitting. Lanthanum was the most effective dopant. The apparent quantum yield at 270 nm amounted to 56% which is the highest quantum yield ever reported for catalysts in pure water splitting. The positive effects on the photocatalytic properties were mainly due to the decrease in the particle size and the ordered surface nanostructure. The effect of the addition of the dopant metal is largely influenced by its concentration in the TiO_2 matrix. As the concentration of the dopant increases, the space-charge region becomes narrower, with the electron/hole pairs within this region being efficiently separated by the large electric field before recombination. On the other hand, when the concentration is high, the space-charge region becomes very narrow and the penetration of light into the catalyst greatly exceeds the space-charge layer. Therefore, the recombination of photogenerated electron/hole pairs in the semiconductor increases, because there is no driving force to separate them.

1.3.3.3 Dye sensitization

Dye sensitization of nanocrystalline semiconductors has attracted considerable attention in the last years since Graetzel first reported on the highly efficient ruthenium complex sensitized nanocrystalline TiO_2-based dye sensitized solar cells [127]. Several dyes possess sharp and intense absorption bands in the visible and near infrared regions and have been employed as sensitizers in a number of technological applications such as electrography [128], xerography [129] and optical data storage [130]. The ability of dyes to sensitize large band-gap semiconductors as well as their application as organic photovoltaic materials have been well investigated [18]. Upon illumination by visible light, the excited dyes can inject electrons to the semiconductor conduction band to initiate the photocatalytic process. The semiconductor surface acts as a quencher accepting an electron from the excited dye molecule. The electrons can in turn be transferred to reduce an acceptor species adsorbed on the surface. Although there are some studies with dye/metal complex sensitized TiO_2 for photocatalytic degradation reactions [130], is in the field of energy production that semiconductor dye sensitization plays it most important role [18]. Dye-sensitized solar cells have attracted a great deal of interest because of their relatively higher

efficiency and low cost compared with conventional inorganic photovoltaic devices.

Dhanalakshmi et al. [131] found that, when TiO_2 and ZnO were sensitized with a new sensitizer ($[Ru\text{-}(dcbpy)_2(dpq)]^{2+}$), they displayed extremely stable and efficient photocatalytic activity for hydrogen production under visible-light irradiation from water even in the absence of an electron donor.

Gratzel and co-workers [132] succeeded in decomposing water by visible light using $Ru(bpy)_3^{2+}$ and its amphiphilic derivatives as sensitizers. Pt/RuO_2-loaded TiO_2 particles proved particularly effective in those systems, acting as photocatalysts for water-splitting process. Nada et al. [133] found that, when copper phthalocyanine was used as a photosensitizer, it was effective for hydrogen production over RuO_2/TiO_2 using UV/solar light irradiation. In fact, copper phthalocyanine exhibited higher efficiency compared to other sensitizers such as ruthenium bipyridyl.

1.3.3.4 Composite semiconductors

The composition of two semiconductors possessing different energy levels for their corresponding conduction and valence bands, is another method to use visible light for photocatalytic applications [18]. When a large band-gap semiconductor is

coupled with a small band-gap semiconductor with a more negative conduction band level, photogenerated electrons can be injected from the small band-gap semiconductor to that with the large band-gap. Thus, this technique provides a more efficient charge separation, an increase in the life time of the charge carriers and an enhanced interfacial charge transfer to adsorbed substrates. Coupled semiconductors including TiO_2/CdS, TiO_2/SnO_2, TiO_2/ZnO and TiO_2/WO_3 have been used intensively for organic photodegradation [134] but in the recent years it received particular attention for their potential application in hydrogen generation from water splitting [135]. It has been reported that coupling CdS (band-gap 2.4 eV) with TiO_2 (band-gap 3.2 eV) hydrogen could be produced since the conduction band of TiO_2 is more negative than hydrogen production level ($E_{H2/H2O}$). In CdS/TiO_2 the photogenerated electrons in CdS are transferred into the TiO_2 particles while the holes remain in the CdS particle. This not only helps for charge separation by isolating electrons and holes in two distinct particles but at the same time, allows the extension of the photoresponse of the photocatalyst in the visible. CdS photocorrsion can be prevented adding Na_2S solution. Other composite systems recently studied for the water splitting reaction are ZnO/ZnS/CdS [136], ZnO/CdS [137], CdS/ZnS [138], InP/CdS [139]. In general, the coupled system exhibit higher efficiency of the photocatalytic process.

Domen and co-workers [140] reported that a NiO-loaded $SrTiO_3$ powder was capable of decomposing pure water as well as water vapor into H_2 and O_2 under UV irradiation. The activity of the photocatalyst was increased considerably by a pretreatment in H_2 and using a concentrated NaOH solution for the photocatalytic reaction. The photocatalytic activity of $SrTiO_3$ was also greatly improved by using a modified preparation method or a suitable concentration of metal cations doping such as La^{3+} and Ga^{3+}.

1.4 Applications of Photocatalysis

In the last decade photocatalysis has become more and more attractive for the research in water splitting to make hydrogen and oxygen using clean and renewable sources, for organic synthesis and for environment and for the industry regarding the development of technologies for purification of water and air. Compared with traditional advanced oxidation processes the technology of photocatalysis is known to have some advantages, such as ease of setup and operation at ambient temperatures, no need for post-processes, low consumption of energy and consequently low costs.

1.4.1 Photocatalytic hydrogen production

Hydrogen is considered as an ideal fuel for the next future. It does not produce any contaminant when it burns in air, it is a clean and a non-polluting energy carrier. It is the most common element on earth, mostly present in water, biomass and hydrocarbons. Nowadays, the most widely used industrial process is the Steam Methane Reforming (SMR), which is also the most economical process for producing hydrogen [141]. This process involves many different catalytic steps, as long as natural gas (or methane) and hydrocarbon fuels that remains at a low or moderate price. However, industrial hydrogen production results in equally large carbon dioxide emissions. Moreover, the emission of greenhouse gases also needs to be reduced to solve the problem of the global warming. Other fuel processing technologies for hydrogen production are partial oxidation and autothermal reforming. Partial oxidation converts hydrocarbons to hydrogen by partially combusting the hydrocarbon with oxygen. The process requires high temperatures with some soot formation and the hydrogen/ carbon oxide ratio from 1:1 to 2:1. Autothermal reforming is typically conducted at a lower pressure than partial oxidation reforming and has a low methane slip. However, these processes require an expensive and complex oxygen separation unit in order to feed pure oxygen to the reactor. Fuel fossil burning which contributes to the

greenhouse gas pool and also the eventual depletion of the world's fossil fuel reserves need a development of cheap and very efficient new technologies. One strategy could be to apply steam reforming methods to alternative renewable materials. Such materials might be derived from crops. Not only do these biomass-conversion schemes turn waste into a valuable product, but in addition, any carbon dioxide in the processes could be soaked up by planting new crops to provide the required biomass. A biomass strategy could represent a useful alternative to the current fossil fuel methods. Solar and wind that are the two major sources of renewable energy, also represent a promising way for sustainable hydrogen production, although their cost still remains high. In the last years there has been a great interest of research in water splitting to make hydrogen and oxygen. Water electrolysis could become a useful alternative for producing clean hydrogen. It is essentially the conversion of electrical energy to chemical energy in the hydrogen form, with oxygen as useful by-product [142]. The most common electrolysis technology is alkaline based, but the research is developing also in proton exchange membrane processes and solid oxide electrolysis cells units. Currently, electrolysis is more expensive than using large-scale fuel processing techniques to produce hydrogen. It can become more competitive as the cost continues to decrease with the technology advancement. Alternatively, photocatalytic water

splitting using semiconductors could offer a promising way for low cost and environmentally friendly hydrogen generation from solar energy. Since Fujishima and Honda reported photoelectrochemical water splitting using a TiO_2 electrode in 1972 [1], many research groups have intensively studied water splitting using photoelectrodes or photocatalysts [18]. Both photocatalytic and photoelectrochemical water splitting are similar to the photosynthesis process of green plants, so are both interesting and promising topics. However, heterogeneous photocatalysis that employees photocatalyst powders has several advantages over photoelectrochemical cells such as greater simplicity and lower processing cost. In both systems the electronic structure of a semiconductor plays a key role for an efficient hydrogen generation [18]. The photocatalytic hydrogen generation using a useful semiconductor is represented in Fig. 2.

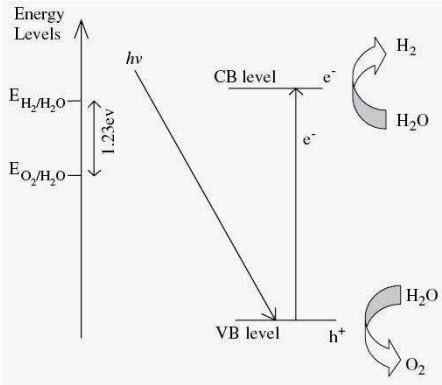

Figure 2. Mechanism of photocatalytic water splitting using a suitable photocatayst.

For hydrogen generation, the conduction band level of the semiconductor should be more negative than hydrogen production level, while the valence band should be more positive than water oxidation level to obtain an efficient oxygen generation from photocatalysis. In the overall water splitting process, oxygen and hydrogen evolution can be modelled as two chemical half-reactions. A simplified equation set that describes these half reactions in addition to the net conversion process can be written:

$2\gamma \rightarrow 2e^-_{CB} + 2h^+_{VB}$	Photon induced e^-/h^+ generation	(13)
$H_2O + 2h^+ \rightarrow 2H^+ + {}^1/_2O_2$	Water oxidation half reaction	(14)
$2H^+ + 2e^- \rightarrow H_2\,(gas)$	Proton reduction half reaction	(15)
$H_2O + 2\gamma \rightarrow H_2\,(gas) + {}^1/_2O_2$	Net overall water splitting	(16)
$\Delta G° = +237.18\ kJ\ mol^{-1}$	Standard Gibbs free energy	(17)
$V°_{rev} = \Delta G°/nF = 1.23\ V$	Standard reversible potential	(18)

where γ is photon energy, e^- is an electron, h^+ is a hole, $\Delta G°$ is the standard Gibbs free energy, $V°_{rev}$ is the standard reversible potential, n (= 2) is the number of electron exchanged and F is the Faraday constant.

It is clear from the equation set that photocatalytic water splitting is a delicate balancing process, where photoproducted

electron-hole pairs can drive the photocatalytic half reactions. In this system, light energy is converted into chemical energy. Thus, the minimum energy required to drive the reaction correspondent to that of two photons is equal to 1.23 V. Presently, hydrogen generation from water splitting has still a low efficiency, mainly due to the recombination of the photogenerated electron-hole pairs, the inability to use visible light using most of known photocatalyst and in many cases to the possible reverse reaction that involves the rapid hydrogen and oxygen recombination.

Since nearly half of the solar energy incident on the Earth's surface lies in the visible region (400 nm< λ< 800 nm) it is of primary importance using visible light to promote hydrogen generation from water splitting. Even if all UV light and visible light up to 600 nm are utilized, the conversion efficiency would be 16 %, and a further extension up to 800 nm would increase the conversion efficiency up to 32% as shown in Fig. 3.

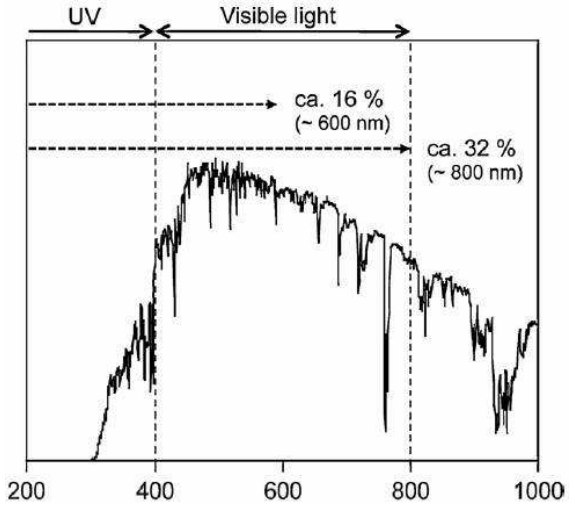

Figure 3. Solar spectrum and maximum visible solar light conversion for water splitting reaction.

The first example of water splitting using visible light irradiation was reported only a decade ago by Sayama et al. [143] in 2001 and it is inspired by photosynthesis in nature. In this study overall water splitting process takes place using a mixture of two different photocatalysts, Pt/WO_3 for oxygen evolution and $Pt/SrTiO_3$(Cr–Ta-doped) for hydrogen generation using visible light irradiation (λ> 420 nm) and IO^{3-}/I^- redox couple as an electron mediator. The overall water splitting proceeded by the redox cycle between IO_3^- and I^- under basic conditions as follows: (a) water reduction to H_2 and I^- oxidation to IO_3^- over Pt-TiO_2-anatase and (b) IO_3^- reduction to I^- and water oxidation to O_2 over TiO_2-rutile. An advantage of this system was that H_2 gas was evolved only over the Pt-TiO_2-anatase photocatalyst

and that O_2 gas was evolved over the TiO_2-rutile photocatalyst only, even from a mixture of IO_3^- and I^- in a basic aqueous solution. Many others Z-scheme systems using reversible redox mediators has been investigated to carry out the overall water splitting into H_2 and O_2. For example, Arakawa et al. [144] constructed an artificial Z-scheme system using WO_3 photocatalyst and a Fe^{2+}/Fe^{3+} redox mediator. Kozlova et al. [145] investigated the overall water splitting over a Pt/TiO_2 catalyst with a Ce^{3+}/Ce^{4+} shuttle charge transfer system. However, in these studies, the photocatalytic activities for O_2 and H_2 production were low, due to the back-reaction and the interactional reaction characteristics. Fujihara et al. [146] constructed a Z-scheme water splitting system using a TiO_2-rutile photocatalyst and two redox mediators (Br_2/Br^- and Fe^{3+}/Fe^{2+}) in a two-compartment cell. As the production of H_2 and O_2 were carried out in separated compartments, the reversible reactions on photocatalysts, which often suffered from the effects of back reactions, were largely prevented. Other approach for hydrogen and oxygen generation is to use a one-step system, using a single photocatalyst. To absorb visible light and have sufficiently high potential for decomponing water, innovative photocatalysts materials are required to satisfy the following requirements: (i) have a sufficiently narrow band-gap (1.23 eV < *E*g < 3.0 eV) to harvest visible light and possess the correct band structure, (ii) are stable under photoirradiation, (iii)

have suitable conduction and valence band for hydrogen and oxygen generation. Several methods have been investigated, including modification by noble metal loading and mixing with other semiconductors. Up until now, the highest photocatalytic activities for hydrogen production from water using visible-light irradiation are from photocatalysts loaded with Pt as the cocatalyst [147]. Some other noble metals, such as Au [148] Ru [149] Pd [134] Ag [134] and Rh [134] have also been reported as efficient cocatalysts. Another promising one-step water splitting system that is based on the $(Ga_{1-x}Zn_x)(N_{1-x}O_x)$ has been proposed by Maeda et al. [150] in 2005. The result of the solid solution was that the band position of $(Ga_{1-x}Zn_x)(N_{1-x}O_x)$ was suitable for the overall water splitting under visible light irradiation. The quantum efficiency at 420-440 nm was 2.5% using $Rh_{2-y}Cr_yO_3$ as cocatalyst [151] that is greater than that of others systems like Ni-$InTaO_4$ (0.66% at 402 nm) [152] and $BiYWO_6$ (0.17% at 420 nm) [153]. The photocatalytic efficiency of the $Rh_{2-y}Cr_yO_3$-loaded $(Ga_{1-x}Zn_x)(N_{1-x}O_x)$ system mainly consists in the ability to prevent the electron-hole recombination and to enhance the reactivity of the photoproduced holes in the oxygen generation.

1.4.2 Photocatalytic synthesis

Photocatalytic oxidation of benzylic and allylic alcohols in presence of oxygen give the correspondent carbonyl derivates. Mohamed et al. [154] reported the photocatalytic oxidation of 1-phenylethanol in dry acetonitrile using TiO_2 and a slow stream of oxygen.

Another application of phtocatalysis in synthetic processes is the mild oxidation of sulfides to sulfoxides. Using 2,4,6-triphenylthiapyrylium salt (TPTP) encapsulated within a HY zeolite through a ship-in-the-bottle synthesis as photocatalyst [155], alkylaryl and diaryl sulfides were cleanly oxidized. Several studies reported the selective oxidation of hydrocarbons in aqueous and organic phase [156]. Palmisano et al. [157] investigated substitent group influence the photocatalytic benzene oxidation, observing that organic molecules containing an electron withdrawing group (cyanobenzene, nitrobenzene, benzoic acid, etc.) were unselectively converted in a mixture of mono-hydroxy derivates, while in the presence of an electron donor group (phenol, phenylamine, N-phenylacetamide) the attack of OH radicals was selective in the ortho and para positions. Park and Choi [158] studying the photocatalytic conversion of benzene to phenol, showed the possibility to enhance the phenol production yield and selectivity adding Fe^{3+}

or/and H_2O_2 to the TiO_2 suspension or modifying the catalyst surface by loading Pt nanoparticles (Pt/TiO_2).

Selective benzene oxidation was also carried out using transition metal-exchanged BEA zeolites dispersed in benzene-acetonitrile-water mixtures [159]. The one-step conversion of benzene to phenol was studied by Molinari et al. [37] in a photocatalytic membrane reactor (PMR) in which both the reaction and product separation occurred simultaneously by means of a membrane contactor. The system was operated using benzene both as reactant and extraction solvent, employing a polypropylene membrane to separate the organic phase from the aqueous one. The PMR allowed the production and separation of phenol, although formation of intermediate oxidation by-products was observed. The operative pH of 3.1 allowed control of the selectivity towards the by-products.

The photocatalytic conversion of methane into methanol at room temperature in the aqueous solution using oxides semiconductors was investigated by many research groups [160]. An increase in the methanol production was observed when hydrogen peroxide was added to the reactive solution. Moreover, selective photo oxidation reactions were also reported to convert alcohols to carbonyls [161]. Palmisano G. et al [162] studied the selective oxidation of 4-methoxybenzyl

alcohol to p-anisaldehyde in organic-free aqueous TiO_2 suspensions, obtaining a considerable yield of 41.5% mol.

Colmenares et al. [163] reported the use of different metal doped TiO_2 systems for the gas phase selective photo-oxidation of 2-propanol to acetone. Doping the catalyst with Pd, Pt or Ag caused an increase in molar conversion as compared to bare TiO_2, whereas the presence of Fe and Zr had a detrimental effect.

Photocatalytic reductions are less frequent than oxidations, probably because the reducing power of conduction band electron is considerably lower than the oxidizing ability of valence band. However, many works are reported in literature, such as the conversion of aromatic and aliphatic nitro compounds to the corresponding amines [164], carbonate to methane and methanol [165].

1.4.3 Photocatalytic depollution

A further main use of the photocatalytic techniques is the recovery of industrial water and air purification of the pollutants. This application appears advantageous since it does not require chemicals addition and permits to operate at mild operational conditions. Often it is coupled with biological treatments for enhancing the depollution efficiency [166, 167].

Photodegradation can be carried out under homogeneous and heterogeneous conditions, even if solid semiconductors are more widely used because they are cheaper, more robust and easily recovered than soluble photocatalysts. The mechanism for the photooxidative degradation of many organic pollutants over titanium dioxide has been extensively studied [168] and it is due to the uniformly high (mostly 106 to 109 mol^{-1} s^{-1}) rate of reaction of OH^- radicals with organic materials that involves in many cases the complete pollutant mineralization. Photodegradation processes permit to convert carbon to CO_2, hydrogen to H_2O, nitrogen to nitrate, sulphur to sulphates and phosphorus to phosphate. Many studies have been carried out with the aim to remove, by photocatalytic reactions, the most common pollutants: dyes [169], pesticides and herbicides [170]; pharmaceutical compounds [171]; hormones [172]. Modifications of photocatalyst surface such as platinization and fluorination increase the cyanuric acid degradation [173]. Also electron acceptors like hydrogen peroxide, bromate and persulfate increase hydroxyl radicals formation and inhibit at the same time the electron-hole recombination [174]. The air treatment was also reported as a promising field of application of these processes. Several VOCs such as MTBE [175], toluene [176], bromomethane [177], benzene [178], etc., were successfully degraded by photocatalytic processes.

In the last years, the purification property of the TiO_2 was exploited in building materials not only at laboratory levels but also in concrete structures for maintaining their aesthetic characteristics, such as the church "Dives in Misericordia" in Rome (Italy), 'l'Ecole de Musique' in Chambe´ (France), the Marunouchi Building in Tokyo (Japan).

Photoreduction of several heavy metal such as Cr(VI) [179], Hg [180], Pd(II) [181], Ni [182], Cu [182], Pb [183] and others has been studied not only in pollution application but also in recovery and reuse of valuable metal products with environmental and economic concerns, respectively. Interesting recent researches investigated the possibility to use the photogeneration of active oxygenated radicals to attack the cell membrane of microorganisms and to cause their inactivation. The antimicrobial activity of UV-irradiated photocatalyst has been tested against several types of bacteria, yeasts, algae and viruses [184].

1.5 Membranes in Photocatalysis

A membrane can be defined as a selective separation barrier. The membrane module can act as a molecular filter allowing separation both of solid particles and specific ions/molecules. The simplest classification of membrane is based on its nature

and provides the main division into biological and synthetic membranes (organic and inorganic). Membranes can be solid or liquid, symmetric and asymmetric, homogeneous and heterogeneous. Another distinction is based on morphology and structure of membranes. This type of classification is very important because the structure of the membrane can determine the separation mechanism and thus its application. Porous membranes allow permeation through their pores, then the mechanisms (Knudsen diffusion or microporous separation) are different depending on the pore size. In dense membrane the permeate forms a solution with the membrane, then diffuses through the thickness allowing the separation. The differences between different types of morphologies can be both in the macroscopic structure (films, tubes, hollow fibres) and in the microscopic one (symmetrical, asymmetrical, porous, dense or mixed structure). In symmetric membranes structural and transport properties are the same throughout its section, and the thickness of the entire membrane determines the flow. In asymmetric membranes the structural and transport properties change along the membrane thickness. They are mainly used in separation processes that use hydrostatic pressure as driving force. An asymmetric membrane consists of two parts: a dense thin layer supported by a porous layer which acts as mechanical support of the fragile skin layer, and has a small effect on separation and transport through the membrane. This type of

structure combines the high selectivity of a dense membrane with the high permeation rate of a thin layer membrane. Depending on membrane pore size, different pressure driven processes can occur: reverse osmosis (RO), nanofiltration (NF), ultrafiltration (UF) and microfiltration (MF). Others characteristics that must be considered are the ability to transport electrical charges (ion exchange or bipolar mixed conduction) and the possibility of including in the porous structure or deposited on the surface a catalyst that has some affinity with the membrane. Another classification is based on surface properties of a membrane (hydrophobic/hydrophilic character).

Most of the photocatalytic membrane reactors (PMRs) involves the use of catalyst in suspension, combined with pressure driven processes as MF, UF and NF. NF has the advantage to retain molecules with lower molecular weight than MF and UF membranes although these appear to be energetically more convenient. Other kind of membrane operation used in processes coupled with photocatalysis is membrane distillation (MD). The choice of the material used for producing membranes depends mainly on their different applications. For porous membranes (used for MF and UF processes) the material used is strongly determined by the requirements of the process, the tendency to give rise to fouling and the chemical and thermal stability of the materials. The performance depends directly by the material

characteristics, e.g. dense non porous membranes are generally used for pervaporation or gas separation applications. In photocatalysis generally polymeric membranes are used. Damodar et al. [185] reported the preparation and testing of composite PVDF/TiO_2 membranes with self cleaning/antifouling, bactericidal and photoactive properties based on UV/ TiO_2 photocatalytic mechanism. Another study [186] reported the photocatalytic mineralization of Reactive Black 5 dye in a photocatalytic membrane reactor, using a flat plate novel PTFE membrane module that was placed at the axis of the tank and surrounded by two UV lamps. The obtained data demonstrated that the membrane maintains a high performance even after cleaning, regaining its original behaviour. Moreover, the authors reported that no fouling occurred under the chosen operating conditions. Another hydrophobic polymer is polypropylene (PP). PP membranes may be synthesized by stretching and phase-inversion. PP hollow fibre membranes were used by Erdim et al. [187] to study the effect of natural organic matter (NOM) fouling. Synthetic and natural raw waters were used in their photocatalytic experiments. The obtained data showed that the increase in NOM concentration increased the pressure, and raw water experiments showed higher pressure increase and lower removal efficiencies compared with that of synthetic water. Because of their hydrophobic nature, PP membranes can be used in membrane distillation (MD), in fact

they are not wetted by water or other liquids with a high surface tension [188]. Grzechulska-Damszel et al. [189] studied various configurations of photocatalytic membrane reactor for the removal of different azo-dyes. PP membrane was used in a MD process using the permeate of the initial suspension as the feed. Non-volatile compounds were retained in the feed side whereas the volatile ones were transferred through the pores of the MD membrane, and then condensed or dissolved in cold distillate. The authors reported a better removal of organic species from the treated solution by using MD process with respect to a nanofiltration process. The use of PP membranes was also reported by Molinari et al. [37] in a work regarding the study of the partial photooxidation of benzene to phenol. In the proposed system the separation of phenol was obtained by using benzene both as reactant and extraction solvent. The organic phase was separated from the aqueous environment by means of a PP membrane. Benzene filled the PP membrane pores due to the capillary force, but its passage into the aqueous reactive suspension was reduced by operating with a suitable pressure. In order to verify the efficiency of the phenol extraction with PP membrane, preliminary transport tests were carried out. The results demonstrated that PP membrane can be used for the separation of phenol from the aqueous phase. Moreover it assured a constant restock of benzene in the reactive suspension.

Polymeric membranes consisting of hydrophilic materials were also tested in recent years for photocatalytic applications. The best known class of these polymers is cellulose (CA) based. The performance of CA membrane was examined by Lee et al. [190] in photodegradation of humic acids in drinking water treatment by coupling photocatalytic reaction and cross-flow UF process using a plate-and-frame CA module. CA membrane showed a good resistance during the photocatalytic runs and ensured the separation of TiO_2 catalysts from the reaction environment. The experiments showed a partial photocatalytic mineralization of organic species and their transformation in less absorbable molecules enhanced the UF flux. Mounir et al. [191] studied the photodegradation of Basic Red-46 under visible, UV and solar light, using two different catalysts based on cellulose fibres and TiO_2 particles. In the first case the TiO_2 catalyst was deposited on cellulose fibres (catalyst I), while in the second case it (catalyst II) consisted of three layers: the central one of carbon fibres, one of the outer layers of cellulose fibres containing the deposited TiO_2 and the other made of non-modified cellulose fibres. The catalyst (II) was more efficient than catalyst (I) in the photocatalytic process of dye degradation. By using sunlight, the discoloration yield was 100% for the most complex catalyst, and 70% for the catalyst (I), with a simpler structure. Choo et al. [192] proposed the use of a membrane module consisting of three hollow fibres for the photocatalytic removal of

trichloroethylene in water. A better membrane system performance was obtained by using three fibres instead of a single one. The clogging of a single fibre did not affect the process. The use of the photocatalytic reactor coupled with this membrane system allowed the complete separation of suspended catalyst from the reaction environment, also in the case of particle size of the catalyst smaller than the pore size of the membrane. Indeed, the larger TiO_2 particles, formed a layer on the membrane surface hindering the passage of the smaller ones. A reduction in efficiency of the membrane occurred when humic acid was used as background species in the feedwater.

In the mid-1960s DuPont introduced a novel polymer: Nafion® [193]. Nafion® is a copolymer of tetrafluoroethylene and perfluoro(4-methyl-3,6-dioxa-7-octene-1-sulfonyl-fluoride).

Nafion® polymer is a thermoplastic resin that can be produced into different shapes such as beads, film, and tubing.

The perfluorinated composition of the copolymer imparts chemical and thermal stability rarely available with non-fluorinated polymers. When the pendant sulfonyl fluoride groups (SO_2F) are chemically converted to sulfonic acid (SO_3H) a ionic functionality is introduced. For example, by simple immersion in an acidic solution, the film can be saturated with H^+ ions (Fig. 4).

The unique functional properties of Nafion® polymer have enabled a broad range of applications. Many efforts have been

made to incorporate semiconductor nanoparticles in a Nafion film [194-197]. Deposition of Pt metal on one side of the film is one startegy used to reduce H^+ into H_2 [194]. However, most of the recent studies that report photocatalytic water splitting reaction employ a photoelectrochemical cell consisting of a three-electrode system (semiconductor photoanode, Pt counterelectrode, and reference electrode) and often require an applied anodic bias to generate hydrogen and oxygen [198, 199].

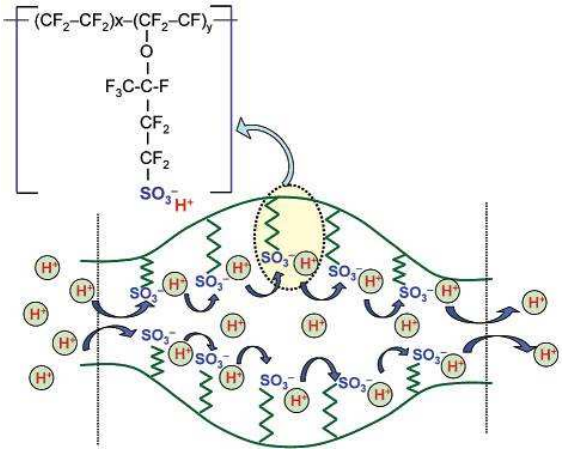

Figure 4. Nafion with sulfonic acid groups that contribute to the H^+ ion activity in a proton exchange membrane (PEM).

In a typical proton exchange membrane (PEM)-based fuel cell, hydrogen or methanol is oxidized and oxygen is reduced at the electrocatalyst surface. Metal like Pt-Ru or Pt alloy

nanoparticles dispersed on support provide a large electrochemically active surface area to induce redox processes. The two electrodes are separated by a thin proton exchange nafion membrane that assists in transporting H^+ ions selectively from the anode to the cathode compartment [200]. Photoactive anode provides the water oxidation reaction while hydrogen is generated at the cathode. Ceramic membranes are attractive for PMR applications as they generally present higher chemical and thermal stability with respect to polymeric ones, but have the drawback of higher costs [201]. Ceramics are prepared by the combination of a metal with a non metal to form an oxide, nitride or carbide. Ceramic membranes prepared from materials as aluminium oxide and zirconium oxide or zirconia constitute the main class of inorganic membranes. Alem et al. [202] prepared a titania multilayer membrane, which consisted of an Al_2O_3 support, a colloidal sol gel derived intermediate layer and finally a sol gel top layer. Methyl orange degradation was chosen to test the photoactivity of the obtained titania membrane. The results showed a high stability and catalytical activity per unit mass of TiO_2, ensuring both the photodegradation reactions and the physical separation of pollutant.

The same authors reported the study of different techniques to prepare a crack-free mesoporous titania membrane on alumina support. The titania colloidal sol was prepared with the sol-gel

technique and its photocatalytic performance was evaluated with the photodegradation of methyl orange in aqueous solution. The membrane performance was strongly dependent from various factors, mainly the calcination time and temperature. An increase of calcination time and temperature caused a decrease in the specific surface area and in the photoactivity of the catalyst. Other factors, like crystallite size, allotropic phase of titania and membrane thickness, play an important role in the photocatalytic activity of the membrane.

1.6 Photocatalytic reactors

The development of photocatalytic applications requires an efficient design of photocatalytic reactors for industrial-scale use and commercial applications. Several aspects such as the type of irradiation source (natural or artificial), the light source position (immersed or external), the catalyst (slurry or immobilized on a support) play an important role in the photocatalytic efficiency of the process. The most usual geometries applied for heterogeneous photocatalysis include: immersion well photoreactor [203], multilamp photoreactor [204], annular photoreactors [205] and fuidized bed photoreactor [206]. In a photochemical reactor the catalyst can be either suspended in aqueous medium or immobilized on

support materials, e.g. cellulose fibers, glass, ceramic membrane [207]. In a slurry reactor, the catalyst particles are suspended in the fluid phase. Some advantages of this system include the fairly uniform catalyst distribution, minimum catalyst fouling effects and practically no mass transfer limitations. However, in this type of configuration light scattering can occur, lowering the efficiency of the treatment process. In addition, a post-process of catalyst separation is needed to isolate the catalyst particles from the reaction solution. Immobilized photocatalytic reactors allow the continuous use of the photocatalyst, eliminating the problem of the catalyst post-separation. Drawbacks of the use of this kind of reactors are the possibility of mass transfer limitations, catalyst fouling or wash-out, low surface to volume ratio and significant pressure drop. Slurry photocatalytic systems usually show largest photocatalytic activity when compared to immobilized photocatalytic reactors [208]. Increasing attention has being taken to recently developed photocatalytic membrane reactors that could allow the selective separation of the product(s) and/or intermediates from the reactive environment. The use of hybrid systems in which photocatalysis is coupled with a membrane module [37] could have a significant impact in the near future to design processes for synthetic reactions and pollutant abatement.

2

Influence of excitation wavelength on the photocatalytic activity of Au/TiO_2 for the generation of hydrogen or oxygen from water*.

**: C. G. Silva, R. Juàrez, T. Marino, R. Molinari and H. Garcìa, The Journal of the American Chemical Society, 133 (2011) 595.*

2.1 Introduction

As already reported in the introduction, one potentially important application of photocatalysis is the conversion of light into chemical energy. In this regard, photocatalytic water splitting is still a challenging process due to the low efficiency of the system. In this chapter, the catalytic behaviour of a series of gold supported on TiO_2 P25 samples with gold loadings ranging from 0-2.2 wt% was studied in order to investigate which are the characteristics of the gold deposited on the titania

surface that can control and influence the water splitting reaction.

As a result of this study, first of all, a deposition-precipitation synthesis procedure with well controlled steps has been developed allowing the preparation of active catalysts. Successively, the samples were characterised by means of XRD, S_{BET}, TEM and UV-Vis techniques and tested in the photocatalytic generation of hydrogen or oxygen from water.

The influence of different parameters involved in the synthesis procedure, such as pH and calcinations temperature, have also been taken into consideration and are going to be addressed in the following paragraphs. The obtained data showed that Au/TiO_2 exhibits for photocatalytic water splitting two distinctive operating mechanisms depending on the excitation (UV or visible light) wavelength. Importantly, the catalytic performances of the solids seems to depend on the gold content, the particle size and the operation of visible light water splitting arises from the excitation of the gold surface plasmon. While there are some reports in the literature describing the use of Au/TiO_2 as photocatalyst, even using visible light illumination [209] none of them have dealt with visible light photocatalytic water splitting. In a related precedent, Haruta studied the photocatalytic activity for water splitting upon UV excitation of some gold catalysts compared with platinum.[210] It was observed that the activity of gold samples was about 30% lower

than that of platinum. In addition, they observed that the activity of titania supported gold was very sensitive to the preparation procedure [198]. But the experimental results were explained just considering Au nanoparticles as catalytic centers for gas generation without being responsible for light absorption. Recently, Wark and co-workers have reported the use of Au/TiO_2 to enhance the photocatalytic activity of TiO_2 for methanol oxidation to formaldehyde irradiating at wavelengths longer than 320 nm [211]. In other cases, it has been observed that the presence of Au nanoparticles is even detrimental for the inherent photocatalytic activity of TiO_2. For instance, Mul and coworkers have checked Au/TiO_2 to promote the aerobic oxyfunctionalization of cyclohexane to mixtures of cyclohexanol/cyclohexanone and found that Au nanoparticles decrease the photocatalytic activity due to the reduction of the surface OH population required in the photocatalytic process [212]. Thus, the present situation does not allow concluding the positive or negative effect of gold nanoparticles on the photocatalytic activity of titania [212]. As we have indicated, these prior studies were performed using light in the UV range, and therefore exciting directly the TiO_2 semiconductor absorption band. The possibility of using the surface plasmon band of gold nanoparticles (from 500 to 600 nm) to excite photochemically the Au/TiO_2 system has been up to now mostly neglected. Only a few scattered precedents have reported visible

light photoactivity of Au/TiO_2 such as in the degradation of chemical warfare agents [213]. In this chapter it is presented also the visible light photocatalytic activity of Au/TiO_2. The main difference with the previous work is that gold nanoparticles exhibit a dual role as light harvesters injecting electrons into the semiconductor conduction band and also as catalytic sites for gas generation. Besides the photocatalytic activity for hydrogen generation using sacrificial electron donors, it was also determined the activity of Au/TiO_2 for the visible light oxygen formation adding sacrificial electron acceptors. Considering the interest in gold catalysis, our finding can open new avenues aimed at applying this type of catalyst into photocatalysis.

2.2 Experimental

2.2.1 Photocatalyst preparation

$Au(1.5\ wt\ \%)/TiO_2$ consists of 1.5 wt% gold on P25 TiO_2 and was supplied by Gold World Council (reference catalyst Type A). Materials containing different gold percentages were prepared by deposition-precipitation. The adeguate amount of $HAuCl_4 \cdot 3H_2O$ (Alfa Aesar) to obtain 0.25 and 2.2 wt% in the final catalysts was dissolved in 100 mL of ultrapure water

(obtained from Milli-Q equipment by Millipore) and the pH of the solution adjusted to 9.0 by addition of NaOH (Aldrich) 0.2 M (using a WTW Inolab Terminal Level 3 pH meter with a glass pH electrode SenTix). The solution was heated to 70 °C and then the support (TiO_2 Degussa P25) was added and kept under continuos stirring during 2 hours maintaining constant the pH at value of 9.0. The catalyst is then recovered, filtered, washed with deionized water, and dried at 100 °C overnight. Finally, the powder was calcined at 400 °C in air for 4 hours [214]. Particles of different sizes were obtained by changing the pH used in the deposition of gold nanoparticles over the TiO_2 support and the calcination temperature. Thus, a solution of $HAuCl_4 \cdot 3H_2O$ in 100 mL of Milli-Q water was brought to pH 4.5, 6.0, or 9.0 by addition of a 0.2 M solution of NaOH. Once the pH value was stable P25 TiO_2 was added. The amount of $HAuCl_4 \cdot 3H_2O$ added was calculed according the designed loading amount of gold in the Au/TiO_2 samples. The slurry was vigorously stirred overnight. The Au/TiO_2 catalyst was then filtered and exhaustively washed with Milli-Q water. The catalyst was dried at 100 °C during 8 hours and calcined at 200 or 400 °C. The temperature program starts at room temperature increasing at a rate of 5 °C min^{-1} up to the final temperature that was maintained for 4 hours.

2.2.2 Characterization techniques

Room temperature diffuse reflectance UV-vis-NIR spectra of solid samples were recorded by the diffuse reflectance mode using an integrating sphere with a Varian Cary 5000 UV-vis-NIR scanning spectrophotometer. The gold content of the catalysts was determined using an inductively coupled plasma optical emission spectrometer (ICP-OES, Varian). Transmission electron microscopy (TEM) images were obtained using a Jeol 200 Cx microscope operating at 200 kV. The samples were dispersed in dichloromethane by sonication and dropped on a copper grid coated with a carbon film. The X-ray diffraction (XRD) patterns were taken in a PANalytical X'Pert PRO diffractometer using Cu K_α radiation (λ = 1.5418 Å) at 45 keV and 40 mA.

2.2.3 Photocatalytic tests

The photocatalytic experiments were carried out in a 30 mL Pyrex reactor. The headspace of the reactor was connected to an inverted buret filled with water at atmospheric pressure, allowing the measurement of the evolved gas. In the photocatalytic reactions for hydrogen generation, Au/TiO_2 powders were dispersed in water/methanol solutions

(H_2O:methanol of 3:1 v/v %) or water containing 0.01 M of ethylenediamine tetraacetic acid (EDTA). In the case of the photocatalytic oxygen generation reactions, the same amount of catalyst was dispersed in a 0.01 M $AgNO_3$ aqueous solution in the reaction cell. In both cases, the total volume of the suspensions was of 22.5 mL. The suspensions were purged with an argon flow for at least 30 minutes before irradiation in order to remove dissolved air. Then the suspensions were irradiated for 3 hours using either a 200 W xenon-doped mercury lamp (Hamamatsu Lightningcure LC8, 1 cm distance) or the second harmonic of a Nd:YAG laser (532 nm, 7 ns pulse width, 50 mJ × $pulse^{-1}$). For polychromatic visible light irradiation the output of the 220 W xenon-doped mercury lamp was filtered through a cutoff filter ($\lambda > 400$ nm). The stationary temperature of the reactor, reached at 5 minutes of irradiation, was 38 °C. The formation of hydrogen and oxygen was confirmed by injecting 0.5 mL of the reactor headspace gas in a gas chromatograph (HP 5890) operating at isothermal conditions (50 °C) using a semicapillary column (molecular sieve, 530 μm diameter, 15 m length) equipped with a thermal conductivity detector and argon as carrier gas.

2.2.4 Electrochemical measurements

Electrochemical measurements were carried out using the conventional three electrode setup connected to an Amel potentiostat (model 7050) that was controlled by software allowing data storage and management. As working electrode a thin film of Au/TiO_2 was deposited using the doctor blade technique on a fluorine-doped tin oxide (FTO) conductive support. A paste of methylcellulose (1.19 g) and terpineol (20 mL) in acetone (40 mL) containing about 30% Au/TiO_2 in weight was prepared by mechanical mixing and then spread on the FTO electrode. Before measurements the paste was dried at room temperature and then calcined at 400 °C heating from room temperature at 5 °C min^{-1} and maintaining the maximum temperature for 1 hour. As counter and reference electrodes a platinum wire and a 0.1 M Ag/AgCl standard solution were used, respectively. The FTO electrode containing the Au/TiO_2 film and the counter electrode were immersed into 0.1 M tetrabutylammonium perchlorate electrolyte in acetonitrile. Measurements were carried out at a scan rate of 50 mV s^{-1} in the range -2.0/+2 V.

2.2.5 Apparent quantum yield measurements

Photon flux was determined using a 150 W mercury lamp at 560 nm using a monochromator (half-width 12 nm) by potassium ferrioxalate actinometry being of 4.38 Einstein s^{-1}. The actinometer solution was irradiated for 2 minutes using monochromatic light. The number of photons entering the reaction system is determined by measuring Fe^{2+} formation via the visible absorption spectroscopy of Fe^{2+}-phenanthroline complex at 510 nm, knowing that, at the working conditions, this photocomplexation reaction has a quantum yield of 1.21 [215]. Then, photocatalytic hydrogen or oxygen generation reactions were performed using monochromatic light. After 3 hours of irradiation the amount of gas evolved was determined by gas chromatography. The quantum yield of the photocatalytic reactions was determined by the ratio between the number of reacted electrons/holes that are related to the number of hydrogen/oxygen molecules formed, and the number of incident photons.

2.3 Results and discussion

The overall water splitting consists of the combination of the reduction to hydrogen and oxidation to oxygen semireactions. In order to gain understanding on the rate-determining process that eventually can lead to more efficient photocatalysts it is very convenient to study both semireactions separately. This can be carried out by adding sacrificial electron donors when studying the reduction process and sacrificial electron acceptors when performing the oxidation semireaction. In the present study we started addressing the photocatalytic hydrogen formation with either UV or visible light in the presence of a series of gold nanoparticles supported on P25 titania (Au/TiO_2) photocatalysts using methanol or EDTA as sacrificial reducing agents. We have selected a commercial P25 powder as titania support because the junction between its two constituent phases (anatase and rutile) already provides a very good path for electron-hole separation and so minimises the influence of this mechanism on the catalytic activity, allowing to discern the improve of the activity due to gold introduction.

2.3.1 Characterization

The presence of Au nanoparticles on Au/TiO_2 can be ascertained by the TEM images of the samples. TEM also allows to estimate that titania crystallites have about 20 nm particle size that is a common dimension for many titania photocatalysts. As an example Fig.e 5 shows a comparison between the unmodified TiO_2 P25 and $Au(2.2\ wt\%)/TiO_2$.

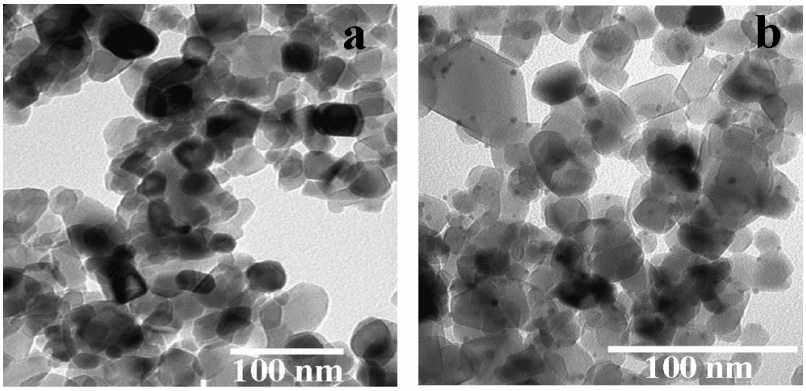

Figure 5. Typical TEM micrographs of the catalysts studied; a: TiO_2 P25 and b: $Au(2.2\ wt\%)/TiO_2$.

The loaded catalysts $Au(2.2\ wt\%)/TiO_2$ (Fig. 5b) presents a regular distribution of spherical gold nanoparticles on the whole support, with a diameter ranging from 5.5 to 10 nm. The UV-Vis spectra of the studied samples are shown in Fig. 6.

As expected, due to the presence of gold nanoparticles, the Au/TiO_2 samples exhibits in optical spectroscopy two bands: one in the visible region between 500 and 650 nm and another, stronger, with onset at 320 nm that is due to the bandgap transition of TiO_2 semiconductor. The band in the visible region is reflected by the characteristic pink color that arises from the surface plasmon resonance of the Au metal particles and it is mainly affected by the gold particle size and shape. The intensity increases along the percentage of Au in the samples.

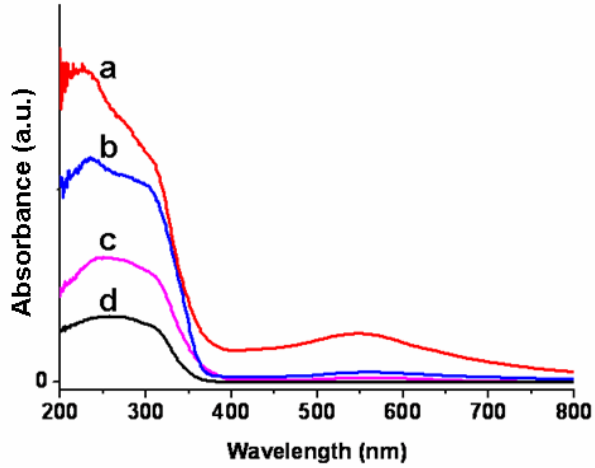

Figure 6. Diffuse UV-Vis reflectance spectra of samples containing different gold loading. a: Au(2.2 wt%)/TiO_2, b: Au(1.5 wt%)/TiO_2, c: Au(0.25 wt%)/TiO_2, d: TiO_2 P25.

Absorption in the visible region can be useful to increase the photocatalytic efficiency of a material compared to the plain TiO_2. The presence of gold on Au/TiO_2 as well as the crystallographic TiO_2 phase can be determined by powder XRD. Fig. 7 presents the diffractograms of selected Au/TiO_2 samples.

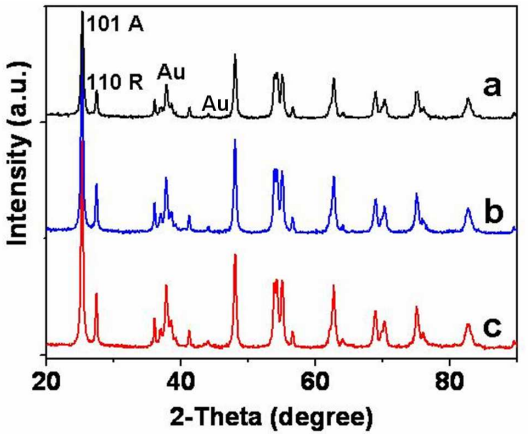

Figure 7. XRD patterns obtained for a: Au(0.25 wt%)/TiO_2, b: Au(1.5 wt%)/TiO_2, c: Au(2.2 wt%)/TiO_2. A: anatase, R: rutile.

Even though the gold content is low, the higher gold atomic weight relative to titanium makes XRD to be more sensitive for this heavier element. Two peaks at 2θ value of around 38.2° and 44.1° were observed revealing the presence of metallic gold (Au) particles into TiO_2. In all the samples along with anatase phase, peaks corresponding to rutile phase were also observed.

2.3.2 Photocatalytic tests

2.3.2.1 UV light photocatalytic hydrogen generation

Preliminary tests by irradiating suspensions of Au/TiO_2 in water/EDTA and water/methanol solution for several days and analysis of the gold leaching in the solution demonstrated the stability of the Au/TiO_2 upon exposure to the light and the possibility to use it as photocatalyst. In the first stage of our work we checked the ability of Au(1.5 wt %)/TiO_2 to generate hydrogen upon irradiation with a Xe-doped Hg lamp of water containing EDTA as sacrificial electron and the obtained data was compared to that obtained using TiO_2 P25 (Figure 8).

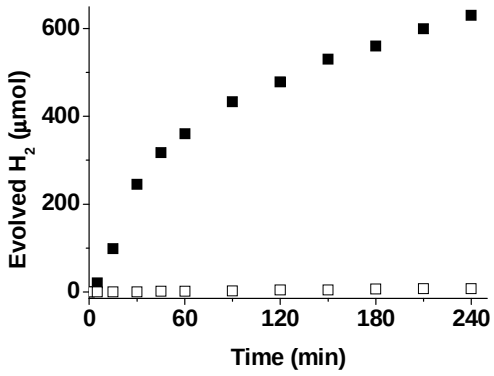

Figure 8. Temporal hydrogen evolution under UV irradiation using □: TiO_2 and ■: Au(1.5 wt%)/TiO_2.
Operational conditions: catalyst 2 g L^{-1}; 0.01 M EDTA; pH 2.65.

The obtained data showed that gold nanoparticles, by increasing the efficiency of charge separation and decreasing the charge carrier recombination speed, highly enhance the photocatalytic activity of titania. In this case, following the previous studies the most reasonable rationalization is indicated in Scheme 2 and assumes direct photoexcitation of TiO_2 with photons with energy larger than the bandgap (λ < 380 nm) leading to the generation of electrons in the semiconductor conduction band and electron holes in the valence band. The electron in the conduction band will move to the gold nanoparticles acting as electron buffer and catalytic sites for hydrogen generation. The electron holes will be quenched by EDTA.

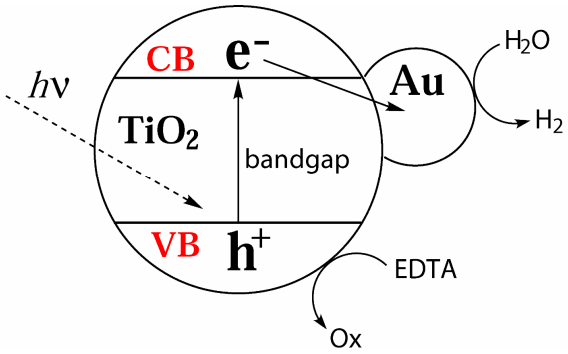

Scheme 2. Proposed rationalization of the photocatalytic activity of Au/TiO_2 under UV light excitation

To understand as the initial amount of photocatalyst influences its activity, photocatalytic tests using four different initial Au(1.5 wt%)/TiO_2 concentration were carried out (Fig. 9).

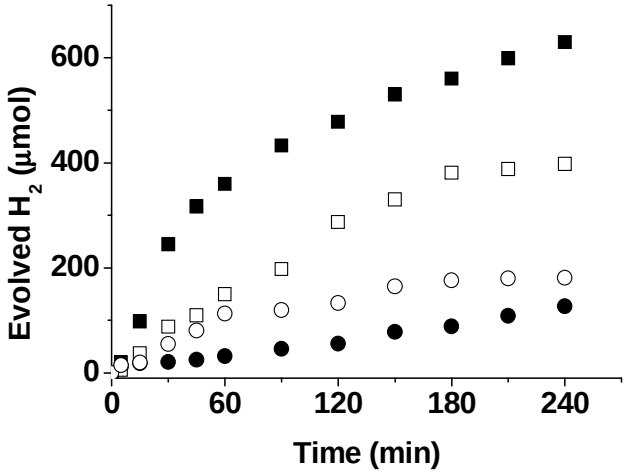

Figure 9. Temporal hydrogen evolution under UV irradiation using different concentration of Au(1.5 wt%)/TiO_2 ■: 2 g L^{-1}; □: 1 g L^{-1}; ○: 3 g L^{-1}; ●: 0.5 g L^{-1}.

The obtained results showed that hydrogen evolution increases with the increasing of catalyst concentration up to a concentration of 2 g L^{-1}. When the catalyst concentration is higher, hydrogen generation strongly decreases. This is probably due to an excessive opacity and turbidity of the suspension that impedes further penetration of light in the reactor. Thus, a concentration of 2 g L^{-1} was chosen for the others photocatalytic runs. Another important parameter which influences the

photocatalytic process leading to the preferential formation of different reaction products because of the acid-base character of TiO_2 is the pH. This effect was studied by adding to the aqueous suspension of Au/TiO_2 at initial pH 2.65, a diluted solution of NaOH (0.2 M). The results are presented in Fig. 10.

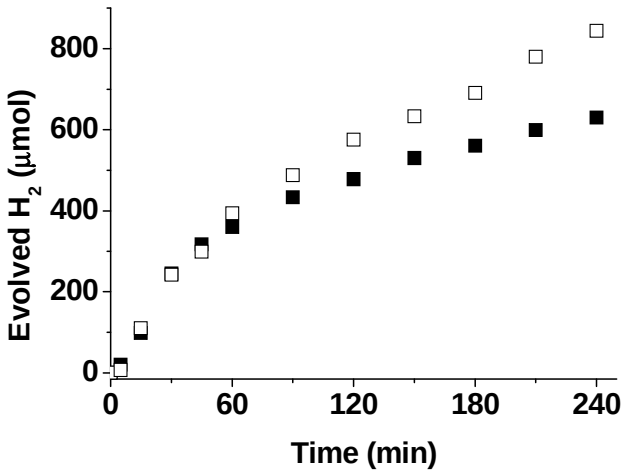

Figure 10. Influence of pH on the volume of hydrogen evolved during the photocatalytic runs using Au(1.5 wt %)/TiO_2 catalyst and EDTA as sacrificial electron donor at two different initial pH values. □: pH 7.00; ■: pH 2.65.

The influence of the pH in the photocatalytic activity is compatible with Scheme 2 since at higher pH EDTA will be unprotonated and more prone to give electrons to the titania valence band holes. Although the obtained results showed a similar initial hydrogen evolution, a significant increase of its

generation at neutral pH was observed after the first hour. This evidence can be explained by considering a lower EDTA adsorption on the catalyst surface with a consequent decrease of its photooxidation. Both titania and EDTA are positively charged at strongly acidic pH leading to a repulsion between the catalyst particles and the sacrificial agent molecules.

2.3.2.2 Visible light photocatalytic hydrogen generation

Gold nanoparticles supported in titania exhibit a surface plasmon band with λ_{max} at about 550 nm. In order to firmly prove the visible light photocatalytic activity of Au(1.5 wt%)/TiO_2 for hydrogen generation upon irradiation of aqueous solutions containing EDTA, a polychromatic lamp light of wavelength greater than 400 nm was used. Figure 11 shows a comparison of the hydrogen evolved using gold loading catalyst and plain TiO_2. As it can be seen there, the control shows that as expected TiO_2 is devoid of any photocatalytic activity under these conditions.

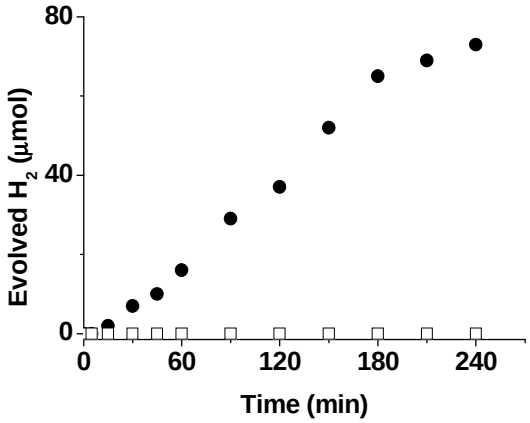

Figure 11. Hydrogen evolved during the photocatalytic runs using TiO_2 and Au(1.5 wt %)/TiO_2 as catalysts and EDTA as sacrificial electron donor, under polychromatic light ($\lambda > 400$ nm). ●: Au/TiO_2, □: TiO_2.

It is well known that gold nanoparticles are very effective electron acceptor centre due to the formation of a Schottky junction between the metal and the semiconductor. Acting as sinks for photogenerated electrons, noble metal particles can contribute to the separation of electron-hole pairs reducing the recombination rate and therefore enhancing the photocatalytic efficiency. Furthermore, when gold particles on titania are very small these could behave not longer as metallic but as semiconducting due to a quantum size effect. The most reasonable mechanism for the photocatalytic hydrogen generation based on semiconductor-semiconductor contact is

depicted in Scheme 3. As it can be seen there, upon photoexcitation of Au nanoparticles, electrons from Au are injected into the TiO_2 conduction band leading to the generation of holes in the Au nanoparticles and electrons in the TiO_2 conduction band. The latter are known to affect hydrogen generation, and the holes will be quenched by EDTA as sacrificial electron donor.

Evidence in support of the proposed mechanism is the fact that the photocatalytic response for hydrogen generation agrees with the absorption of the gold surface plasmon band (see Figure 6). Moreover, controls where colloidal solutions of gold nanoparticles, stabilized with citrate were submitted to irradiation under the same conditions did not lead to observation of hydrogen evolution. Obviously the mechanism of photochemical process indicated in Scheme 3 is an oversimplification since it has been determined that, due to the gold/titania interfacial contact, the conduction band of the semiconductor undergoes shift toward more negative potentials, the energy level being bent at the interface of titania by the influence of gold. Thus, the charge distribution between the gold nanoparticles and the semiconductor causes a shift of the Fermi level toward more negative potentials.

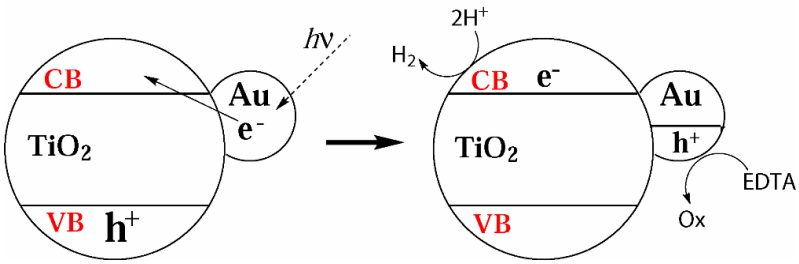

Scheme 3. Proposed rationalization of the photocatalytic activity of Au/TiO_2 under visible light excitation.

The photogeneration of hydrogen using different gold containing samples and methanol as sacrificial agent was also performed using visible light (cutoff filter, $\lambda > 400$ nm) from a Hg-Xe lamp, whereby the formation of hydrogen was also confirmed (see Fig. 12).

As it can be seen in Fig. 12, $Au(0.25\ wt\%)/TiO_2$ has the highest performance in the hydrogen generation. The influence of the gold loading on the catalyst efficiency is discussed more detailed in the next paragraph. Reusability of the Au/TiO_2 catalyst after its use for 4 hours was checked by filtering the catalyst and using it for a second run under the same conditions. Essentially the same kinetic profile shown in Figure 12 was obtained. Moreover, after two consecutive uses the filtered catalyst was characterized by chemical analysis and electron microscopy without observing changes with respect to those of the fresh catalyst.

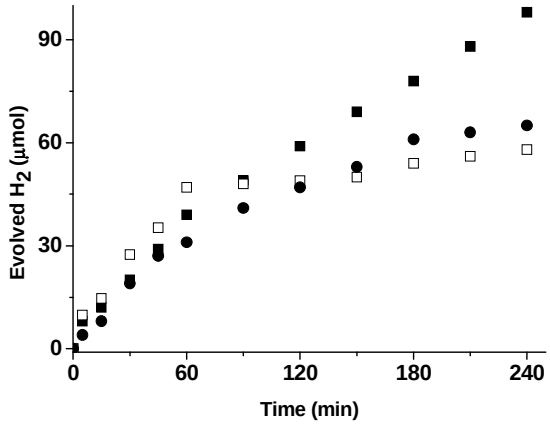

Figure 12. Hydrogen evolved during the photocatalytic runs using gold loading samples and methanol as sacrificial electron donor, under polychromatic light λ > 400 nm. ■: Au (0.25 wt%)/TiO_2, □: Au (1.5 wt%)/TiO_2 and ●: Au(2.2%)/TiO_2.

Chemical analyses of the solutions after the reaction detected the presence of Au in a concentration that corresponds to 0.22% of the total Au content present in the fresh Au/TiO_2 (0.11 mg of Au in 45 mg of Au/TiO_2). We also checked the influence of by-product in the photocatalytic activity of Au/TiO_2. Using methanol as sacrificial electron donor, oxidized derivates, particularly formaldehyde and formic acid, are generated as by-products, and it is of interest to determine how these two by-products affect the photocatalytic activity of Au/TiO_2. Aimed at this purpose we carried out two additional experiments where

fresh Au/TiO_2 photocatalyst was irradiated in water-methanol solutions containing 0.1 M of these by-products (Fig. 13).

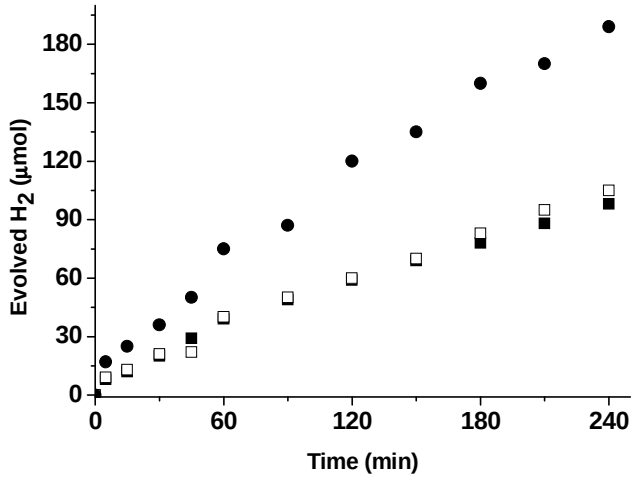

Figure 13. Hydrogen evolved during the photocatalytic runs using Au (0.25 wt%)/TiO_2 as catalyst in water-methanol solutions containing 0.1 M of different byproducts, under polychromatic light $\lambda > 400$ nm. ■: water-methanol, □: water-methanol and formaldehyde, ●: water-methanol and formic acid.

The results show that the presence of formaldehyde plays a minor role in hydrogen evolution since an essentially similar temporal profile is shown in the absence or presence of formaldehyde. In contrast, it was observed that the presence of a 0.1 M concentration of formic acid increases significantly the rate of hydrogen evolution, probably due to the effect of acid pH

on hydrogen evolution or the easier photocatalytic decomposition of formic acid to generate hydrogen.

In order to firmly prove the visible light photocatalytic activity of Au/TiO_2 for hydrogen generation from water, another photocatalytic test using the second harmonic of a Nd:YAG laser operating at 532 nm was used. Gold nanoparticles supported in titania exhibit a surface plasmon band with λ_{max} at about 550 nm, very close to the excitation wavelength used in this experiments. Fig. 14 shows the temporal evolution of hydrogen upon 532 nm laser irradiation of $Au(0.25\ wt\%)/TiO_2$.

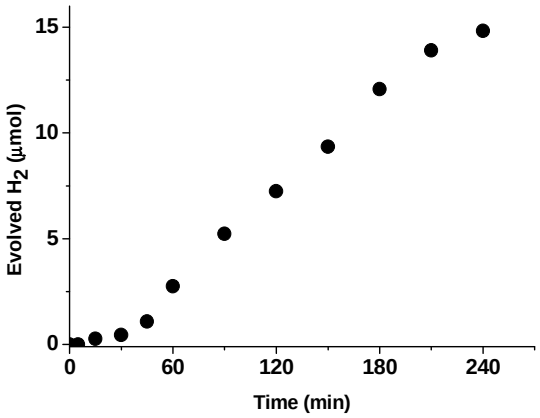

Figure 14. Hydrogen evolved during the photocatalytic runs using Au $(0.25\ wt\%)/TiO_2$ as catalyst in water-methanol solution under 532 nm laser irradiation.

The results obtained using monochromatic laser excitation were consistent with the photocatalytic hydrogen generation using polychromatic lamp light of wavelength longer than 400 nm. We notice that the hydrogen evolution using monochromatic 532 nm laser pulses exhibits an increase in the formation rate that could be due to several reasons, including (i) initial hydrogen absorption on the solid, (ii) changes in the gold particle size caused by the laser energy producing growth or agglomeration of gold nanoparticles, and (iii) titania phase change from anatase to rutile due to the local heat effect generated by the laser pulse. It should be noted, however, that thermal water splitting is very unlikely to be responsible for the observed hydrogen evolution since it requires temperatures well above 1000 °C.

2.3.2.3 Influence of Au loading and particle size in visible light photocatalytic hydrogen generation

In gold catalysis, it is well known that gold loading is a very important parameter that determines the activity of the resulting material [216]. When changing the gold loading, several parameters such as gold particle size and morphology, TiO_2 surface coverage and population of residual hydroxy groups and

metal dispersion are varied simultaneously. The balanced combination of all these factors determines that generally an optimal gold loading is observed for having the maximum catalyst efficiency. Typically, the most active materials in heterogeneous catalysis are those containing around 1 wt % gold loading. In the present case we prepared three samples of Au/TiO_2 using the standard deposition-precipitation method and compared their activities for visible light hydrogen generation with that of P25 TiO_2 devoid of any gold nanoparticles. The results are shown in Fig. 12. As it can be seen there, we found a remarkable influence of gold loading in the range 0-2.2 wt % in agreement with many precedents in gold catalysis [216]. In our photocatalytic study two figures of merit, namely the initial reaction rate (r_0) and the total hydrogen (μmol) at final time (4 hours), can be considered to assess the optimum catalyst performance. Table 2 lists both parameters for the series of Au/TiO_2 under study.

Table 2. Initial reaction rate (r_0) and amount of hydrogen evolved at 4 hours of irradiation for visible light photocatalytic runs using Au/TiO_2 catalysts with different gold loadings and methanol as sacrifical agent.

Catalyst	$r_0 \times 10^2$ (μmol min^{-1})	μmol H_2, 4h
Au(0.25 wt %)/TiO_2	65.6	98.2
Au(1.5 wt %)/TiO_2	81.0	58.8
Au(2.2 wt %)/TiO_2	55.8	65.2

As it can be seen in Table 2, as well as in Fig. 12, Au(0.25 wt %)/TiO_2 combines a high initial rate with high hydrogen productivity at 4 hours, and it has the additional advantage of presenting a high gold economy. For this reason this loading was selected for additional studies. One point that deserves a comment is that at least one of the photocatalysts (Au(1.5 wt %)/TiO_2) exhibits fatigue during the hydrogen generation. This decrease in photocatalytic activity during the reaction is typically due to deactivation probably caused by absorption of some by-product (formic acid, formaldehyde, etc.) arising from the sacrificial agent decomposition during the course of the reaction. In any case the data presented showed that the materials exhibit a notable visible light activity that varies

depending on the loading. In gold catalysis, one important point is the preparation procedure, particularly calcination temperature as well as the gold particle size, shape and the plane of exposed gold crystallites. Haruta has previously reported that it is possible to control the gold particle size by careful control of the suspension pH value during the deposition process [109]. Based on this knowledge, we have prepared two sets of Au/TiO_2 samples, three of which were calcined at 200 °C and other three at 400 °C. In principle, higher calcination temperature causes the growth of the gold particle size but also the sintering between the gold and titania interphase. On the other hand, varying the pH value from 4.5 to 9.0 units allows gaining a certain control on the particle size distribution of gold. To illustrate the variation in the particle size distribution as a function of the calcination temperature and pH of the deposition step, Fig. 15 shows representative TEM images of two of the Au/TiO_2 samples prepared as well as the corresponding statistical size distribution analysis showing the differences on the average gold particle size as a function of the preparation procedure. Unfortunately, higher resolution and deeper analysis of the images will be necessary to determine if the photocatalytic process is sensitive to the morphology of the particles and, moreover, if the exposed Au crystal face also varies depending on the preparation procedure and deposition pH and if these parameters influence the photocatalytic activity.

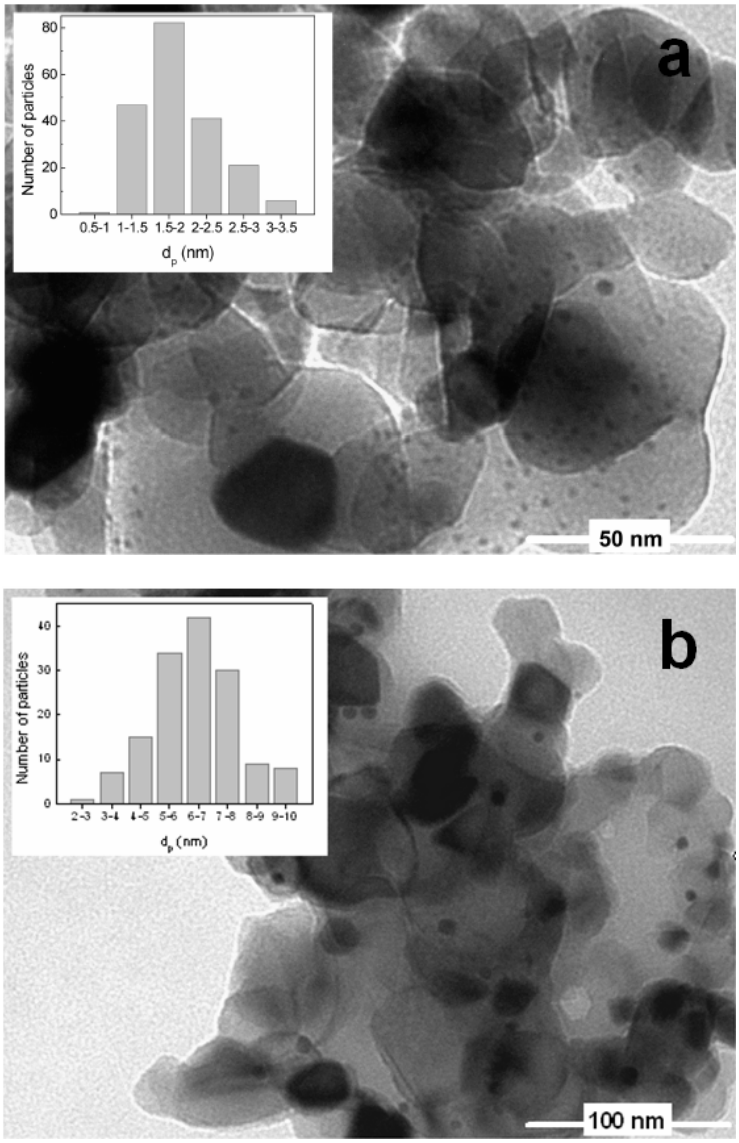

Figure 15. TEM micrographs and particle size distribution (insets) of Au/TiO_2 samples obtained at 200 °C and pH= 9.0 (a) and at 400 °C and pH= 4.5 (b).

Table 3 lists the codes of the Au/TiO_2 samples with indication of the preparation conditions and the average particle size. Importantly, it should be remarked that all the samples contained in Table 3 have a very similar gold loading around the optimum 0.25 wt % value previously determined.

Table 3. Preparation conditions (deposition pH and calcination temperature), average gold particle size (d_p) and wavelength for the maximum absorption of the surface Plasmon band (λ_{max}) for the different Au/TiO_2 samples.

Catalyst	pH	T_{calc} (ºC)	d_p (nm)	λ_{max} (nm)
Au/TiO_2-1	4.5	200	4.91	550
Au/TiO_2-2	6.5	200	2.85	547
Au/TiO_2-3	9.0	200	1.87	552
Au/TiO_2-4	4.5	400	6.40	562
Au/TiO_2-5	6.5	400	4.20	560
Au/TiO_2-6	9.0	400	4.11	561

As expected, due to the presence of gold nanoparticles, the UV-visible spectrum of the Au/TiO_2 samples exhibit in optical spectroscopy two bands: one in the visible region between 500 and 650 nm typical of the gold surface plasmon band, and

another, stronger, with onset at 370 nm that is due to the bandgap transition of TiO_2 semiconductor (Fig. 16).

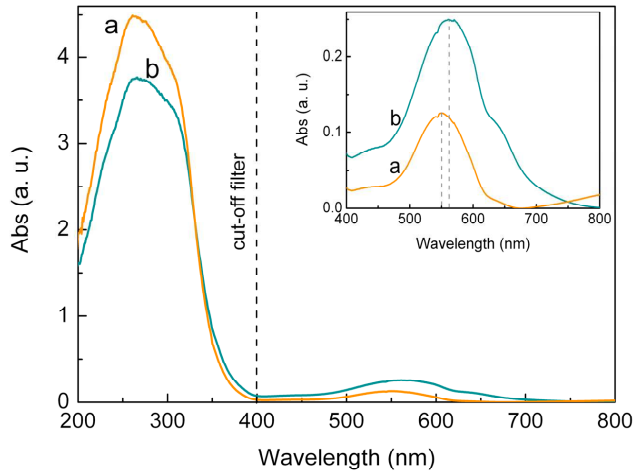

Figure 16. UV-vis spectra of the Au/TiO_2-1 (a) and Au/TiO_2-6 (b) photocatalysts plotted as the Kubelka-Munk function of the reflectance. The inset shows an expansion of the gold surface plasmon band. The dashed vertical line indicates the cutoff wavelength of the filter used in the photocatalytic experiments.

Considering that our excitation light contains radiation of wavelength longer than 400 nm and also the influence of the presence of gold on the photocatalytic activity, we attribute this enhanced photocatalytic activity observed in Fig. 12 to the contribution of gold nanoparticles as light harvesters and ability to inject electrons into the TiO_2 conduction band. Careful

inspection of the position of the surface plasmon band reveals that the samples calcined at 200 °C exhibit very similar wavelength maxima around 550 nm that is different and blue-shifted from the other set of samples calcined at 400 °C where the wavelength maxima of the gold surface plasmon band appears around 561 nm. The actual wavelength maximum for each sample is also given in Table 3. With this set of samples, photocatalytic hydrogen generation using methanol as sacrificial electron donor and visible light was carried out. Fig. 17 shows the temporal evolution of hydrogen formation as a function of the irradiation time and the catalyst present.

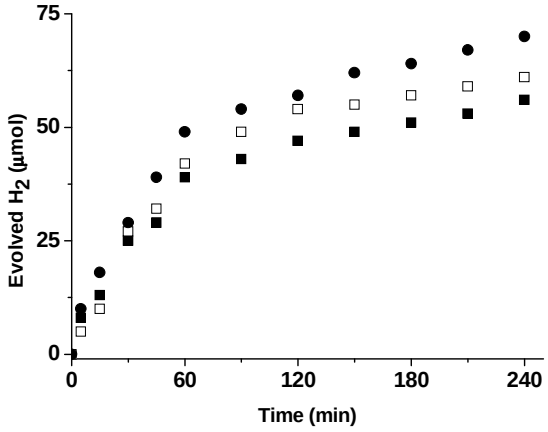

Figure 17. Evolved hydrogen (µmol) during the photocatalytic runs using methanol/water (3/1 v/v) in the presence of catalysts obtained at 200 °C and different pH. ■: Au/TiO_2-1, □: Au/TiO_2-2 and ●: Au/TiO_2-3.

Those samples calcined at lower temperature exhibited higher activity than those calcined at 400 °C. Also for the most active samples (200 °C calcination temperature), the initial reaction rate of hydrogen formation increases as the gold particle size decreases. Therefore, based on this it can be concluded that the intrinsically more efficient samples of Au/TiO_2 should contain the optimum gold loading with the smallest particle size. However, we notice that for the series of Au/TiO_2 calcined at 400 °C the trend of the pH deposition on the photocatalytic activity is opposite (see Fig. 18).

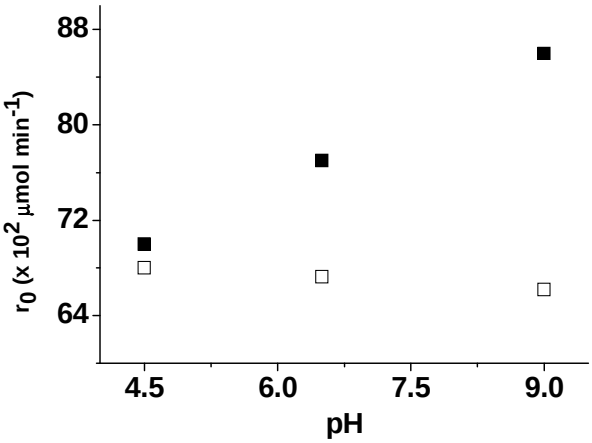

Figure 18. Initial reaction rates (r_0) obtained for the catalysts synthesized at different calcination temperature and different pH

■: T_{calc} 200 °C □: T_{calc} 400 °C.

Therefore, it appears that other factors besides the particle size are coming into play. The previous discussion on the photocatalytic activity is based on the initial reaction rate that reports on the intrinsic photocatalytic activity of fresh samples. However, as commented earlier when observing deactivation of some photocatalysts, long-term hydrogen productivity depends not only on the intrinsic activity but also on the catalytic stability and deactivation processes. Thus, it is frequently observed in catalysis that the most active material becomes rapidly deactivated and the long-term performance is worse than that of other materials exhibiting a good balance between initial activity and long term stability. This is apparently the case here since those samples calcined at 400 °C exhibit better stability during operation of the photocatalytic hydrogen generation. This is not surprising since higher calcination temperatures increase catalytic stability by promoting the grafting and the interfacial contact between gold and the support. Therefore, concerning the total hydrogen production at 4 hours irradiation time, the differences observed based on the initial reaction rate disappear and the performance of the samples calcined at 400 °C becomes similar to the performance of those prepared at 200 °C.

2.3.2.4 UV and visible light photocatalytic oxygen generation

Once the study of the reduction semireaction was complete, we used the same set of samples and the same excitation source to determine the possibility of photocatalytic oxygen generation. Oxygen generation from water requires much higher oxidation potential than the reduction potential needed for hydrogen evolution. In addition to the thermodynamic requirement of holes having higher oxidation potential than 1.26 V, oxygen evolution is considered mechanistically a complex process since the formation of one oxygen molecule involves four electrons and the creation of oxygen-oxygen bonds absent in the water molecule. For the mechanistic complexity, oxygen generation is considered frequently the bottleneck for the overall water splitting [217]. The samples under study containing gold nanoparticles were found also to exhibit photocatalytic activity for O_2 generation from water under both UV and visible light excitation. Fig. 19 shows a temporal profile of O_2 evolution for Au(0.25 wt %)/TiO_2 and P25 TiO_2 under UV and visible light (λ > 400 nm) excitation using $AgNO_3$ as sacrificial electron acceptor.

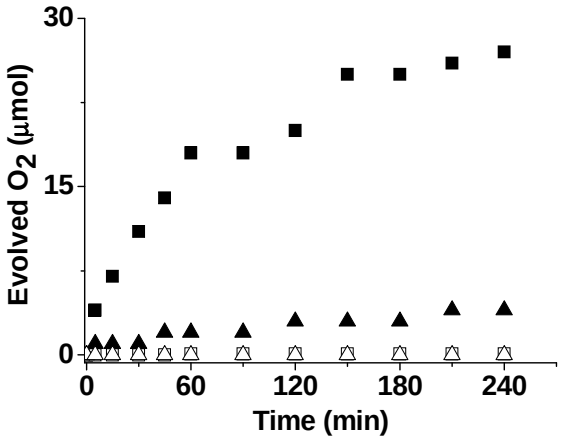

Figure 19. Evolved oxygen during the photocatalytic runs using Au(0.25 wt%)/TiO_2 and P25 TiO_2 under UV and Visible light (λ > 400 nm) using $AgNO_3$ as sacrificial electron acceptors. ■: Au/TiO_2, UV; ▲: Au/TiO_2, Vis; □: TiO_2, UV; Δ: TiO_2, Vis.

As it can be seen in Fig. 19, $AgNO_3$ as sacrificial electron acceptor promotes oxygen evolution, although reusability of the catalyst is not allowed with this sacrifical agent, probably because the formation of black silver particles or formation of core/shell Au/Ag particles reduces the efficiency of the photocatalytic oxygen evolution. Recently it has been observed that core/shell Au/Ag nanoparticles can be formed upon photolysis of Au nanoparticles in the presence of Ag salts, and a similar process can occur here. If this were the case, then the photocatalytic activity would decrease due to the coverage of Au nanoparticles by a shell of Ag. On the contrary, similar

photocatalytic experiments in which $(NH_4)_2Ce(NO_3)_6$ was used as sacrifical agent, demonstrated the possibility to use the same catalyst sample in consecutive photocatalytic runs without observing relevant changes in comparison with the fresh catalyst. Firm experimental evidence of oxygen evolution upon excitation at the gold surface plasmon band was again obtained by using as excitation light a monochromatic laser operating at 532 nm. The results show that no oxygen is evolved performing the experiment using P25 TiO_2, while in contrast the presence of Au nanoparticles in Au/TiO_2 samples introduces visible light photoactivity. According to Scheme 4, the positive holes located on Au nanoparticles should have an oxidation potential higher than 1.26 V.

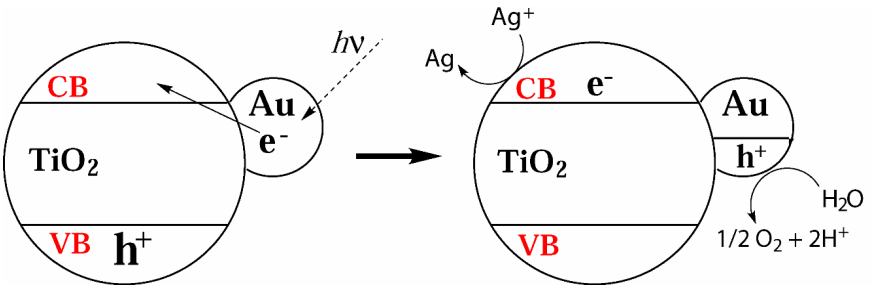

Scheme 4. Proposed rationalization of the photocatalytic activity of Au/TiO_2 forming O_2 upon excitation of the gold surface plasmon band.

Typically metals are devoid of any oxidation activity. However, when the particle size is reduced a transition between the band theory predicts a change from the characteristic bands of bulk metals to discrete atomic orbitals present in atoms occurring in the nanometric scale. Small Au clusters (below 2-3 nm) can exhibit frontier HOMO/LUMO orbitals, and electron holes in the HOMO orbital can have higher oxidation potential than larger nanoparticles. The situation is, however, complex since variation of the HOMO/LUMO orbital energy and the presence of separate valence and conduction bands will influence also the absorption of light and intensity of the corresponding surface plasmon band associated with the nanoparticles. Thus, very likely small nanoparticles having discrete energy levels are those that do not have intense visible light absorption. Attempts to obtain electrochemical evidence of the oxidation potential of Au/TiO_2 allowed detection of some reversible oxidation peaks at -1.14 V semipotential in films of this material supported on conductive FTO electrode (Fig. 20).

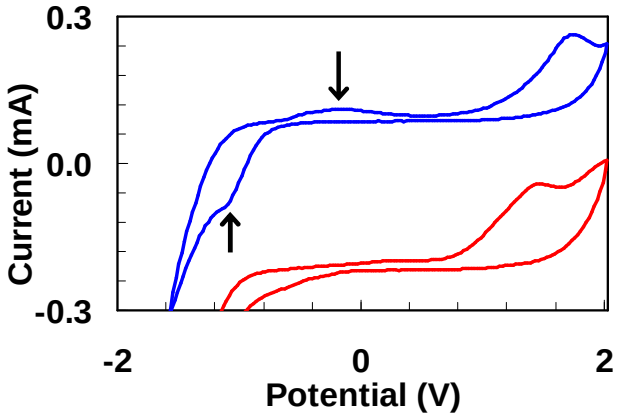

Figure 20. Cyclic voltammetry of a film of Au/TiO_2 supported on a FTO electrode immersed in electrolyte. The bottom voltammogram corresponds to the response of TiO_2 film on FTO electrode recorded under identical conditions. The arrows point to the specific peaks observed for Au(1.5 wt %)/TiO_2 during the reduction (pointing up) and the oxidation (pointing down) scan.

These peaks could be attributable to the electrochemical generation of holes on Au nanoparticles since analogous measurements with P25 TiO_2 (pH of zero point charge about 6.0) do not allowed detection of any peak in the available oxidation window. Although further studies are necessary to firmly assign the electrochemical peaks observed for Au/TiO_2 to the positive holes generated in photocatalysis, the presence of electrochemical response Au/TiO_2 is compatible with the observed photocatalytic oxygen evolution. We noticed however that the oxidation power of the electrochemical oxidation peak

at the maximum of the current intensity (-1.14 V) is lower than the thermodynamic oxidation potential required to generate oxygen from water (1.26 V). In this regard it has to be commented that cyclic voltammetry shows broad peaks, probably reflecting a distribution of Au nanoparticles with different oxidation potentials, depending on the particle size. It could be that not all the particles could be able to oxidize water generating oxygen, but only the fraction of the gold nanoparticles in where the oxidation potential fulfills the thermodynamic requirements, i.e. those with oxidation potential higher than 1.26 V. The others, even if they are photochemically excited, will not have enough oxidation capacity to generate oxygen. In general agreement with the previous findings for the photocatalytic hydrogen generation, we also observed that the initial reaction rates and the final oxygen volume at 4 hours depend on the gold particle size and calcination temperature. We have observed for oxygen the same trend as for hydrogen, the most active Au(0.25 wt %)/TiO_2 photocatalyst for oxygen generation being the same as for hydrogen generation, i.e., the Au/TiO_2 material prepared at pH 9.0 and calcined at 200 °C (Au/TiO_2-3), with a gold average particle size of 1.87 nm (Table 4).

Table 4. Initial reaction rate (r_0) and amount of oxygen evolved at 4 hours of irradiation for photocatalytic runs using Au/TiO_2 catalysts obtained at different calcination temperature and pH (see Table 3 for conditions).

Catalyst	$r_0 \times 10^2$ (μmol min^{-1})	μmol O_2, 4h
Au/TiO_2-1	23.5	11.75
Au/TiO_2-2	29.4	12.74
Au/TiO_2-3	31.4	13.73
Au/TiO_2-4	22.5	11.72
Au/TiO_2-5	21.5	10.75
Au/TiO_2-6	21.5	9.77
TiO_2	--	--

2.3.2.5 Quantum yields for visible light hydrogen and oxygen generation

The most important finding of our study is the visible light photocatalytic activity for water splitting of Au/TiO_2. We determined the quantum yield for the independent hydrogen and oxygen semireactions using sacrificial reagents for the most efficient Au/TiO_2-3 sample using monochromatic light. In order to ensure the selective excitation of gold surface plasmon band

we selected for the quantum yield measurements 560 nm that is close to the λ_{max} for gold nanoparticles and far from the onset of the TiO_2. For comparison we have attempted to measure the quantum yield of hydrogen and oxygen generation for TiO_2 at the same excitation wavelength (Table 5).

Table 5. Quantum yield (Φ) of hydrogen and oxygen generation determined by ferrioxalate actinometry at 560 nm.

Catalyst	Φ_{H2} (%)	Φ_{O2} (%)
TiO_2	**< 0.1**	**< 0.1**
Au-TiO_2-3	**7.5**	**5.0**

The results obtained (Table 5) prove quantitatively the photocatalytic activity for water splitting of titania as a consequence of the presence of gold nanoparticles. In this context Domen and coworkers have reported $(Ga_{1-x}Zn_x)(N_{1-x}O_x)$ photocatalysts as one of the most efficient materials for water splitting, having an efficiency of 2-3% [218]. Therefore, our Au/TiO_2 absorbing at long wavelengths exhibits an activity that is not far from that of other visible light water splitting photocatalysts. The low quantum yield values for TiO_2 are compatible with the negligible absorption of TiO_2 at this long wavelength. In any case, the data of Table 5 clearly show that the light harvesting component is gold nanoparticles at least for long wavelengths.

2.4 Conclusions

In the present work, by using a UV cutoff filter ($\lambda > 400$ nm) and a monochromatic 532 nm laser excitation that ensure that the light is absorbed exclusively by gold nanoparticles in combination with the quantum yield measurements we have demonstrated that gold can have an additional role as light harvester besides gas evolution center. We have found that, using excitation wavelengths corresponding to gold plasmon band, gold nanoparticles absorb photons and inject electrons into the semiconductor conduction band (Schemes 2 and 3). This photoinduced electron injection into the conduction band of a semiconductor is unusual for a metal, but the nanometric size of the gold particles and the operation of quantum size effects should be responsible for the occurrence of this mechanism. Electrons in the titania conduction band and holes in certain gold nanoparticles have adequate potential to generate hydrogen and oxygen from water, respectively. We have also found that the gold particle size and calcination temperature play a certain role, influencing the catalytic activity. Apparently the combination of appropriate loading, small particle size and the presence of surface hydroxyl groups (low calcination temperatures) favors the photocatalytic activity of the materials.

3

Efficient visible-light photocatalytic water splitting by minute amounts of gold supported on nanoparticulate CeO_2 obtained by a biopolymer templating method*.

**: A. Primo, T. Marino, A. Corma, R. Molinari and H. Garcìa, The Journal of the American Chemical Society, 133 (2011) 6930.*

3.1 Introduction

In the overall water splitting, water becomes reduced to hydrogen and simultaneously oxidized to oxygen. Of these two semireactions, hydrogen generation is considered simpler since, in principle, the process consists in protons present in the water

accepting electrons and noble metals acting as hydrogen evolution centers. In contrast to the simplicity of hydrogen generation, formation of oxygen from water is conceptually more challenging since mechanistically it has to occur through several steps requiring four positive holes and the formation of O-O bonds [219]. For this reason, oxygen evolution is frequently the bottleneck determining the overall efficiency in the overall photocatalytic water splitting. Both semi-reactions, hydrogen and oxygen generation from water, can be independently studied by adding during the photocatalytic process sacrificial electron donors (for hydrogen generation) and electron acceptors (for oxygen formation). Therefore, it is possible to decouple both semi-reactions and focus the study on one of them. Considering the importance in developing novel efficient photocatalysts with visible-light activity with comparable or higher efficiency than those currently known [220] and also the interest in having efficient semiconductors for oxygen evolution, in the present contribution we describe that nanoparticulated ceria prepared by a novel biopolymer-templating methodology and containing appropriate gold loadings is a stable and efficient photocatalyst for oxygen evolution. Characterization of the catalyst samples using SEM, TEM, XRD, XPS and S_{BET} is presented in the following. A comparison between the photocatalytic efficiency of the synthesised ceria (CeO_2(A)) and a commercial one (CeO_2(B)) is

reported to study the influence of their physical-chemical properties on the photocatalytic oxygen generation from water. The relevance of our finding is two-fold. On one hand, our report shows how, by reducing the particle size down to the nanometer scale, a conventional metal oxide insulator is converted into a semiconductor whose photocatalytic activity strongly depends on the particle size in the nanometer scale. On the other hand, we show that by supporting gold nanoparticles it is possible to introduce visible-light response in the nanoparticulated ceria that otherwise would be inactive under visible-light irradiation. It is well documented that conventional ceria of large particle size behaves as insulator devoid of any photocatalytic activity [221]. Scattered precedents have reported that reducing the particle size of ceria to the nanometer scale introduces some photovoltaic activity [222]. Part of this work is based on a novel preparation method of very small nanoparticle-sized ceria using a biopolymer (alginate) as template with the resulting nanoparticulated ceria exhibiting a high photoactivity as a semiconductor.

3.2 Experimental

3.2.1 Synthesis of nanoparticulated ceria

The most active sample for the visible-light photocatalytic generation of oxygen reported here, called CeO_2(A), was prepared as indicated in Scheme 5.

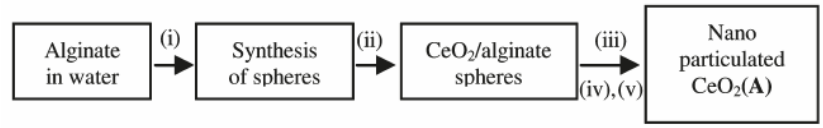

Scheme 5. Biopolymer templated synthesis of CeO_2(A) nanoparticles, i) alginate precipitation by $(NH_4)_2Ce(NO_3)_6$; ii) maturation (19 hours); iii) water by ethanol exchange; iv) supercritical CO_2 drying; v) air calcination.

The first step consists in the anionic exchange Ce^{4+} into alginate dissolved in water that precipitates when a sufficient large uptake of Ce^{4+} is achieved. Thus, a 1.0 % (w/w) solution of sodium alginate is added dropwise at room temperature to a stirred 0.1 M aqueous $(NH_4)_2Ce(NO_3)_6$ solution using a syringe with a 0.8 mm internal diameter needle. The gel beads are left overnight and then filtered and washed with distilled water. At this point the Ce^{4+} loading determined by chemical analysis was

77.5 wt %. The subsequent step in the synthesis is the supercritical CO_2 drying of the sample that requires a prior gradual exchange of water for ethanol since, in contrast to ethanol, water is immiscible in supercritical CO_2. The supercritical CO_2 drying is crucial, as has already been demonstrated [223] to achieve a highly porous alginate with remarkably high surface area. Thus, hydrogel beads are dehydrated by a series of consecutive washings using ethanol-water solutions of increasing alcohol concentration (10, 30, 50, 70, 90 and 100 %) for 14 min each. The alcogel beads are then dried under supercritical CO_2 conditions (slightly above 73 bar and 31 °C), yielding aerogel beads. For removing all the organic part, the beads are calcined in air at 540 °C. In our case, at this moment Ce^{4+} ion is still compensating for the negative charge of carboxylate groups present in the biopolymer. For the sake of comparison with CeO_2(A) we have included in our study also a commercial nanoparticulate CeO_2 sample (CeO_2(B) from Aldrich). Furthermore, a commercial nanopowder WO_3 sample (Aldrich) was used in the present study as reference photocatalyst. The material presents spherical shape crystallites with diameter up to 33.1 nm [224].

3.2.2 Deposition-precipitation procedure

The deposition precipitation procedure is done at 70 °C and pH 9 using 0.2 M NaOH to maintain the pH constant. Under these conditions, gold deposition occurs with ~80 % efficiency. The catalyst is then recovered, filtered, washed with deionized water, and dried at 100 °C. Finally, the powder is calcined at 400 °C in air for 4 hours. Following this procedure, 3.5 nm gold nanoparticles supported on CeO_2 are obtained.

3.2.3 Characterization techniques

To characterize photocatalysts samples by Uv-Vis spectra, ICP, TEM and XRD analysis, the same apparatus described in Chapter 2 (see paragraph 2.2.2) were used.

The interaction of gold nanoparticles with ceria support was addressed by X-ray photoelectron spectroscopy (XPS) using a SPECS spectrometer equipped with a Phoibos 150 9MCD detector and a non-monochromatic X-ray source (Al and Mg) operating at 200 W.

3.2.4 Photocatalytic tests

The photocatalytic experiments were performed using the system described in Chapter 2 (see paragraph 2.2.3), in which the headspace of the reactor was connected to an inverted burette filled with water at atmospheric pressure, allowing the measurement of the evolved gas. In the photocatalytic reactions the photocatalyst powder (45 mg) was dispersed in water containing 0.01 M of $AgNO_3$ or $(NH_4)_2Ce(NO_3)_6$. The total volume of the suspension was of 22.5 mL. The suspension was purged with an argon flow for at least 30 minutes before irradiation in order to remove dissolved air. Then it was irradiated for 4 h using a 200 W xenon doped mercury lamp (Hamamatsu Lightningcure LC8, 1 cm distance). For polychromatic visible light irradiation the output of the 220 W xenon-doped mercury lamp was filtered through a cutoff filter (λ > 400 nm). The stationary temperature of the reactor, reached at 5 min of irradiation, was 38 °C. The formation of oxygen was confirmed by injecting 0.5 mL of the reactor headspace gas in a gas chromatograph (HP 5890) operating at isothermal conditions (50 °C) using a semi-capillary column (molecular sieve, 530 μm diameter, 15 m length) equipped with a thermal conductivity detector and argon as carrier gas. To explain our proposal photocatalytic mechanism we performed photocatalytic tests based on the monochromatic irradiation of the suspension containing Au(0.25 wt%)/CeO_2(A). To carry out these

experiments, we used a 150 W XBO lamp (Osram) equipped with water cooled housing, LPS 200 power supply (Photon Technology International) and a computer controlled monochromator.

3.2.5 Electrochemical characterization

The potential corresponding to the positive hole (assuming that it is located on gold nanoparticles) has been calculated from cyclic voltammograms for Au/CeO_2 microparticulate deposits on paraffin-impregnated graphite electrodes immersed into aqueous 0.10 M NaOH and 0.10 M Bu_4NPF_6/MeCN.

3.3 Results and discussion

Au/CeO_2 are important heterogeneous catalysts for low temperature CO oxidation, alcohol oxidation and aromatic amine carbamoylation among other reactions [222]. Due to its ample use in heterogeneous catalysts, there is a considerable amount of information about the Au/CeO_2 preparation. The most widely used procedure is the deposition-precipitation method, as discussed in Chapter 1. Here we have followed this procedure and deposited gold nanoparticles on CeO_2(A) at different

loading levels and we carried out photocatalytic experiments for oxygen generation from water under UV and visible irradiation. The data presented below show that the influence of gold favoring or disfavoring the photocatalytic activity is different, depending on the UV or visible irradiation wavelength. Photocatalysis under visible-light irradiation is considerably more challenging due to the lower photon energy that is generally unable to excite wide band gap semiconductors and also because about 45% of the solar light corresponds to the visible range. However, herein the initial experiments with ceria materials were performed with UV light with the aim of obtaining data supporting the photocatalytic activity of this metal oxide for oxygen generation from water. Experiments submitting a suspension of CeO_2 or Au/CeO_2 in water containing EDTA or methanol as sacrificial electron donors failed to generate hydrogen in the range of pH 1-7. In contrast analogous experiments using Ag^+ or Ce^{4+} as electron scavengers gave rise to the photocatalytic generation of oxygen.

3.3.1 Characterization

Fig. 21 shows an image of the millimetric alginate spheres obtained by coagulation of the aqueous alginate solution with Ce^{4+} as well as a representative TEM image of the corresponding material.

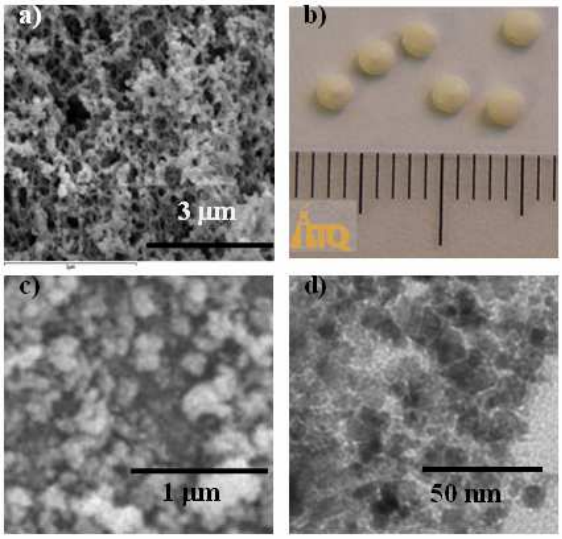

Figure 21. a) SEM CeO_2(A) before calcination b) spheres before calcination c) SEM CeO_2(A) after calcination d) TEM Au(1.0 wt%)/CeO_2(A).

Isothermal N_2 adsorption measurements give a specific surface area for alginate containing Ce^{4+} of 229 m^2g^{-1}. This sample was submitted to mild aerobic calcination to effect the controlled

combustion of the biopolymer and formation of CeO_2(A). The novel CeO_2(A) material was characterized by conventional techniques in material sciences. Fig. 22 shows UV-Vis absorption spectra of the unmodified ceria and gold containing samples.

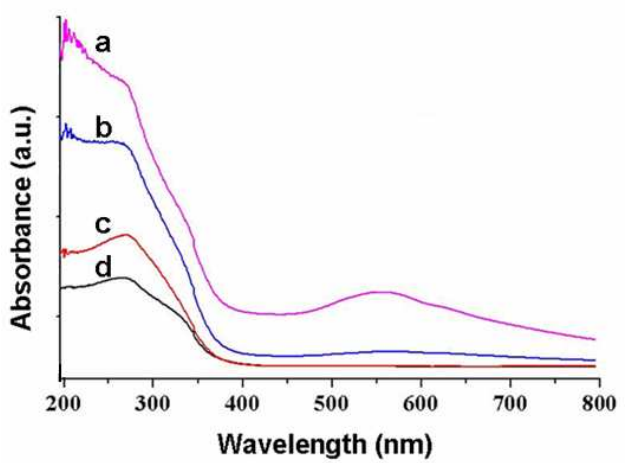

Figure 22. Diffuse UV-Vis reflectance spectra of samples containing or not gold loading. a: Au(3 wt%)/CeO_2(A), b: Au(1 wt%)/CeO_2(A), c: CeO_2(A), d: CeO_2(B).

The spectra show that CeO_2 has intense broad band with a maximum at ca. 270 nm while Au/CeO_2 samples exhibit a significant ultraviolet absorption and a surface plasmon resonance centered at 560 nm.

The crystal structure of the products was examined by powder X-ray diffraction (XRD). Peaks corresponding to CeO_2 (111),

(200), (220) and (311) planes were observed, indicating a face-centered cubic phase CeO_2 (Fig. 23).

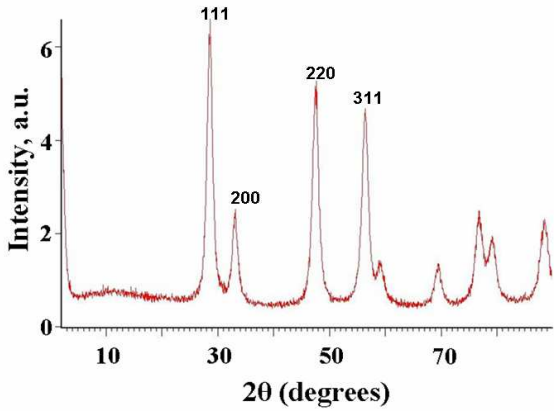

Figure 23. XRD patterns of the as-obtained CeO_2(A) sample.

Ce 3d electron core level XPS spectra for CeO_2(A) is shown in Fig. 24.

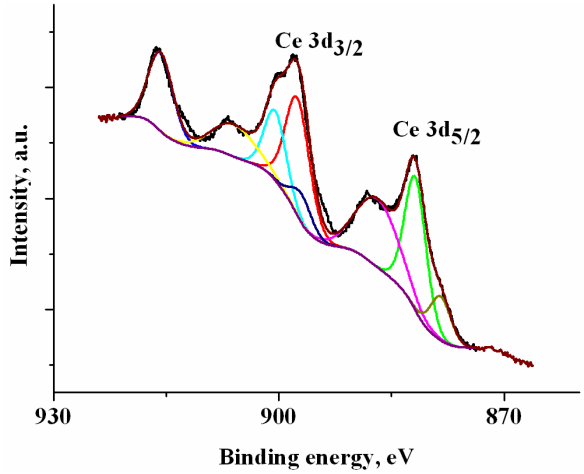

Figure 24. XPS spectra for CeO_2(A) sample.

The 3d level is formed by two series of peaks: $3d_{5/2}$ and two very pronounced "shake-up" satellites and $3d_{3/2}$ with the same characteristics. XPS shows that most of the Ce atoms (over 90%) are in the +4 oxidation state.

BET surface area measurement gives a value of 93 m^2g^{-1}. The average particle size of CeO_2(A), determined by counting a statistical relevant number of nanoparticles, was 4.9±0.1 nm. Overall, the data obtained are consistent with a well-crystallized CeO_2(A) sample with a 5 nm particle size and a large specific surface area that originates from the templating effect of alginate dried under supercritical CO_2. For the sake of comparison with CeO_2(A) we have included in our study also a commercial nanoparticulate CeO_2 sample (CeO_2(B) from Aldrich). XRD and BET measurements indicate that CeO_2(B) has the same crystal phase as CeO_2(A), similar surface area (102 m^2g^{-1}) and larger average particle size (20 nm) than CeO_2(A) sample. Also in our study we have used WO_3 as a reference photocatalyst for oxygen generation [8]. It is generally considered that WO_3 is a benchmark material for oxygen generation to which novel photocatalysts should be compared to establish relative efficiencies.

3.3.2 Photocatalytic tests

3.3.2.1 UV light photocatalytic oxygen generation

A first set of photocatalytic experiments were performed in order to compare the catalytic efficiency of the photocatalysts in the oxygen generation from water splitting under UV irradiation. Fig. 25 shows the temporal profile of oxygen evolution under UV irradiation of CeO_2(A) and CeO_2(B). For the sake of comparison we also include the photocatalytic behaviour of WO_3 as reference.

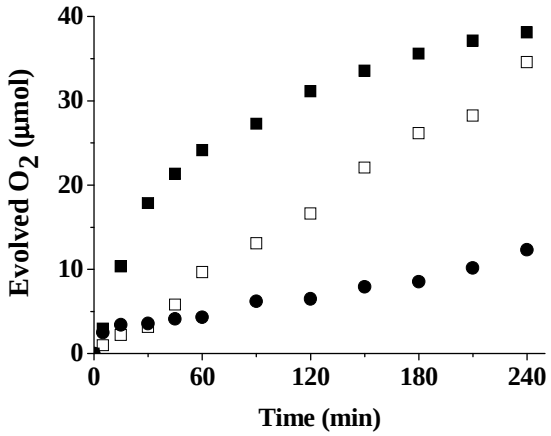

Figure 25. Oxygen evolution upon UV irradiation of an aqueous suspension of $AgNO_3$ containing ■: WO_3, □: CeO_2(A), and ●: CeO_2(B).

As can be seen in Fig. 25, although WO_3 exhibits a high initial rate under these conditions as well as a slightly higher oxygen amount generated by the end of the reaction, the relevance of the obtained data is that both ceria materials exhibit photocatalytic activity for oxygen generation under UV light irradiation. The temporal profiles for oxygen generation determined for CeO_2(A) and CeO_2(B) are remarkably different. While commercial CeO_2(B) seems to exhibit a higher initial rate, even comparable to that of WO_3, the slope of the O_2 formation curve decreases remarkably even at short times. In contrast in the case of CeO_2(A) the initial reaction rate was smaller, but it maintains the activity over the time and after 45 minutes is more efficient than CeO_2(B), reaching photocatalytic activity comparable to that of WO_3 at 4 hours. These differences can be rationalized, considering that CeO_2(B) undergoes fast deactivation, probably by deposition of Ag particles, under these conditions. In contrast, CeO_2(A) with the smaller particle size becomes more active due to its lower tendency to deactivate.

The use of Ag^+ should be limited for the reusability of the catalyst because it is difficult for silver metal to be oxidized back to silver ion. In contrast, other reduced ions could be reoxidized to the oxidized form without any catalyst deactivation. Thus, two different photocatalytic runs, using $AgNO_3$ or $(NH_4)_2Ce(NO_3)_6$, were performed. The obtained results are shown in Fig. 26.

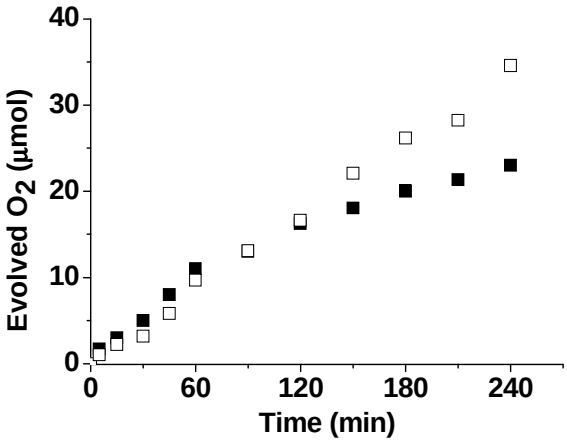

Figure 26. Oxygen evolution upon UV irradiation of an aqueous suspension using CeO_2(A) as catalyst and different electron acceptor □: $AgNO_3$, ■: $(NH_4)_2Ce(NO_3)_6$.

As it can be seen, Fig. 26 shows that Ag^+ promotes oxygen evolution with higher efficiency than when Ce^{4+} was used. These results do not correlate well with the redox potential of electrolytes. Probably other kinetic factors might be involved in this process. In order to verify the possibility of reuse of ceria after one photocatalytic run for 4 hours, the catalyst was filtered and it was used for a second experiment under the same operational conditions. The same kinetic profile shown in Fig. 26 was essentially obtained when Ce^{4+} was used as electron acceptor, while a lower efficiency of the catalyst was observed in the case of Ag^+, probably because the formation of metallic silver causes its precipitation on the ceria nanoparticles.

In order to understand the effect of gold on CeO_2 catalysts for the oxygen generation from water, different amounts of gold were loaded on CeO_2(A) and CeO_2(B) from 0.25 to 3.0 wt% and the catalytic activity of Au/CeO_2 samples was investigated under UV light irradiation (Fig. 27).

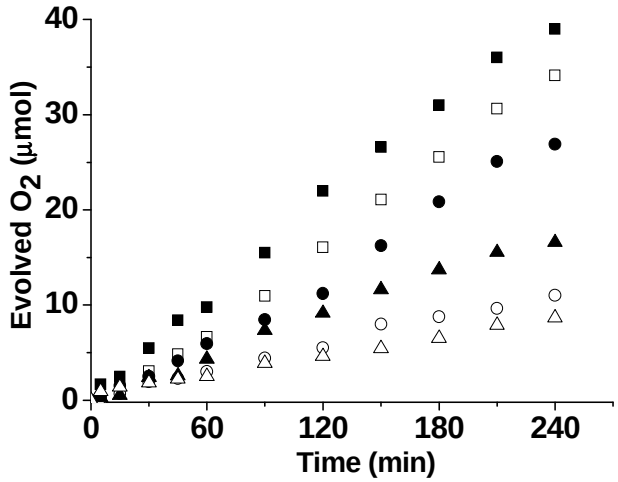

Figure 27. Oxygen evolved upon UV light illumination of an aqueous $AgNO_3$ suspension containing the photocatalyst. ■: Au(0.25 wt%)/CeO_2(A), □: Au(1.0 wt%)/CeO_2(A), O: Au(3.0 wt%)/CeO_2(A) , ●: Au(0.25 wt%)/CeO_2(B) , ▲: Au(1.0 wt%)/CeO_2(B), Δ: Au(3.0 wt%)/CeO_2(B).

As it can be seen in Fig. 27, when ceria samples containing gold nanoparticles at 0.25, 1.0 or 3.0 wt % were tested under the same conditions, it was observed that the presence of gold at 3.0 wt % loading is highly detrimental for the photocatalytic

efficiency. However, with regard to the final moles of oxygen formed, samples with 0.25 and 1.0 wt % Au loading exhibit photocatalytic activity similar to that of ceria without gold. It can be concluded that under UV irradiation the presence of Au plays a minor (0.25 and 1.0 wt %) or notable (3.0 wt %) negative influence on the photocatalytic activity of CeO_2 under UV irradiation. The negative influence of gold might be due to the role of Au nanoparticles acting as charge (e^-/h^+) recombination centres when the semiconductor is excited in the band gap.

3.3.2.2 Visible light photocatalytic oxygen generation

Photocatalytic experiments using UV light similar to those previously referenced were performed under visible light ($\lambda >$ 400 nm). Under these conditions CeO_2(A) or CeO_2(B) did not give rise to the generation of any oxygen. Only WO_3 exhibited a low photocatalytic oxygen generation activity in agreement with its low performance under visible light illumination. In sharp contrast, all the Au/CeO_2 samples exhibited visible light activity.

Fig. 28 shows the obtained results using visible light irradiation.

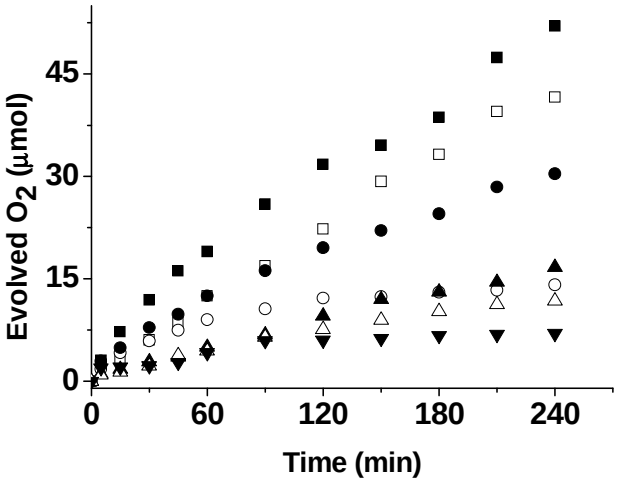

Figure 28. Oxygen evolved upon visible light (λ > 400 nm) illumination of an aqueous $AgNO_3$ suspension containing the photocatalyst. ■: Au(0.25 wt%)/CeO_2(A), □: Au(1.0 wt%)/CeO_2(A), O: Au(3.0 wt%)/CeO_2(A) , ●: Au(0.25 wt%)/CeO_2(B) , ▲: Au(1.0 wt%)/CeO_2(B), Δ: Au(3.0 wt%)/CeO_2(B), ▼: WO_3.

It can be observed from Fig. 28 that around 0.25 wt% gold loading represents the best amount for the efficient water oxidation. When the amount of gold loaded on CeO_2 more than 0.25 wt%, shielding of light by gold will occur which may prevent the excitation of electrons from the valence to conduction band. These all the experiments illustrates the importance of optimizing the amount metal particles on CeO_2 to maximizing the photocatalytic activity of the catalysts.

Moreover, the photocatalytic activity of Au(0.25 wt %)/CeO_2(A) using visible light was higher than that achieved with CeO_2(A) under UV irradiation. This behaviour is remarkable because, typically for titania and other semiconductors, the photocatalytic activity under UV is considerably reduced using visible light, whereas here the performance for Au/CeO_2 can be better using visible light. It is remarkable that with the use of Au/CeO_2(A) the final moles of oxygen evolved are higher than those obtained for WO_3 using UV light. Fig. 28 shows selected plots of the oxygen formed over the time for visible light illumination for the series of Au/CeO_2. For comparison, we have included also in this Fig. 28 the activity of WO_3 under the same conditions. With respect to the influence of Au loading we observed again that 0.25 Au renders a more efficient photocatalyst than 1.0 and 3.0 wt% Au. Also as commented using UV irradiation, the ceria sample prepared by the novel biopolymer template procedure described previously and having smaller particle size is far more efficient than larger particle size in the conversion of commercial CeO_2(B).

Concerning the mechanism of O_2 formation, the photo action spectrum of Au/CeO_2(A) was studied using monochromatic light in the range 410-650 nm; the ability to generate O_2 was found to follow the surface plasmon band profile (Fig. 29).

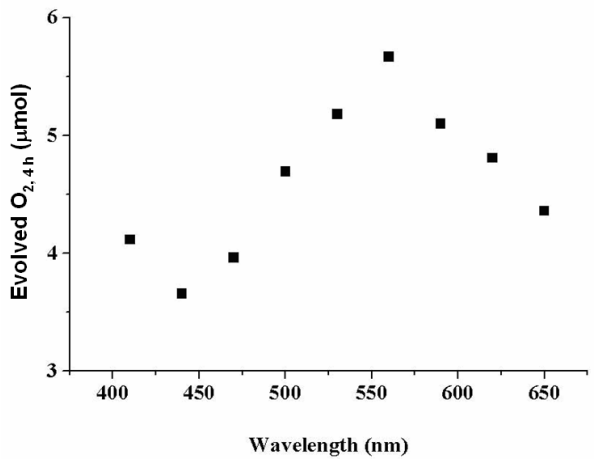

Figure 29. Oxygen evolution upon monochromatic irradiation of an aqueous suspension of $AgNO_3$ containing ■: Au(0.2 wt%)/CeO_2(A).

This supports that gold nanoparticles are the species responsible for light absorption and trigger the photochemical events. In addition, preliminary experiments using cyclic voltammetry reveal for Au/CeO_2(A) the presence of an oxidation peak at about +1.49 V that is absent in CeO_2 (Table 6).

Table 6. Potential corresponding to the positive hole calculated from cyclic voltammograms for Au/CeO_2 microparticulate deposits on paraffin-impregnated graphite electrodes immersed into aqueous 0.10 M NaOH and 0.10 M Bu_4NPF_6/MeCN.

Material	E (V vs. AgCl/Ag)	E (vs. SHE)
Au/CeO_2**(A)**	+1.28	+1.49
Au/CeO_2**(B)**	+1.00	+1.21

If this were the oxidation potential of the positive holes in Au/CeO_2(A) they would have enough energy to promote water oxidation. Scheme 6 summarizes our proposal to rationalize the photocatalytic behavior of Au/CeO_2 under visible irradiation.

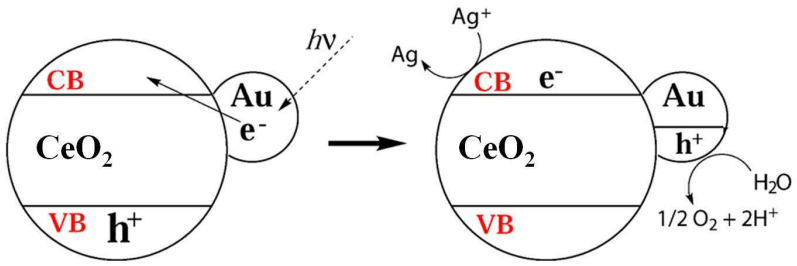

Scheme 6. Proposed rationalization of the photocatalytic activity of Au/TiO_2 forming O_2 upon excitation of the gold surface plasmon band.

3.4 Conclusions

In this study, we have reported the unprecedented photocatalytic activity of ceria nanoparticles for oxygen generation from water. The photocatalytic activity depends on the ceria particle size, and a novel ceria preparation based on templation by alginate is reported. In addition, we have also shown that deposition of gold nanoparticles at low loading increases the photocatalytic activity for visible-light-producing samples that exhibit higher photocatalytic activity than the same material upon irradiation at its bandgap. Moreover, the ceria samples containing gold under visible light irradiation outperform the photocatalytic activity of WO_3 under UV irradiation. Our finding opens the way for using ceria as a photocatalyst for other reactions.

4

Visible light photocatalytic overall water splitting by combining gold nanoparticles supported on TiO_2 and CeO_2*

* *T. Marino, A. Primo, A. Corma, R. Molinari and H. Garcìa, submitted to Chemical Communication, 2011.*

4.1 Introduction

The photocatalytic splitting of water under visible light irradiation is a greatly desired reaction system for hydrogen production. However, powdered photocatalysts always produce a gas mixture of hydrogen and oxygen in a such splitting reaction and, thus, a separation process for the gas mixture is required before the hydrogen can be effectively utilized. Construction of a photocatalytic system enabling the separate

evolution of hydrogen and oxygen from water under visible light irradiation is, therefore, of vital interest.

In Chapter 2 has been reported that gold nanoparticles supported on titania (Au/TiO_2) is a suitable photocatalyst for the generation of hydrogen [225]. In this system gold nanoparticles act as a durable and stable photosensitizer, absorbing visible light and injecting electrons in the conduction band of the TiO_2. Also, in Chapter 3 has been shown that ceria, above of small average particle size, can behave as semiconductor with a remarkable high efficiency for the photocatalytic generation of oxygen from water [226]. The best performing CeO_2 sample was the one that was prepared using a biopolymer "alginate" as templating agent to synthesize particles upper than 5 nm of average size with a BET of 93 $m^2 \times g^{-1}$. Also in this case visible light photocatalytic activity was implemented by depositing gold nanoparticles on CeO_2 (Au/CeO_2) [226]. Considering the above precedents and the visible light photocatalytic activity for independent hydrogen and oxygen generation using Au/TiO_2 or Au/CeO_2 respectively, in the presence of appropriate sacrificial agents, it is useful that these two photocatalysts could also work in a system to perform the overall water splitting in the absence of sacrificial agents using a Z-scheme [227]. In this Z-scheme methodology, hydrogen and oxygen are generated photocatalytically in different cells that are illuminated and separated by a membrane. An electrolyte is used to ensure the

electroneutrality in each cell and to allow charge transfer from one compartment to the other. One suitable electrolyte is the Fe^{2+}/Fe^{3+} redox pair. In the present work we want to describe the overall photocatalytic water splitting using Au nanoparticles as sensitizer of TiO_2 and CeO_2 semiconductors irradiating with visible light in combination with Nafion film as membrane separating both cells and ferric sulphate as electrolyte. Nafion membrane was used as barrier between the two compartments of the reactor because of its chemical and physical properties [228] and for its affinity for iron species [229]. Ramirez et al. [229] investigated the uptake characteristic of different cations (Fe^{3+} , Cu^{2+} and Ni^{2+}) by Nafion 117 which is commonly used as separator for different chemical processes. The membrane exhibits its affinity in the order $Fe^{3+} \geq Ni^{2+} \geq Cu^{2+}$ similar to that reported in a previous study [230]. In another study [231] Nafion/Fe membrane has been reported to resist attack of the highly oxidative radical ($E°_{\cdot OH/-OH}$= 1.90 eV NHE) and does not allow leaching out of the Fe exchanged on the sulfonic groups within the 3000 hours testing period. Kiwi et al. [232] demonstrated that iron compounds supported on a nafion membrane can give good results in a photo-Fenton water treatment process, where the Fe-ions have been fixed and remain active in H_2O_2 decomposition.

4.2 Experimental

4.2.1 Photocatalyst preparation

TiO_2 was a commercial P25 sample supplied by Degussa. CeO_2 was prepared by starting from an aqueous solution of alginate that was flocculated with cerium nitrate followed by calcination as previously reported. Gold nanoparticles were deposited on TiO_2 and CeO_2 following the deposition-precipitation method starting from $HAuCl_4$ and controlling the pH value at 10 as described in detail (Chapter 2, paragraph 2.2.1) The average particle size of gold and cerium nanoparticles was determined by measuring a statistically relevant number of particles in the TEM images of the samples and resulted in 2.7 and 5.0 nm, respectively.

4.2.2 Photocatalytic tests

The Z-scheme system (Fig. 30) used for photocatalytic experiments consists of two-compartment pyrex cell, each one with a volume of 50 mL, separated by a Nafion modified membrane with an exposed membrane surface area of 3.14 cm^2. Each compartment, containing 60 mg of photocatalyst suspended in 30 mL of Milli-Q water, was irradiated with a 125 W medium pressure mercury lamp (DLU, HDLM E27)

equipped with a pyrex glass jacket which allows to maintain the system at a temperature of 20 °C. The suspensions were purged with argon flow for at least 30 minutes before irradiation in order to remove dissolved air. For polychromatic visible light irradiation an $Fe_2(SO_4)_3$ solution (3% w/v) was used as cut-off filter (λ> 400 nm). Hydrogen and oxygen generation was determined injecting 0.1 mL of each pyrex cell headspace gas in a GC (Agilent 7890A) operating at isothermal conditions (50 °C) using a capillary column (CP-PoraPLOT Q, molecular sieve, 530 μm inner diameter, 15 m length) equipped with a thermal conductivity detector and argon as carrier gas.

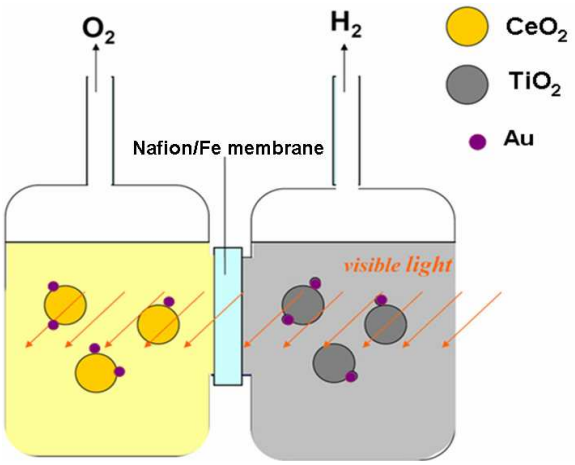

Figure 30. Schematic diagram of the twin reactor system.

4.2.3 Membrane preparation

The nafion 117 membrane (Aldrich, thickness of 178 μm) was modified using the following procedure before its use. In the first step, the membrane was boiled in a 1 M HNO_3 solution for 2 hours to remove any contaminant. Thus, the membrane was washed with Milli-Q water and then it was immersed in a 1 M NaOH solution followed by 1 M H_2SO_4 solution for 4 hours each. Finally, the membrane was immersed in a 0.5 M $Fe_2(SO_4)_3$ solution for 24 hours to change its functional groups H^+ with Fe^{3+} ions. The iron content in the membrane was extimated by SEM-EDX analysis using a Joel scanning electron microscope (JSM 6300) equipped with a SATW-window with a Si(Li) detector and applying an accelering 20 kV voltage. EDX analysis showed a loading of 1.3% before and after the membrane use. The same membrane can be used for different photocatalytic experiments without relevant changes in its efficiency.

4.2.4 Spectrophotometric iron determination

Spectrophotometric analysis were performed using 1,10-phenanthroline (Fluka, Aquanal Plus kit) with a maximum absorbance at λ= 510 nm and potassium thiocyanate (Aldrich) with a maximum absorbance at λ= 477 nm, for total iron and

ferric ions determination, respectively. Ferrous iron ions concentration present in solution was calculed by the difference between total and ferric iron concentration. UV-vis spectra were recorded using a Varian Cary-300 UV-vis specthrophotometer.

4.3 Results and discussion

In a Z-scheme membrane system, the water splitting reaction is broken up into two stages: one for hydrogen evolution and the other for oxygen evolution; these are combined by using a shuttle redox couple (Fe^{2+}/Fe^{3+}) in the solution. Over a hydrogen evolution photocatalyst (TiO_2), the photoexcited electrons reduce water to hydrogen and holes in the valence band oxidize the reductant (Fe^{2+}) to an oxidant (Fe^{3+}). The oxidant is reduced back to the reductant by photoexcited electrons generated over an oxygen evolution photocatalyst (CeO_2), where the holes oxidize water to oxygen. Scheme 7 illustrates the system used in the present work.

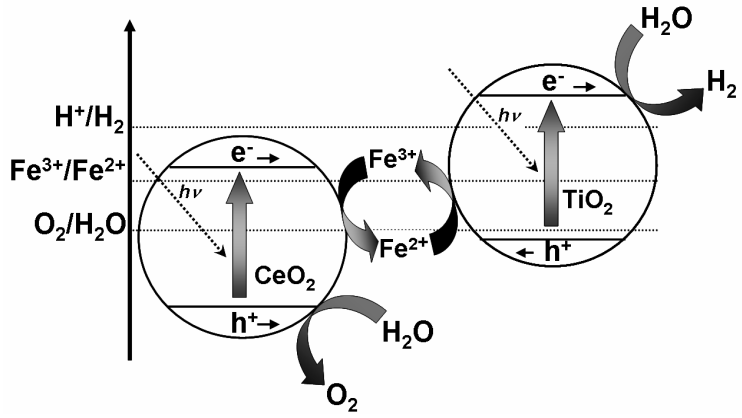

Scheme 7. Diagram of the Z-scheme overall water splitting using Au/CeO_2 as photocatalyst for oxygen generation, Au/TiO_2 for hydrogen generation and Fe^{3+}/Fe^{2+} as redox couple. Catalyst 2 g L^{-1}; pH Au/TiO_2 side: 6.5; pH Au/CeO_2 side: 2.65; Temperature: 20 °C; irradiation source for each suspension: 125 W medium pressure mercury lamp.

Before its use, we submitted the commercial Nafion film to exhaustive ionic exchange using aqueous ferric sulfate solution to introduce Fe^{3+} as counter cation of Nafion polymer. This iron containing Nafion was tested to determine its ability to allow diffusion of iron species. We carried out different experiments in which a 5 mM Fe^{2+} (or Fe^{3+}) aqueous solution (150 μmol of iron ions in 30 mL of ultrapure water) was placed in one compartment of the system and ultrapure water was placed in the other compartment. The presence of corresponding iron species in the last compartment, due to the ions diffusion, was

determined over the time. The corresponding profiles of iron species diffusing through the membrane are provided in Fig. 31.

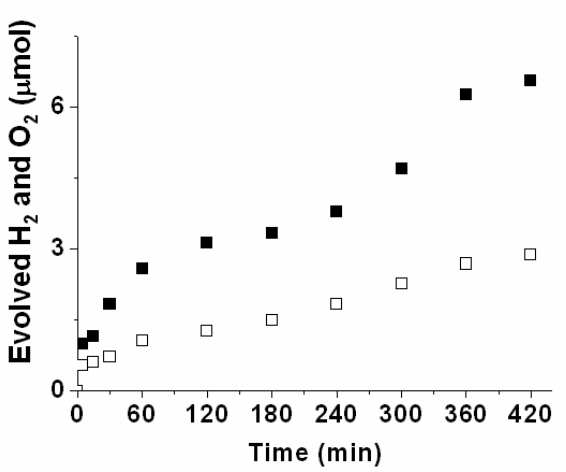

Figure 31. ■: Fe^{2+} (μmol) diffusion and □: Fe^{3+} (μmol) diffusion over the time. Iinitial concentration of Fe^{2+} or Fe^{3+}: 5 mM.

It was observed that while Fe^{3+} diffusion in the chamber containing pure water grew linearly with the time and could be fitted to a straight line, similar experiments with Fe^{2+} salt clearly reveal two regimes. We interpret these results considering that in the first regime, Fe^{2+} ions exchange Fe^{3+} in the Nafion membrane concomitantly to the diffusion to the other cell and in the second regime the Nafion membrane behaves essentially as a Fe^{2+} exchanged membrane. This interpretation was confirmed by independent experiments starting with a Fe^{2+} exchanged

Nafion membrane.

For irradiation two 125 W medium pressure mercury lamps were used. These lamps exhibit emission peaks at discrete wavelengths, mostly in the visible region (total irradiance 2133 mW/m^2 with a 61% in the visible). Preliminary photocatalytic tests were carried out using initially Fe^{2+} salt in the cell containing Au/TiO_2 and Fe^{3+} in the cell containing Au/CeO_2 However, these experiments lead consistently to the generation of oxygen in both cells (Fig. 32).

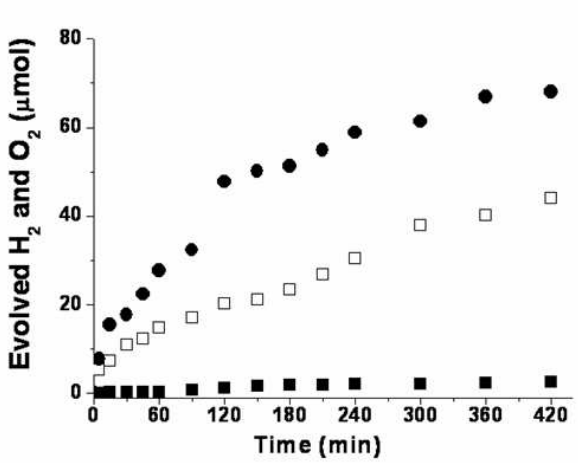

Figure 32. ●: Evolved oxygen using Au(0.25 wt%)/CeO_2; □: evolved oxygen and ■: evolved hydrogen using Au(0.25 wt%)/TiO_2. Initial concentration of Fe^{2+} (in the Au/CeO_2 side) and Fe^{3+} (in the Au/TiO_2 side): 5 mM.

We suggest that the reason why oxygen is generated in Au/TiO_2 is because Fe^{3+} salt is formed during the preparation of work-up

cell and during the early stages of the photocatalytic experiments (less than 15 min) in where hydrogen generation (instead of oxygen) is observed before changing to continuous oxygen generation. This percentage of Fe^{3+} would be quenching the generation of hydrogen and promoting the formation of oxygen, due to the preferential reduction of Fe^{3+} by photogenerated electrons with respect to the photoreduction of water. Analysis of the Fe^{3+} concentration after addition of Fe^{2+} to the Au/TiO_2 cell allowed to estimate that about 22% of Fe^{2+} ions (initial concentration: 5 mM) has became oxidized to Fe^{3+} in the process.

From the previous preliminary results advising to avoid the presence of Fe^{2+} in the Au/TiO_2 cell at the beginning of the photocatalytic reaction, we proceeded under conditions in where Fe^{3+} solution is only added to the cell containing Au/CeO_2. It should be commented that Au/CeO_2 has been found unable to generate hydrogen. It has been proposed that the reason for this is that the energy of the electrons in the conduction band of Au/CeO_2 will be not sufficient for water reduction. In contrast, these electrons of conduction band will be able to reduce Fe^{3+} to Fe^{2+}. Under the conditions in which only Fe^{3+} is added to the cell containing Au/CeO_2 we have been able to observe the simultaneous generation of hydrogen and oxygen in the Au/TiO_2 and Au/CeO_2 cells, respectively.

The concentration of electrolyte in the range from 2 to 50 mM

was tested and it was found that the best performing concentration was 5 mM (Table 7).

Table 7. Photocatalytic activity (initial reaction rate, r_0, evolved hydrogen and oxygen at 4 hours) of the series of ferric aqueous solution under study, using Au(0.25 wt%)/TiO_2 and Au(0.25 wt%)/CeO_2 for hydrogen and oxygen generation, respectively.

C_0 Fe^{3+} (mM)	Evolved $H_{2,\ 4h}$ (μmol)	Evolved $O_{2,\ 4h}$ (μmol)	H_2 $r_0 \times 10^2$ (μmol min^{-1})	O_2 $r_0 \times 10^2$ (μmol min^{-1})
2	56.2	28.1	34.2	20.7
5	166.1	75.6	114.0	53.4
10	86.2	43.0	96.3	32.5
20	43.2	24.2	34.8	21.1
50	25.5	16.3	33.4	23.5

Fig. 33 shows the temporal hydrogen evolution in the Au(0.25 wt%)/TiO_2 cell and oxygen in the Au(0.25 wt%)/TiO_2 cell when Fe^{3+} 5 mM is added in the Au/CeO_2 cell. The influence of the presence of Au in the photocatalytic performance of Z-scheme overall water splitting by TiO_2 and CeO_2 was determined by comparing the activity for the Au containing semiconductors in comparison with the same semiconductors in the absence of Au (Fig. 33).

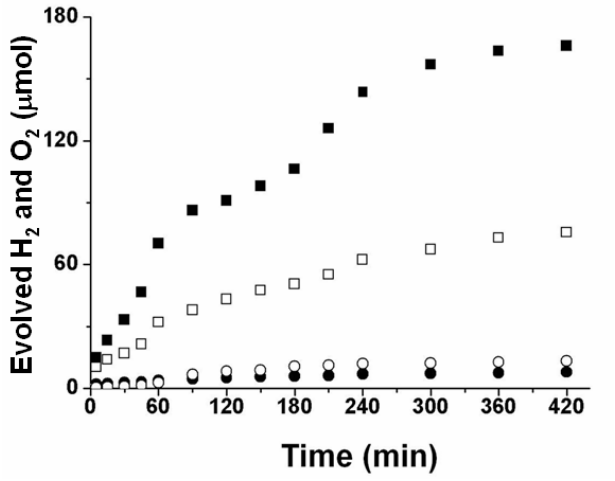

Figure 33. ■: Hydrogen and □: oxygen production using Au(0.25 wt%)/TiO_2 and Au(0.25 wt%)/CeO_2. Similar experiments using TiO_2 and CeO_2 as semiconductors for ●: hydrogen and ○**:** oxygen production, respectively, led to significantly lower photoactivity.

Even though the light used for excitation is not exclusively visible light, a positive effect of the presence of Au was observed. The Au loading plays an important role on the photocatalytic efficiency of the system. To demonstrate this point, in the present study we checked out a systems in where the Au loading on the TiO_2 and CeO_2 was the same and varied from 0.25 to 1.0 wt%. By measuring the initial rate and the final amount of hydrogen generated, it was concluded that the optimum loading under these conditions was the lowest Au content, corresponding to 0.25 wt% (Table 8).

Table 8. Photocatalytic activity (initial reaction rate, r_0, evolved hydrogen and oxygen at 4 hours) of the series of gold containing samples under study, using a 5 mM ferric solution and TiO_2 and CeO_2 as photocatalyst for hydrogen and oxygen generation, respectively.

Au loading (wt%)	Evolved $H_{2,\ 4h}$ (μmol)	Evolved $O_{2,\ 4h}$ (μmol)	H_2 $r_0 \times 10^2$ (μmol min^{-1})	O_2 $r_0 \times 10^2$ (μmol min^{-1})
0.25	166.1	75.6	114.0	53.4
0.6	152.0	61.3	112.1	70.8
1.0	71.0	25.1	67.0	32.2

Chemical analysis of the water after the reaction showed that the Au content was below the detection limit (0.1 ppm) and TEM did not reveal changes in the morphology of the photocatalyst after use. In a related precedent it has also been observed that Au loading is a key parameter controlling the photocatalytic activity of Au/TiO_2 and that there is an optimal percentage for the maximum photocatalytic activity [218]. Since the presence of Au nanoparticles is detrimental for the efficiency of TiO_2 photocatalysis under UV irradiation, but enhances the photocatalytic efficiency for visible light irradiation, we interpret the beneficial effect of Au observed here considering that under our conditions the largest contribution to the total photocatalytic water splitting is visible light. In view of the above data we propose for the water splitting the mechanism

shown in Scheme 8.

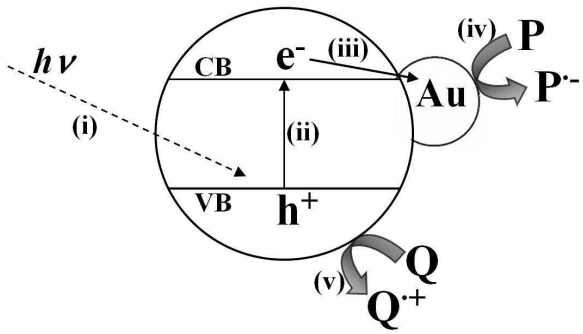

Scheme 8. Elementary steps occurring in the photocatalytic reaction upon irradiation of Au containing photocatalyst sample under UV irradiation: i) photon absorption; ii) charge separation; iii) electron migration to Au; iv) electron quenching by P; v) Q oxidation by hole.

Upon light absorption (mostly visible) electrons (in the conduction band) and holes (in the valence band) are generated in Au/CeO_2. It has been found that electrons in Au/CeO_2 are inefficient to generate hydrogen and therefore they will be captured by Fe^{3+}, forming Fe^{2+} ions that will diffuse to the Au/TiO_2 cell. The holes located on Au of the Au/CeO_2 photocatalyst have sufficient oxidation power to generate oxygen as it has been previously proved [219]. In the Au/TiO_2 cell similar charge separation as in the Au/CeO_2 cell would occur upon photon absorption, but in this case the reduction potential of TiO_2 conduction band has enough energy to form hydrogen. The holes on Au will be in this case quenched by Fe^{2+}

diffusing from Au/CeO_2 cell. To demonstrate the photocatalytic activity of the pair Au/TiO_2 and Au/CeO_2 for the overall water splitting through a Z-scheme using visible light, we performed analogous experiments filtering light to remove almost completely the wavelength below 400 nm (Fig. 34). Under these conditions the irradiance decreased from 2133 mW/m^2 to 570 mW/m^2 from UV and visible light to almost visible light. The inset of the Fig. 34 shows the emission spectrum of the lamp used.

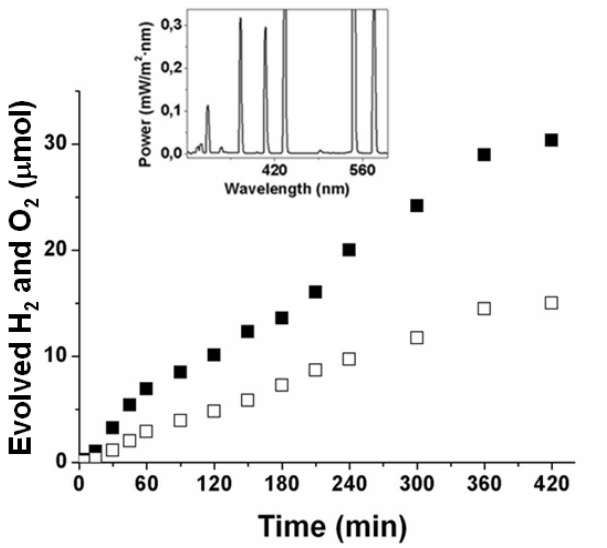

Figure 34. ■: Hydrogen and □: oxygen production using Au(0.25 wt%)/TiO_2 and Au(0.25 wt%)/CeO_2, under visible light irradiation.

Also under these conditions observation of generation of hydrogen and oxygen in stoichiometric amount in the Au/TiO_2 and Au/CeO_2 cells, respectively, was observed (Table 9).

Table 9. Photocatalytic activity (initial reaction rate, r_0, evolved hydrogen and oxygen at 4 hours) of the Au(0.25 wt%)/TiO_2 and Au(0.25 wt%)/CeO_2 samples using a 5 mM ferric solution for hydrogen and oxygen generation, respectively, under visible light irradiation.

Au loading (wt%)	Evolved $H_{2,\,4h}$ (μmol)	Evolved $O_{2,\,4h}$ (μmol)	H_2 $r_0 \times 10^2$ (μmol min^{-1})	O_2 $r_0 \times 10^2$ (μmol min^{-1})
0.25	30.36	14.89	11.0	4.2

4.4 Conclusions

Herein we have combined the reported high activity of Au/TiO_2 to generate photocatalytically hydrogen and that of Au/CeO_2 to generate oxygen from water to develop an overall water splitting operating through a Z-scheme using a Nafion membrane and Fe^{3+} as electrolyte. The obtained results had showed that Au acts as photosensitizer allowing the operation of the system with visible light.

5

Hydrogen photoproduction under visible irradiation of Au-TiO_2/Activated Carbon*

**J. Matos, T. Marino, A. García, R. Molinari and H. García, submitted to Applied Catalysis A: General, 2011.*

5.1 Introduction

The main objective of the present work is to study the photoproduction of hydrogen under ultraviolet and visible irradiation of Au/TiO_2 supported on activated carbon (AC) prepared by different activation methods in order to verify the influence of functionalization of AC upon the Au/TiO_2 photoactivity in hydrogen generation from water splitting. TiO_2 is the best catalyst for photocatalytic applications. However, two

of the most important operational limitations are that most of commercial TiO_2 has low surface area and its photoactivity is limited to UV irradiation. Several studies have been performed to solve the first limitation employing co-supports [233]. Particularly, activated carbons (AC) have shown to increase remarkably TiO_2 photoactivity for photodegradation of pollutants in waste waters and poisonous chemicals [234]. This cooperative effect has been attributed not only to the high surface area of AC but also to the low-strength of adsorption that permits the diffusion of pollutants from support to active phase [235]. Concerning to the second limitation, the influence of carbon deposits or carbon-doped titania has been studied and different points of view have been proposed [236]. Most of works suggest that enhanced photocatalytic activity on TiO_2-AC catalysts is not due to a change in band energy of semiconductor but to a remarkable influence of the functional surface groups of AC on TiO_2 optoelectronic properties, primarily by the interaction between some of these groups, mainly carboxyl anions or cyclic ethers with Ti atoms as proposed some authors and us [236]. Another way to solve the second limitation of TiO_2 corresponds to the deposition of noble metal nanoparticle exhibiting surface plasmon band as gold supported on TiO_2 because the possibility of gold photosensitization of titania by electron injection into the conduction band [237]. The combination of Au nanoparticles deposited on TiO_2 and

simultaneously supported on AC for the photoproduction of hydrogen is reported in this Chapter.

5.2 Experimental

5.2.1 Activated Carbon synthesis

AC powders were prepared from sawdust of Tabebuia Pentaphyla wood by changing experimental conditions and the activation temperature in order to introduce different physicochemical properties, mainly texture and the nature and density of the functional groups on carbon surface [238]. Physical activation by gasification under CO_2 flow at 800 ºC and pyrolysis under N_2 flow at 1000 ºC by 1 hour where firstly performed [239]. These AC were denoted AC_{CO2} and AC_{N2}. Chemical activation [240] was also performed after impregnation of the sawdust with 5% w/w aqueous solutions of $ZnCl_2$ and H_3PO_4 followed by activation under N_2 flow at 450 ºC by 1 hour. These AC, denoted as AC_{ZnCl2} and AC_{H3PO4}, were extensively washed and then dry under static air at 100 ºC by 2 hours. These conditions of synthesis for the AC were selected because they showed the highest synergy effect in presence of TiO_2 during the photocatalytic degradation of 4-chlorophenol [239,240].

5.2.2 Au/TiO_2-AC preparation

The synthesis of Au/TiO_2-AC photocatalysts was performed in a two-step procedure. Au was firstly deposited on TiO_2-P25 (Degussa) following the method described elsewhere [241]. In a typical synthesis, a solution (3 mL) of $HAuCl_4$ (0.034 g) in deionized water was brought to pH 10 by the addition of 2 mL NaOH 0.2 M. Once pH was stable, the solution was added to a slurry containing TiO_2 (0.627 g) in H_2O(12.5 mL) previously basified with 1 mL NaOH 0.2 M. After adding gold solution to the slurry, a final adjusting to pH 10 with additional 3 mL of NaOH 0.2 M was performed and the slurry was vigorously stirred for 18 hours at room temperature. After this time the solid was isolated by filtration and extensively washed until free of chloride and dried 150 min at 100 ºC. After this, the $Au\text{-}TiO_2$ catalyst was not calcined. The total Au content of the final catalysts was 2.4% as determined by chemical analysis. In a second step, Au/TiO_2-AC photocatalysts were obtained by a similar method reported elsewhere [242]. Au/TiO_2-AC samples were obtained with the relative amount of semiconductor:AC ratio, expressed in mass, i.e. 10:1, by mixing about 250 mg $Au\text{-}TiO_2$ with 25 mg AC in 80 mL of deionized H_2O and this slurry was vigorously stirred for 20 minutes at room temperature. After this, the mixture was filtered and dried by 2 hours at 100 ºC. The following photocatalysts $Au/TiO_2\text{-}AC_{CO_2}$, $Au/TiO_2\text{-}AC_{N2}$,

Au/TiO_2-AC_{ZnCl_2}, and Au/TiO_2-$AC_{H_3PO_4}$ were prepared by this method.

5.2.3 Characterization

Characterization of TiO_2, AC and Au/TiO_2-AC was performed by adsorption-desorption N_2 isotherms, surface pH (pH_{PZC}), infrared spectroscopy (FTIR), X-ray photoelectronic spectroscopy (XPS), diffuse reflectance UV-visible spectra (DR/UV-vis) and transmission electron microscopy (TEM). Textural characterization was performed by adsorption-desorption N_2 isotherms at 350 °C. The full isotherms in the range of 4×10^{-3} to 84 kPa were measured in a Micromeritics ASAP-2020. Equivalent surface area, micropore area and volume, and pore diameters were obtained by Brunauer-Emmet-Teller (BET), Harkins-Jura (HJ) and Horvath-Kawazoe (HK) methods, respectively [243]. HJ and HK were employed because they are better suited algorithms having slits and spherical shapes. Surface pH_{PZC} of bare AC were obtained by the drift method [244] by comparing the pH measured after 48 hours stirring (to achieve the equilibrium of charges) against the pH of initial buffer solutions. Fourier transformed infrared (FTIR) spectra were recorded on a spectrophotometer Magna-IR 560 from Nicolet. The powders were mixed with KBr in a 5% (w/w)

mixture. The mixed powder was pressed as tablets of 1 cm diameter at 10 tons for 1 minute. The transparent tablets were inserted in the apparatus and the spectra were recorded from 4000 to 400 cm^{-1} with a resolution on 5 cm^{-1}. KBr reference spectrum and CO_2 from ambient have been subtracted from every spectrum. Diffuse reflectance ultraviolet/visible spectra of samples (DR/UV-vis) were recorded using a UV-VIS-NIR spectrophotometer (Cary 5000 from Varian). X-ray photoelectron spectroscopy (XPS) measurements were performed on a SPECS spectrometer with a MCD-9 detector and using a non monochromatic Al Kα (1486.6 eV) X-ray source. Spectra were recorded using analyzer pass energy of 50 V, an X-ray power of 50 W and under an operating pressure of 10^{-9} mbar. Spectrum treatment has been performed using the CASA software. Binding energies (BE) were referenced to C1s at 284.5 eV. A transmission electron microscope (TEM) operating at 100 keV accelerating voltage was used also for this work for the microscopy study.

5.2.4 Photocatalytic tests

The photocatalytic experiments were carried out in the same system provided of a burette described in Chapter 2 (paragraph 2.1.3). In the photocatalytic reactions the Au/TiO_2-AC

photocatalyst powder (2.0 g L^{-1}) was dispersed in water containing 0.01 M EDTA. The total volume of the suspension was of 22.5 mL with an initial pH of 4.65. The suspension was purged with an argon flow for at least 30 minutes before irradiation in order to remove dissolved air. Then it was irradiated for 4 hours using a 200 W xenon-doped mercury lamp (Hamamatsu Lightningcure LC8, 1 cm distance). For polychromatic visible light irradiation the output of the 200 W xenon-doped mercury lamp was filtered through a cut-off filter (λ> 400 nm). Radiation was verified with a radiometer and total intensity of radiation was about to 14.1 W m^{-2} and 13.5 W m^{-2} without and with the filter, respectively. Total photon flux was estimated by the procedure described elsewhere [245] which permits to convert $W \cdot m^{-2}$ in photons$\cdot cm^{-2} \cdot s^{-1}$. The stationary temperature of the reactor, reached at 5 minutes of irradiation, was 38 °C. The formation of hydrogen was confirmed by injecting 0.5 mL of the reactor headspace gas in a gas chromatograph (HP 5890) operating at isothermal conditions (50 °C) using a semi-capillary column (molecular sieve, 530 μm diameter, 15 m length) equipped with a thermal conductivity detector and argon as carrier gas.

5.3 Results and discussion

5.3.1 TiO_2/AC Characterization

Fig. 35 shows the adsorption-desorption N_2 isotherms of the TiO_2, and the four activated carbons, AC_{CO2}, AC_{ZnCl2}, AC_{N2} and AC_{H3PO4}.

For TiO_2 a type 2 adsorption isotherm with a small and vertical hysteresis phenomenon attributed to aggregation of nanoparticles can be noticed. This isotherm corresponds to a non-porous or relatively large pore sized material in agreement with the low surface area, the negligible micropore volume and the large mean pore diameter reported in Table 10. Adsorption isotherms of AC_{CO2} and AC_{ZnCl2} correspond to a type 1. The framework of these materials is mainly composed by micropores. The small hysteresis loop observed for AC_{CO2} suggests that this sample also possesses some mesopores.

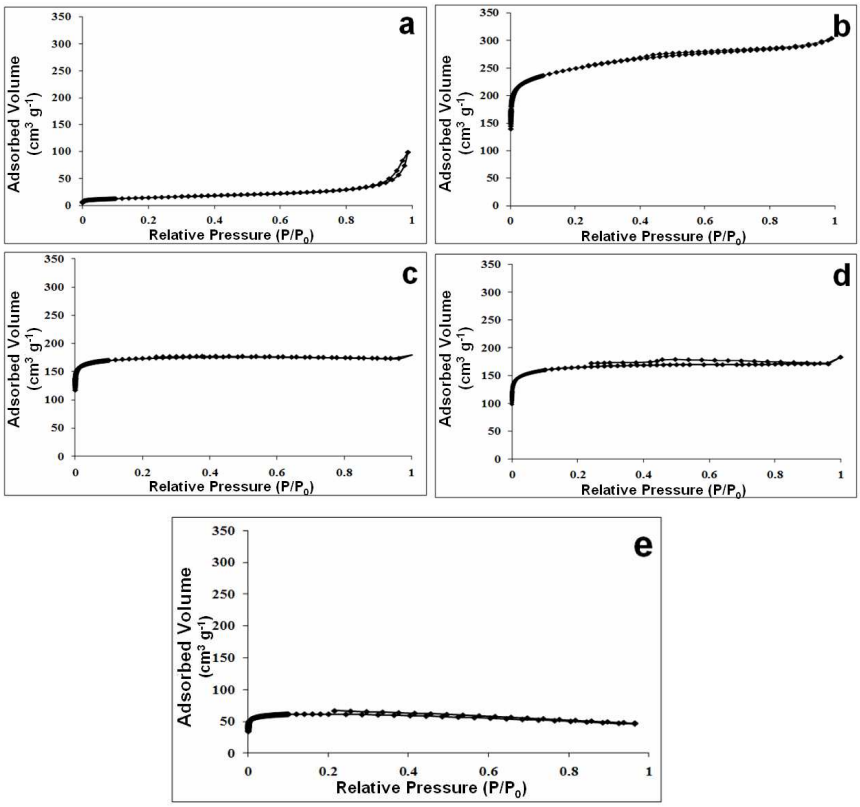

Figure 35. Adsorption-desorption N_2 isotherms; a: TiO_2, b: AC_{CO2}, c: AC_{ZnCl2}, d: AC_{N2}, e: AC_{H3PO4}.

Table 10 shows the surface pH and the textural properties of the studied materials.

Table 10. Summary of surface pH (pH_{PZC}) and textural properties of different materials. Surface BET area (S_{BET}), micropore area ($S_{\mu pore}$), micropore volume ($V_{\mu pore}$), total pore volume (V_{tot}), mean pore diameter (W_{pore}).

Support	**pH_{PZC}**	**S_{BET}** **(m^2g^{-1})**	**$S_{\mu pore}$ [a]** **(m^2g^{-1})**	**$V_{\mu pore}$ [a]** **(cm^3g^{-1})**	**V_{tot} [b]** **(cm^3g^{-1})**	**W_{pore} [b]** **(Å)**
TiO_2 P25	6.5	45.17	-0-	0.0024	0.1525	577.86
TiO_2/AC_{CO2}	6.8	86.46	49.20	0.0261	0.3752	974.01
TiO_2/AC_{N2}	6.8	60.40	13.59	0.0105	0.4159	1051.8
TiO_2/AC_{ZnCl2}	6.2	92.51	41.38	0.0249	0.4820	979.03
TiO_2/AC_{H3PO4}	6.0	63.38	21.15	0.0130	0.3881	1034.4
AC_{CO2}	8.5	942.86	912.59	0.4086	0.4702	6.30
AC_{N2}	8.9	644.27	643.09	0.2635	0.2836	5.90
AC_{ZnCl2}	6.0	689.39	687.75	0.2706	0.2720	5.90
AC_{H3PO4}	4.0	246.66	231.49	0.0889	0.1071	5.94

[a] Obtained by HJ method. [b]Obtained by HK method

AC_{ZnCl2} is composed by ca. 99% of micropores while AC_{CO2} only by ca. 87%, in agreement with the lower mean pore width found for AC_{ZnCl2} against that of AC_{CO2} (5.9 versus 6.3 Å).

This finding can be explained by taking into account the higher activation temperature in the case of AC_{CO2} which induces the destruction of certain fraction of the micropores [246]. This behaviour is the opposite for AC_{N2} and AC_{H3PO4}. In this case, H_3PO_4 is thermally decomposed during the activation leading to in situ formation of water molecules [240]. The diffusion of water molecules from the core to outside of the carbonaceous precursor has been reported to be responsible of the production of an important quantity of mesopores [247], which for the present case corresponds to about 17%. Fig. 36 shows the adsorption-desorption isotherms of TiO_2/AC_{CO2}, TiO_2/AC_{ZnCl2}, TiO_2/AC_{N2} and TiO_2/AC_{H3PO4}.

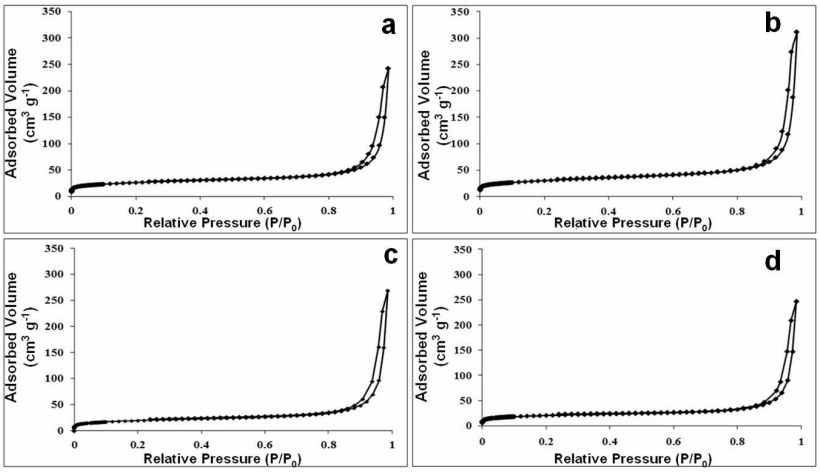

Figure 36. Adsorption-desorption N_2 isotherms; a: TiO_2/AC_{CO2}, b: TiO_2/AC_{ZnCl2}, c: TiO_2/AC_{N2}, d: TiO_2/AC_{H3PO4}.

As it can be seen in this figure the adsorption-desorption isotherms are of type 2 with a remarkably vertical hysteresis phenomenon attributable to aggregation of nanoparticles. These isotherms correspond to non-porous or relatively large porous materials. Interestingly, the values in Table 10 show that TiO_2/AC_{CO2} and TiO_2/AC_{ZnCl2} exhibit moderate surface areas and one order magnitude higher micropore volume than that of TiO_2 alone, indicating that in spite of their relative low proportion AC plays an important role in the adsorption capabilities of TiO_2/AC materials. We also notice the TiO_2/AC_{ZnCl2} sample presents higher S_{BET} value than the TiO_2/AC_{CO2}. This fact could be due to the higher micropore proportion of TiO_2/AC_{ZnCl2} with respect to AC_{CO2}. Also noticeable was that the TiO_2/AC solids have higher mean pore diameter than that of TiO_2, and this data being associated with the surface aggregation of TiO_2 nanoparticles as reported elsewhere [239]. With regards to pH_{PZC} as expected, the higher the activation or pyrolysis temperature the higher the pH_{PZC} which indicate the presence of basic functional groups on the surface of AC (Table 10). Concerning to AC prepared by chemical activation, it can be seen from Table 10 that AC prepared with H_3PO_4 showed lower pH_{PZC} values than those AC prepared with $ZnCl_2$. This data indicates that H_3PO_4 introduces more acidic groups on the AC surface as reported elsewhere [240].

- *XPS spectra*

Fig. 37 shows the XPS spectra in the region C1s of selceted catalysts: TiO_2/AC_{CO2} (Fig. 37a) and TiO_2/AC_{ZnCl2} (Fig. 37b). Data were referenced to C1s level at 284.5 eV.

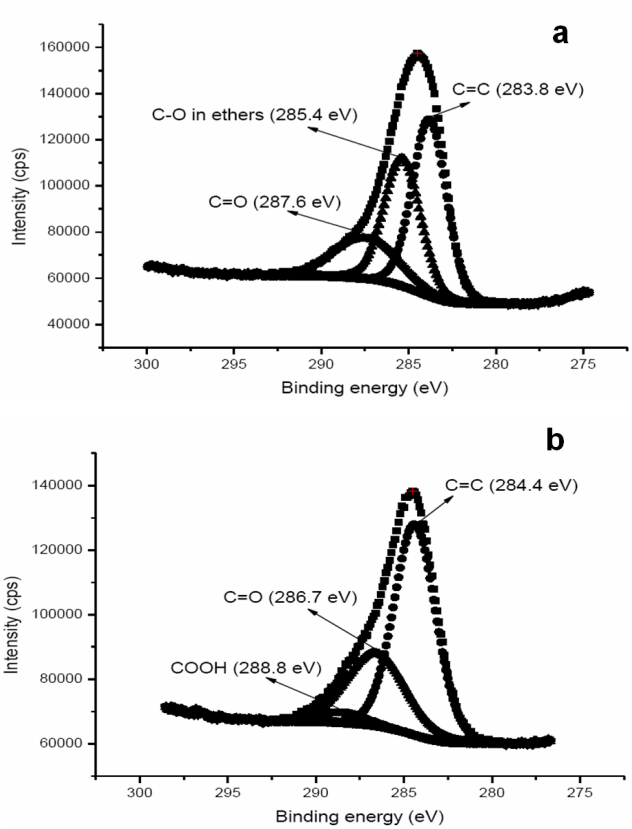

Figure 37. XPS spectra in the region C 1s; a: TiO_2/AC_{CO2}, b: TiO_2/AC_{ZnCl2}. Data were referenced to C1s at 284.5 eV.

Deconvolution of the C1s peak of the two binary solids shown in Fig. 37 clearly indicates differences in chemical composition in the surface of activated carbon [248]. XPS spectra of C1s in Fig. 37a indicated that besides the peak corresponding to the aromatic C=C bonding at about 283.8 eV [249], an important sharp peak attributed to cyclic ethers (-C-O-C) at about 285.4 eV and a broad peak reported for carbonyl groups (C=O) at about 287.6 eV [249] were introduced to the surface of AC during activation. The presence of cyclic ethers groups is in agreement with the basic surface pH (8.5) of AC_{CO2} which increases the surface pH_{PZC} from 6.5 of bare TiO_2 to 6.8 in presence of AC_{CO2} (Table 10). In the case of TiO_2/AC_{ZnCl2} material, besides the peaks of aromatic bonding (C=C) and carbonyl groups (C=O), a small peak at about 288.8 eV is detected and attributed [249] to carboxylic acids (-COOH). In other words, chemical activation by $ZnCl_2$ was able to introduce some acidic functional groups on surface of AC as indicated by the pH_{PZC} of 6.0 for AC_{ZnCl2}. The trends of the other two binary materials (TiO_2/AC_{N2} and TiO_2/AC_{H3PO4}) follow those of TiO_2/AC_{CO2} and TiO_2/AC_{ZnCl2}, respectively. A summary of the main information and binding energies (BE) obtained from XPS of the samples under consideration is compiled in Table 11.

The most important result here concerns to the fact that the BE of Ti $2p_{3/2}$ for TiO_2/AC_{ZnCl2} was clearly higher than that observed in the TiO_2 P25 alone, 459.5 eV against 458.3 eV

(Table 11) suggesting an increase in the positive charge of surface Ti atoms in this binary material. This increase in surface charge can be attributed to the remnant Zn in the carbon material. The atomic concentration (%At) of Zn from full report of XPS spectra was 0.503%, probably as graphite intercalated Zn compound [250].

Table 11. Comparison of the binding energies (BE, eV) in the C1s and Ti $2p_{3/2}$ regions.

Sample	O 1s [a]	Ti $2p_{3/2}$ [a]
TiO_2-P25	529.6	458.3
TiO_2/AC_{CO2}	529.7	458.5
TiO_2/AC_{ZnCl2}	530.92	459.5
TiO_2/AC_{N2}	529.9	458.4
TiO_2/AC_{H3PO4}	529.9	458.5

[a] BE referenced to the C1s (284.5 eV)

- *FTIR spectra*

FTIR spectroscopy is mainly used as a qualitative technique for the study of the surface chemical functional groups. Fig. 38

shows the FTIR spectra of TiO_2 against those for AC and TiO_2/AC samples.

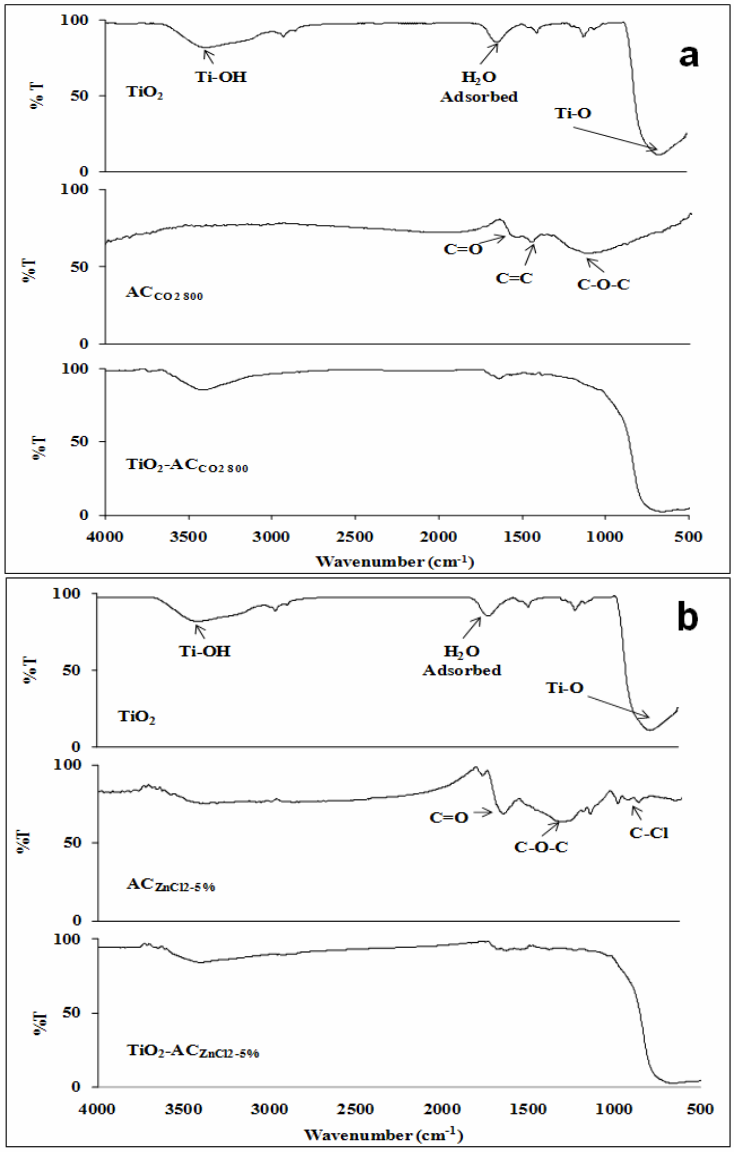

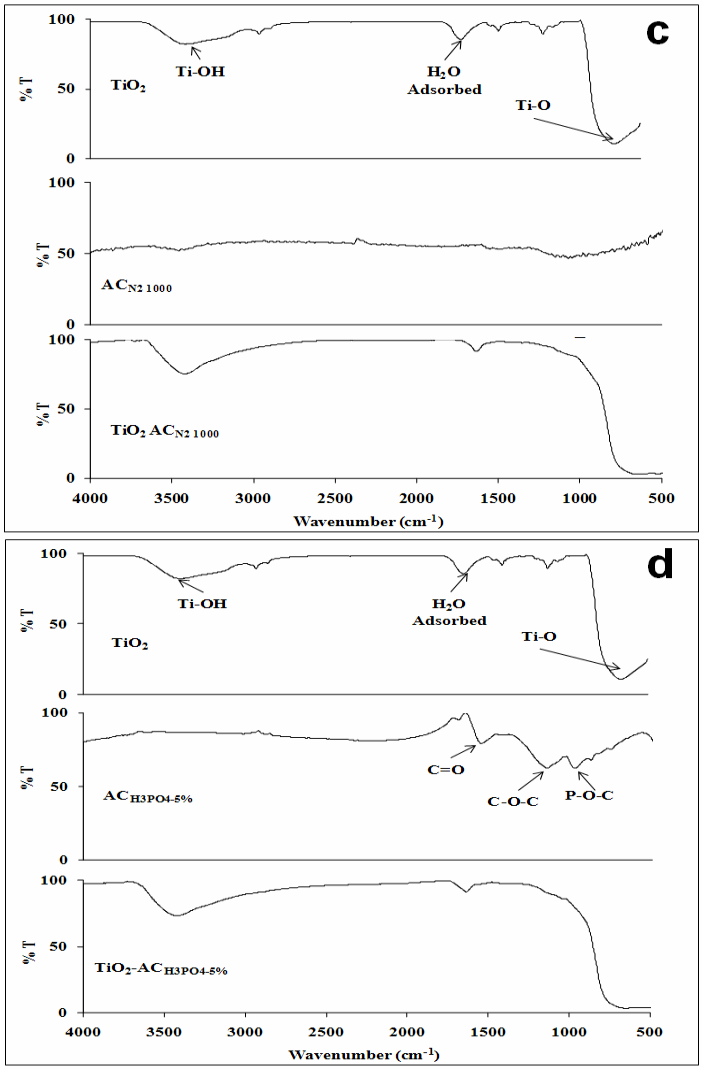

Figure 38. FTIR spectra of TiO_2 and a: AC_{CO2}, TiO_2/AC_{CO2}, b: AC_{ZnCl2}, TiO_2/AC_{ZnCl2}, c: AC_{N2}, TiO_2/AC_{N2}, d: AC_{H3PO4},TiO_2/AC_{H3PO4}.

In the case of AC_{CO2} and TiO_2/AC_{CO2}, it can be seen from Fig. 38a, that the stretching absorption band in 500-1000 cm^{-1} of the

skeletal O-Ti becomes broader in presence of AC_{CO2}. The same feature is observed in presence of AC_{ZnCl2}. This AC is characterized by the presence of a strong signal attributed to C=O at high wavenumber (1671 cm^{-1}) with two associated stretching signal at about 1114 cm^{-1} and at about 943 cm^{-1} attributed to COOH and the -C-OH stretching. The functional groups detected in the FTIR spectra of Fig. 38, mainly a mixture of cyclic ethers and carboxylic acids, are in full agreement with those discussed above in the XPS analysis. The influence of functional groups AC on TiO_2 FTIR spectra has been previously confirmed for other kind of AC [251]. For example, a band corresponding to the stretching of Ti-O-C surface was detected for the case of interaction of TiO_2 with AC [240]. In spite of ACs were washed extensively with hot water (around 80 ºC), some phosphorus and chloride remains on AC forming functional groups on its surface. From the comparison of the functional surface groups detected in the AC samples (Table 12), it can be concluded that acid functional groups as carboxylic acid and phenols practically disappeared when temperature of activation is high as in the case of 800 ºC or 1000 ºC for AC_{CO2} and AC_{N2}, respectively. This observation based on FTIR agrees with a basic pH_{PZC} as indicated in Table 10.

Table 12. Functional surface groups detected in the activated carbon of the present work.

Group or functionality (Assigment regions cm^{-1})	**Activated Carbon**			
	AC_{CO2}	**AC_{N2}**	**AC_{ZnCl2}**	**AC_{H3PO4}**
Carboxylic Acids (1120-1200, 1665-1760, 2500-3300)	x	x	✓ Medium	✓ Strong
Lactones (1160-1370, 1675-1790)	x	x	✓ Low	✓ Strong
Phenolic groups (-C-OH stretching: 1000-1220) (O-H: 1160-1200, 2500-3620 cm^{-1})	x	x	✓ Low	x
C-H stretching (2600-3000)	x	x	x	x
Quinones (1550-1680)	✓ Strong	✓ Medium	✓ Low	✓ Strong
C-O in ethers (stretching) (1000-1300)	✓ Medium	✓ Medium	✓ Strong	✓ Strong
Ketones (1600-1700)	✓ Strong	✓ Médium	✓ Strong	✓ Strong
Aromatic C-C (stretching) (1585-1600)	✓ Medium	✓ Medium	✓ Medium	✓ Strong
Others	-----	-----	C-Cl 843 cm^{-1}	P-O-C 1000 cm^{-1}

- *DR/UV-VIS spectra*

Fig. 39 shows the normalized data of the diffuse reflectance UV/visible spectra of the expansion of the gold surface plasmon band, plotted as the Kubelka-Munk function of the reflectance, for Au/TiO_2 P25 and Au/TiO_2-AC samples. The band in the visible region around 545 nm attributed to the surface plasmon resonance and ascribed to a collective oscillation of the free conduction band electrons of the gold nanoparticles in response to optical excitation, seems to be negligible influenced by the presence of AC as indicates a small increase in the reflectance of Au/TiO_2-AC in comparison of that of Au/TiO_2.

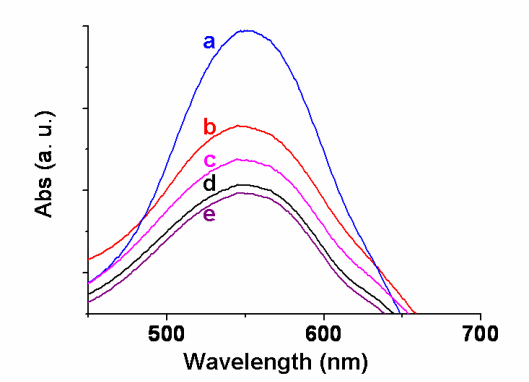

Figure 39. Diffuse reflectance UV/visible spectra, plotted as the Kubelka-Munk function of the reflectance. a: Au/TiO_2-AC_{CO2}; b: Au/TiO_2-AC_{N2}; c: Au/TiO_2-AC_{ZnCl2}; d: Au/TiO_2-AC_{H3PO4}; e: Au/TiO_2.

The normalized data of the diffuse reflectance UV/visible spectra at 545 nm showed a lightly increase on Au-TiO_2/AC_{CO2} and Au-TiO_2/AC_{N2}, while for the case of Au/TiO_2-AC_{ZnCl2} and Au/TiO_2-AC_{H3PO4}, the plasmon results very similar to that of Au/TiO_2. In other words, the absorption due to the plasmon oscillation in the metallic nanoparticles is practically the same in presence of acidic AC (AC_{ZnCl2} and AC_{H3PO4}) while it slightly increases in presence of basic AC (AC_{CO2} and AC_{N2}), suggesting that some functional groups in these AC could influence the structure of the Au nanoparticles. Accordingly to previous works [240], basic AC enhance the dispersion of TiO_2 nanoparticles and concomitantly increases the dispersion of Au nanoparticles which are distributed with very small particles sizes as we discuss below.

5.3.2 Photocatalytic tests

Preliminary runs were performed under the same experimental conditions used for the photoreactivity experiments but in the absence of catalyst or light. No activity was observed in all these cases, so it was concluded that the simultaneous presence of catalyst and irradiation is needed for the occurrence of hydrogen photoproduction. Figs. 40a and 40b show the temporal evolution of hydrogen under UV and visible light irradiation, respectively.

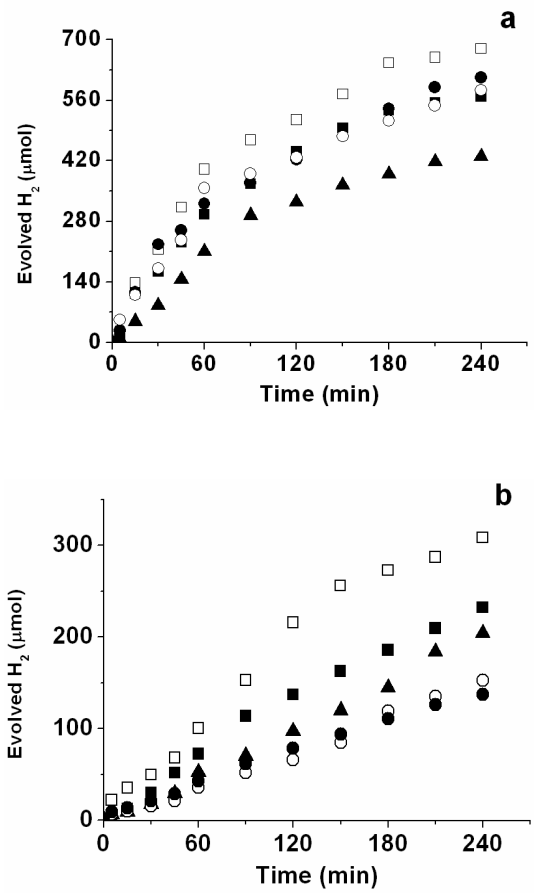

Figure 40. Hydrogen evolved during the photocatalytic runs using □: Au/TiO_2-AC_{CO2}; ▲: Au/TiO_2-$AC_{ZnCl2,}$ ■: Au/TiO_2-AC_{N2}, ●: Au/TiO_2-AC_{H3PO4}, ○: Au/TiO_2, under a: UV irradiation and b: visible irradiation. Reaction conditions: catalyst concentration: 2.0 g L^{-1}, 0.01 M EDTA, 22.5 mL H_2O.

Table 13 reports the initial reaction rates and final moles of hydrogen formed for the photocatalysts studied.

Table 13. Photocatalytic Activity (initial reaction rate, r_0, evolved hydrogen and oxygen at 4 hours) of the catalysts under study, under UV and visible light irradiation.

Catalysts	UV		Visible	
	Evolved $H_{2,\ 4h}$ (μmol)	$H_2\ r_0 \times 10^2$ (μmol min^{-1})	Evolved $H_{2,\ 4h}$ (μmol)	$H_2\ r_0 \times 10^2$ (μmol min^{-1})
$Au/TiO2\text{-}AC_{CO2}$	682.2	714.0	308.5	160.2
$Au/TiO2\text{-}AC_{ZnCl2}$	430.5	312.1	20.4.1	62.3
$Au/TiO2\text{-}AC_{N2}$	568.7	540.2	232.1	97.8
$Au/TiO2\text{-}AC_{H3PO4}$	612.6	595.0	137.4	67.1
Au/TiO_2	587.8	544.6	152.9	49.0

As expected, higher rate constants were obtained under UV irradiation than those obtained under only visible irradiation. Under visible irradiation $Au/TiO_2\text{-}AC_{CO2}$ showed higher photoactivity than that of Au/TiO_2. In addition, it should be noted that this $Au/TiO_2\text{-}AC_{CO2}$ photocatalyst also shows higher photoactivity under UV-vis irradiation than that of Au/TiO_2 alone. Moreover, AC_{CO2} is the only AC that increases the photoactivity of Au/TiO_2 under UV-Vis irradiation. In contrast,

the initial rate obtained for all Au-TiO_2/AC samples under visible light irradiation are higher than that of Au/TiO_2 alone indicating a cooperative effect between photocatalyst and AC support. No photoactivity was detected using bare TiO_2 P25 under irradiation with only visible light, the low photoactivity obtained with Au/TiO_2 indicates that the photoactivity under visible light can be attributed to the surface plasmon effect of Au nanoparticles. Comparison of the BET surface area and surface pH values (Table 10) against the initial rate (Table 13) shows no obvious relationship between these parameters. For the case of visible irradiation it seems to be the more basic the pH_{PZC} of AC the higher the photoactivity and this enhancement is in agreement with the fact that the injection of electron in the conduction band of the semiconductor is the driving-force for the hydrogen photoproduction from water. In terms of the evolved hydrogen, it can be seen from Fig. 40 that the decreasing order of evolved hydrogen after 4 hours irradiation follows the order based on the initial rate. In other words, the higher pH_{PZC} of the AC the higher the initial rate and concomitantly the higher the evolved hydrogen under visible irradiation which is in agreement with the suggestion of interaction between oxygen functional groups on the carbon surface with Ti^{+4} [252] which is strongly influenced by the gold nanoparticles on the surface. In spite that FTIR spectrum of Au/TiO_2-AC_{N2} is very similar to that of Au/TiO_2-AC_{CO2}, it

should be pointed out that Au/TiO_2-AC_{N2} shows the second best photoefficiency under any kind of irradiation. However, pH_{PZC} are very similar, and probably Au/TiO_2-AC_{N2} is less photoactive than Au/TiO_2-AC_{CO2} because two reasons, a) less surface area and b) less oxygen content in the AC_{N2} which is only about 11% against 23% in AC_{CO2}, suggesting that interaction between oxygen groups in AC_{N2} and TiO_2 would be weaker in this case compared to AC_{CO2} and TiO_2. However, it must be noted that Au-TiO_2/AC_{H3PO4} was the second more efficient in photo produce hydrogen (Fig. 40) under UV irradiation suggesting that some specific functional groups as polyphosphates could contribute to the photoactivity of Au/TiO_2. Some authors have reported that the incorporation of P atoms to TiO_2 induces an increase on the band gap [253] from 3.2 eV to 3.8 eV. Colon et al [254] also detected an higher energy band gap attributed to charges in the framework of TiO_2 as consequence of phosphates in the surface of the semiconductor. Functional groups on AC surface introduce some modifications to the surface of the TiO_2 that can lead to changes in the band gap or in the lifetime of charge separation. In other words, the cooperative effect under visible irradiation could be attributed mainly to the presence of low surface concentration of acidic oxygenated groups, particularly carboxyl anions ($-COO^-$) on AC's surface which would coordinate to Ti^{+4} metallic centre of TiO_2. Regarding the stability of gold nanoparticles, the Fig. 41 shows TEM images

of Au/TiO_2-AC_{CO2} before irradiation (Fig. 41a) and after 18 hours irradiation with visible light (Fig. 41b).

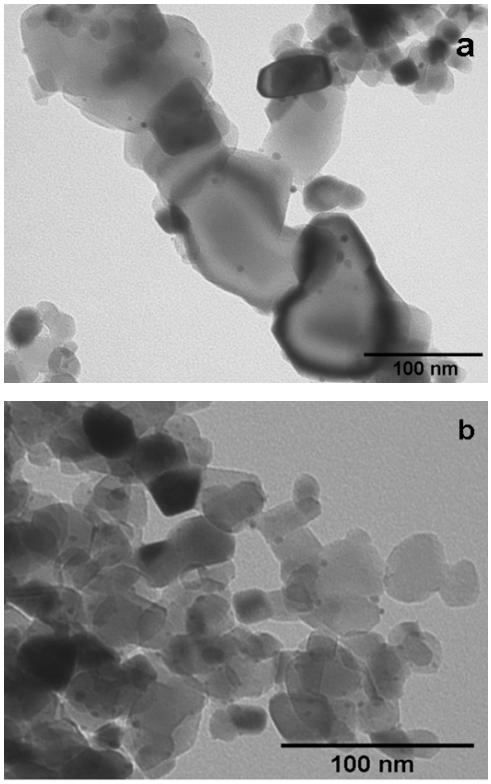

Figure 41. TEM images of Au/TiO_2-AC_{CO2}, a: before irradiation and b: after 18 hours irradiation with visible light.

In both cases, it can be seen a narrow distribution of particle sizes of Au nanoparticles on TiO_2 surface. For example, sizes from 2.4 to 4.8 nm and from 2.3 to 4.60 nm were characterized with mean size values of about 3.36 ± 0.89 nm and 3.39 ± 0.83

nm before and after 18 hours irradiation, respectively. In other words, irradiation with visible light does not seem to influence the stability of gold nanoparticles in the Au/TiO_2-AC_{CO2} photocatalysts. This is in agreement with the very low quantity of Au detected from the leaching experiments of photocatalysts after 4 hours under UV-Vis or visible irradiation which in most of the cases was less than 0.1% of the initial Au composition (2.4% w/w) of photocatalysts. Additional experiments were conducted only under visible irradiation to verify the influence of the TiO_2/AC mass ratio different than 10:1 on the Au/TiO_2-AC_{CO2} efficiency. Additional samples were prepared with TiO_2/AC mass ratio equal to 5:1 and 20:1 and Fig. 42 shows the kinetics of evolved hydrogen as a function of this parameter. Hydrogen evolution rate obtained for Au/TiO_2 P25 were also included for comparative purposes.

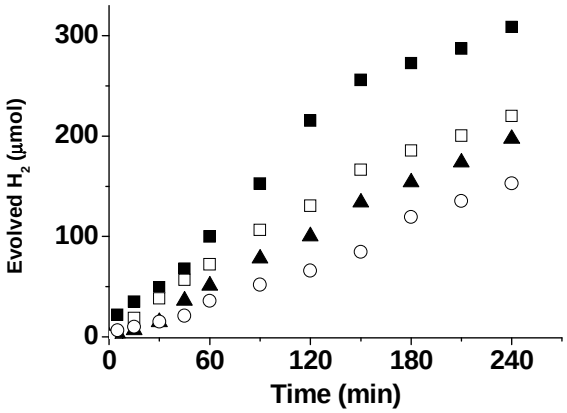

Figure 42. Evolved hydrogen under visible irradiation as a function of the mass ratio Au-TiO_2:AC_{CO2}. □: Au/TiO_2-AC_{CO2}(5:1), ■: Au/TiO_2-AC_{CO2}(10:1), ▲: Au/TiO_2-AC_{CO2}(20:1), ○: Au(2.0 wt%)/TiO_2. Reaction conditions: catalyst concentration: 2.0 g L^{-1}, 0.01 M EDTA, 22.5 mL H_2O, cut-off filter (λ > 400 nm).

It can be seen in Fig. 42 than in any of the three samples conformed by Au/TiO_2-AC_{CO2}, the photoproduction of hydrogen was higher than that obtained using Au/TiO_2 P25 without AC. In terms of initial rate the photoactivity show the following order: Au/TiO_2:AC_{CO2}-10:1> Au/TiO_2:AC_{CO2}-5:1> Au/TiO_2:AC_{CO2}-20:1> Au/TiO_2. In other words, maximum photoactivity was found for the mass ratio Au/TiO_2:AC_{CO2} equal to 10:1 (Table 14).

Table 14. Photocatalytic Activity (initial reaction rate, r_0, evolved hydrogen at 4 hours) of the catalysts under study, under visible irradiation.

Catalysts	Evolved $H_{2,\ 4h}$ (μmol)	$H_2\ r_0 \times 10^2$ (μmol min^{-1})
Au/TiO_2-AC_{CO2}(5:1)	220.1	126.0
Au/TiO_2-AC_{CO2}(10:1)	308.5	160.2
Au/TiO_2-AC_{CO2}(20:1)	197.2	70.0
Au/TiO_2	152.9	49.0

It must be noted the remarkable decrease in the photoactivity at values higher than this maxima and this phenomenon was firstly found to be 5:1 by Matos and Herrmann [235] for the case of phenol photodegradation in aqueous phase and found to be 10:1 by Matos and Marci [242] for the 2-propanol photooxidation in gas-solid regime employing mixtures of binary materials TiO_2/AC. These authors explain this behaviour considering the formation of a common contact interface between both solids which is not accessible to water molecules and consequently the total number of adsorbed molecules on the photocatalyst decreases with the concomitantly decrease in the photoactivity.

5.4 Conclusions

Hydrogen photoproduction has been performed under visible irradiated Au/TiO_2 combined with activated carbon prepared by different activation methods and compared against ultraviolet irradiation. Characterization of TiO_2/AC suggests that carboxylate anions and other basic groups detected on surface of AC interact with the surface Ti atoms of TiO_2 and this surface interaction would be responsible of the enhancement in the photoactivity mainly under visible light irradiation. AC with basic pH enhanced the photoactivity of Au/TiO_2 for the production of hydrogen under only visible light irradiation up to a maxima factor of about 2.6 times higher than that on Au/TiO_2 and infinitely in comparison of TiO_2 in absence of Au. The present results suggest the possibility to study Au/TiO_2 photocatalysts supported on basic AC on real solar conditions.

6

Positive influence of gold nanoparticles on the photocatalytic activity of TiO_2 for the hydroxylation of benzene by water.*

**T. Marino, R. Molinari and H. Garcìa, submitted to Catalysis Today, 2011.*

6.1 Introduction

In contrast to the numerous studies using photocatalysis for pollutant degradation, reports describing photocatalytic processes for the synthesis of valuable organic compounds are considerably less abundant. The term “positive photocatalysis” denotes those processes targeted to the synthesis of a chemical and it is opposed to the term “negative” photocatalysis used to refer to those processes effecting the degradation of pollutants [255]. In principle considering the high reactivity of electrons,

holes and hydroxyl radicals as well as other reactive oxidizing species, one should expect that photocatalysis would also be applicable in organic synthesis (positive photocatalysis). One specific reaction of hydroxyl radicals is its electrophilic attack to benzene giving rise to phenol as the primary product. Benzene is a fairly stable aromatic compound that is reluctant to undergo electrophilic attack. However, the high reactivity of hydroxyl radicals makes the process thermodynamically possible. The main problem of the process of phenol formation from benzene by the attack of hydroxyl radicals is the low selectivity due to the fact that phenol is not stable under the reaction conditions and undergoes consecutive reactions with hydroxyl radicals to give secondary products such as hydroquinone, resorcinol and benzoquinone. In despite of the low selectivity generally obtained for the hydroxyl radical-mediated synthesis of phenol, the main advantage of this process is the convenience and the availability of the starting materials that would be unsubstituted benzene and a source of ˙OH radicals. In the present case to generate the ˙OH radicals we have used the photocatalytic water splitting using gold supported on titania as semiconductor.

The aim of this work is to show that by deposition of small amounts of gold nanoparticles on TiO_2, remarkable differences in the photocatalytic activity and selectivity can be observed. The yield of phenol almost doubles by selecting the appropriate gold loading. Compared to the commercial route for phenol

formation based on cumene oxidation and subsequent sulfuric acid rearrangement [256], the photocatalytic process reported here only uses water as a source of hydroxyl radicals and benzene. Also compared to the ENI process of catalytic benzene oxidation using hydrogen peroxide as oxidant reagent [257], the direct photocatalytic oxidation of benzene has the advantage that does not require any chemical oxidizing reagent except water and the "TiO_2" photocatalyst is considerably more robust compared to titanium silicalite that is the catalyst employed in the ENI process. Recent studies report that selective phenol production is achieved in some TiO_2 systems [258, 259]. Choi et al. [260] reported the photoirradiation of water containing 4% of acetonitrile and benzene with TiO_2 in presence of polyoxometalate ($PW_{12}O_40^{3-}$) obtaining the selective phenol production with relatively high yield (11%), although the mechanism is not clarified. Langford et al. [261] found that TiO_2-loaded ZSM-5 zeolite irradiated in an aerated aqueous solutions (pH 11) containing benzene produce phenol with 21% selectivity, probably due to the lower affinity of phenol on the catalyst surface. Recently, there is some controversy about whether or not the presence of gold increases or decreses the catalytic activity of TiO_2 [262]. While for cyclohexane oxidation it has been found that gold decreases the photocatalytic activity of TiO_2 due to the reduction of surface hydroxyl groups involved in the generation of hydroxyl radicals [263], Garcìa and co-

workers have shown that for visible light water splitting [225] and photocatalytic Fenton reaction [264], the presence of gold introduces visible light photocatalytic activity that is not present in plain TiO_2. In view of the economical importance of the process there is a considerable interest in assessing if, for the photocatalytic transformation of benzene into phenol, gold nanoparticles play or not a positive role enhancing the yield of phenol in respect that achieved for unmodified TiO_2.

6.2 Experimental

6.2.1 Materials

Samples containing gold in different percentages were prepared by deposition of gold from aqueous solutions of $HAuCl_4$ (Alfa Aesar) over suspended TiO_2 (P25 Degussa). Sodium hydroxide (NaOH, purity 98%) for the preparation of gold-containing TiO_2 samples was from Sigma. Benzene (C_6H_6, purity 99.8%) was from Carlo Erba Reagenti. Phenol (C_6H_5OH, purity 99.99%), benzoquinone ($C_6H_4O_2$, purity 99.9%), biphenyl ($C_{12}H_{10}$, purity 99.99%), hydroquinone ($C_6H_6O_2$, purity 99%), resorcinol ($C_6H_6O_2$, purity 98%) and catechol ($C_6H_6O_2$, purity 99.5%) for analytical calibration were from Sigma–Aldrich.

6.2.2 Photocatalyst preparation

For the present work we used four similar samples in which gold nanoparticles have been deposited in the surface of TiO_2. The sample preparation is based on the conventional deposition-precipitation method that has proved to be a suitable experimental procedure for the obtainment of small gold nanoparticles with average dimension below 10 nm and strongly bound to the TiO_2 surface [225], chemical Au analysis in the Au/TiO_2 samples showed that the gold content varies from 0.25 to 2.2 wt%.

6.2.3 Characterization

Photocatalyst samples were characterized using the following techniques: diffuse reflectance UV−vis−NIR spectra, TEM, XRD, Raman spectra (Chapter 2, paragraph 2.2.2). Gas chromatograph mass spectrometer from Shimadzu (GC–MS QP2010S) was used to identify the oxidation products of the photocatalytic tests. Phenol and oxidation by-products concentrations in the aqueous and organic phases were determined by high performance liquid chromatography (HPLC, Agilent 1100 Series instrument) using a Kinetex C18 (50 mm x 2.1 mm) column by UV detector monitoring 265 nm.

The mobile phase consisted of water/acetonitrile 70/30 (v/v) containing 0.1% formic acid fed to a flow-rate of 0.5 mL min^{-1}. The column pressure was 155 bar and the injection volume was 20 μL. All the aqueous samples were filtered by means of a low adsorbing hydrophilic polypropylene membrane (Pall Corporation, mean pore size 0.2 mm) before carrying out the analyses. Ultrapure water used throughout the work was obtained from Milli-Q equipment by Millipore. The UV light intensity was measured by a UVX Digital Radiometer (from UVP).

6.2.4 Photocatalytic tests

Photo-oxidation experiments were carried out in batch reactor equipped with a Pyrex glass jacket at a constant temperature of 25 °C. A 500 W medium pressure Hg lamp (Helios Italquartz) emitting in the UV–Vis range (λ_{max} = 366 nm, emission profile between 240 and 440 nm) with an intensity of 6.0 mW cm^{-2} was placed above the reactor.

The reactive solution consisted of 500 mL of ultrapure water containing the suspended catalyst and 5 mL of benzene. pH was measured using a WTW Inolab Terminal Level pH meter with a glass pH electrode SenTix.

The reactive solution, magnetically stirred, was constituted by 500 mL of ultrapure water containing the suspended catalyst and 5 mL of benzene.

6.3 Results and discussion

6.3.1 Characterization

The presence of Au nanoparticles on Au/TiO_2 can be ascertained by the TEM images of the samples. TEM also allows to estimate that titania crystallites have about 20 nm particle size that is a common dimension for many titania photocatalysts. As an example Fig. 43 shows selected TEM images obtained for Au/TiO_2 samples and the corresponding statistical size distribution.

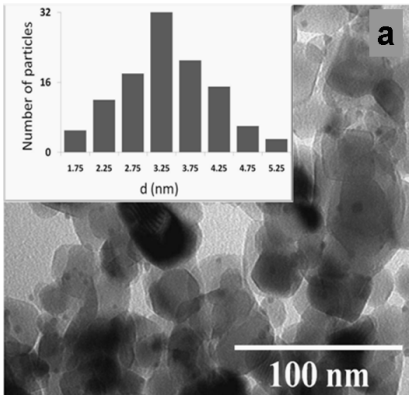

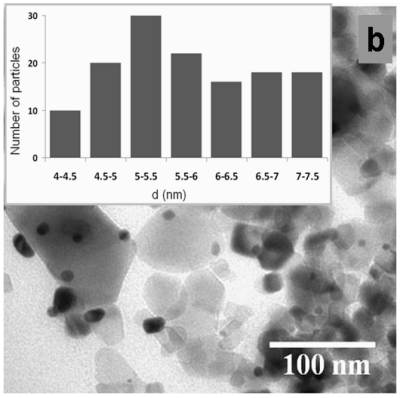

Figure 43. TEM images and corresponding particle size distribution histograms of two selected Au/TiO_2 samples varying in the Au content. a: Au(1.5 wt%)/TiO_2) and d:Au(2.2 wt%)/TiO_2.

Table 15 lists the samples used in this study and their relevant physical-chemical data.

Table 15. List of photocatalysts used in the present study and their corresponding gold loading, calcinations temperature (T_{calc}), particle size (d) and wavelength of the surface Plasmon band (λ_{max}).

Photocatalyst	T_{calc} (ºC)	d_p (nm)	λ_{max} (nm)
TiO_2	--	21.0	320
Au(0.25 wt%)/TiO_2	200	1.80	548
Au(1.0 wt%)/TiO_2	200	2.57	550
Au(1.5 wt%)/TiO_2	200	3.42	543
Au(2.2 wt%)/TiO_2	200	5.70	547

The presence of gold nanoparticles in the four made Au/TiO_2 samples was additionally confirmed by powder X-rays diffraction (XRD), as shown in Fig. 44. Even though the gold content is low, the higher gold atomic weight relative to titanium makes XRD to be more sensitive for this heavier element. Two peaks at 2θ value of ca. 38.2° and 44.1° were observed revealing the presence of metallic gold (Au) particles into TiO_2. The crystalline phase of the support could also be determined by XRD analysis. In particular, we found that to be preferentially anatase, which is the almost active phase of titania, although peaks corresponding to rutile phase were also observed.

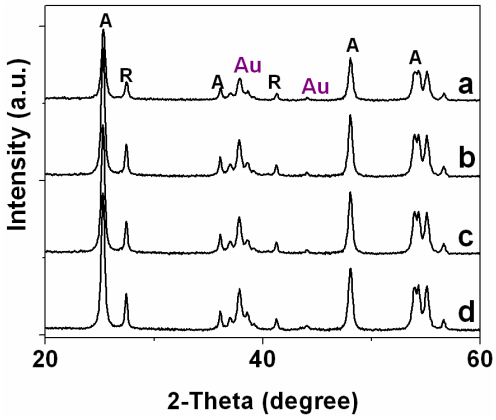

Figure 44. XRD patterns obtained for a: Au(0.25 wt%)/TiO_2, b: Au(1.0 wt%)/TiO_2, c: Au(1.5 wt%)/TiO_2) and d: Au(2.2 wt%)/TiO_2. A: anatase, R: rutile.

The Raman spectra with the assigned vibration peaks for the gold containing catalysts are shown in Fig. 45. At 146 cm^{-1} a well resolved TiO_2 Raman peak is present for all the studied photocatalysts. The presence of the characteristic band at 197, 395, 515 and 640 cm^{-1} confirmed the predominant crystalline phase for the substrate being anatase. However, a broad peak at 448 cm^{-1} is attributable to the rutile phase.

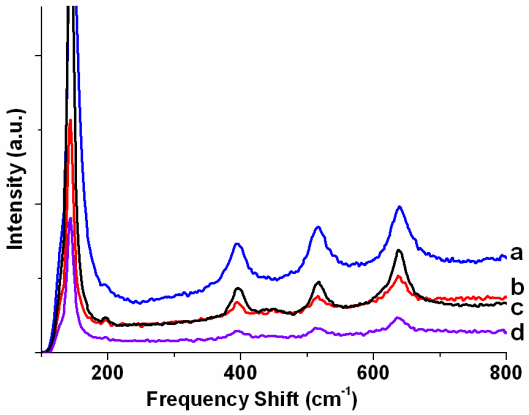

Figure 45. Raman spectra. a: Au(1.0 wt%)/TiO_2, b: Au(2.2 wt%)/TiO_2, c: Au(0.25 wt%)/TiO_2, d: Au(1.5 wt%)/TiO_2).

6.3.2 Photocatalytic tests

The photocatalytic formation of phenol was carried out under batch conditions by irradiating benzene-saturated aqueous suspensions of the corresponding photocatalysts (1.77 g/L) using the output of a medium pressure mercury lamp through pyrex glass. The course of the photocatalytic reactions was followed by analyzing phenol and the byproducts derived from it (hydroquinone, resorcinol, benzoquinone). Fig. 46 shows the temporal evolution of phenol formation depending on the photocatalysts. From this plot it can be seen that TiO_2 is at initial time the most efficient catalyst exhibiting the highest initial reaction rate. However, after 90 minutes irradiation in the presence of TiO_2 the phenol concentration reaches a plateau and finally decreases at longer reaction times. This indicates that TiO_2 is unselective and starts converting phenol into byproducts at lower concentrations than the Au/TiO_2 samples. In contrast all the gold containing photocatalysts exhibit much lower initial reaction rate and in some cases an induction period can even be seen (see inset of Fig. 46).

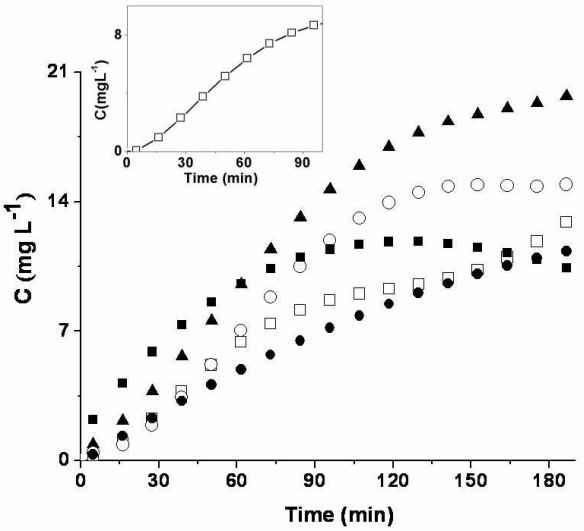

Figure 46. Temporal evolution of phenol concentration for the photocatalytic hydroxylation of benzene (1.77 mgL^{-1}). ■: TiO_2, □: Au(0.25 wt%)/TiO_2 , ▲: Au(1.0 wt%)/TiO_2 , ○: Au(1.5 wt%)/TiO_2 , ●: Au(2.2 wt%)/TiO_2. The inset shows an expansion of the profile for Au(0.25 wt%)/TiO_2 .

We think that this induction period reflects that the first hydroxyl radicals formed are surface bound and react with the photocatalyst producing changes in the either TiO_2 or Au or Au/TiO_2 interface without affecting benzene. After this induction period the photocatalysts equilibrate and then free $^{\cdot}OH$ radicals became available in the solution to attack benzene.

Concerning the influence of Au loading, Fig. 46 shows that Au/TiO_2 samples give higher phenol yield than that reached with TiO_2. In particular the highest phenol yield was achieved

for Au/TiO_2 at 1.0 wt% Au loading. For this Au(1.0 wt%)/TiO_2 the yield of phenol is almost doubles to that obtained for unmodified TiO_2.

This influence of Au decreasing the initial reaction rate, exhibiting an induction period but reaching high phenol yield suggests that gold nanoparticles are acting as catalytic sites controlling the reactivity of photochemically generated ·OH radicals and preventing or disfavouring the subsequent secondary reactions of phenol to hydroquinone, resorcinol and benzoquinone.

Concerning these secondary byproducts, the yields of hydroquinone and resorcinol are relatively low and always below 5%. In contrast, the concentration of benzoquinone can be significantly higher than the other two dihydroxy benzene isomers. Fig. 47 shows the temporal profile of benzoquinone yield depending on the photocatalysts used. As it can be seen there, benzoquinone can reach a significant concentration at final reaction times with similar yield for TiO_2 and Au/TiO_2 at 1.0 wt% loading. This similar benzoquinone concentration contrasts with the higher phenol yield attained for Au/TiO_2 at 1.0 wt% gold loading and could indicate that the conversion of phenol into benzoquinone is slower for the Au containing catalyst.

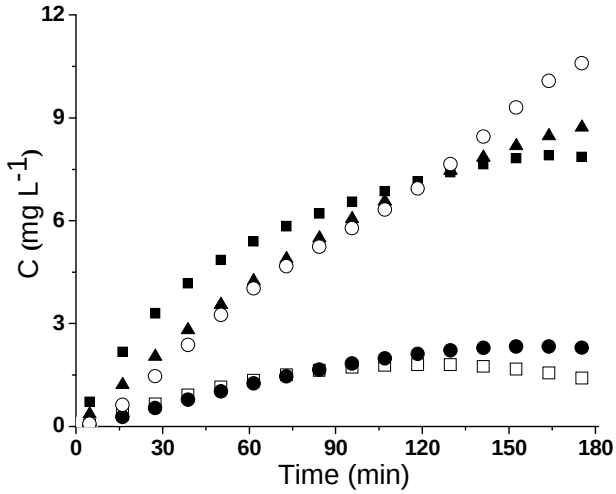

Figure 47. Temporal evolution of benzoquinone yield for the photocatalytic irradiation of benzene in presence of ■: TiO_2, □: Au(0.25 wt%)/TiO_2 , ▲: Au(1.0 wt%)/TiO_2 , ○:Au(1.5 wt%)/TiO_2 , ●: Au(2.2 wt%)/TiO_2.

Concerning catalyst deactivation, in a previous our work [225] in which ·OH radicals came from water, no significant reduction in the activity of the catalyst powders were observed. Reusability of The Au/TiO_2 catalysts after their first use, showed that the same kinetic profile was obtained. Moreover, after two consecutive uses the filtered catalyst was characterized by chemical analysis and electron microscopy without observing changes with respect to those of the fresh catalyst [225].

6.4 Conclusions

The present results have shown that Au nanoparticles at an appropriate loading can exert a positive influence on the photocatalytic performance of TiO_2 for benzene hydroxylation. Although the presence of Au decreases the initial reaction rate, at longer reaction times higher phenol concentrations are obtained for gold containing photocatalysts even though the yield of benzoquinone is similar in both cases.

Thus our finding illustrates again the beneficial influence of the presence of gold nanoparticles supported on titania at low loadings in photocatalysis.

Conclusions

The present study demonstrates the possibility to carry out the water splitting reaction in a membrane reactor and the partial oxidation of benzene into phenol in a batch reactor, to obtain a very sustainable technology in chemical energy production and in organic synthesis. Heterogeneous photocatalysis represents a very promising method that offers the possibility to use two of the main renewable sources, solar light and water, to make chemical processes of increasing interest. Different gold containing catalysts, prepared by the deposition-precipitation method, were employed in the water splitting reaction to generate hydrogen or oxygen under UV and visible light irradiation, using a commercial titanium dioxide or a synthetized cerium oxide as support, respectively. By using visible monochromatic or polychromatic excitation that ensures that light is absorbed exclusively by gold nanoparticles we have demonstrated that gold can have an additional role as light harvester besides gas evolution center. We propose that gold nanoparticles absorb photons and inject electrons into the semiconductor conduction band, due to a quantum size effect of the nanometric metal size. Electrons in the titania conduction band and holes in certain gold nanoparticles could have adequate relative potentials to generate hydrogen and oxygen from water, respectively. We have also found that different

parameters, like gold particle size, pH and calcination temperature influence the catalytic activity. Apparently the combination of appropriate loading, small particle size and low calcination temperatures favors the photocatalytic activity of the materials. A novel biopolymer-templating methodology was developed to synthesize nanoparticulated ceria. The resulting nanoparticulated catalyst exhibits high photoactivity as a semiconductor and when it contains appropriate gold loadings is a stable and efficient photocatalyst for oxygen evolution under visible light irradiation. The overall water splitting reaction was studied in a Z-scheme device. Simultaneous hydrogen and oxygen generation was performed by irradiating Au/TiO_2 and Au/CeO_2 aqueous suspensions separated by a modified Nafion membrane and using Fe^{3+}/Fe^{2+} as redox couple. A stoichiometric amount of hydrogen and oxygen under polychromatic visible light irradiation was obtained. Water splitting reaction to generate hydrogen was also studied employing Au/TiO_2 catalysts supported on activated carbons that were prepared by thermal and chemical methods, under UV and visible light irradiation. The achieved data showed that the performance of Au/TiO_2 supported on activated carbon could be enhanced under visible light when basic groups are present on the carbon surface.

Application of gold supported photocatalysts was also investigated in the one step photooxidation of benzene to

phenol. The organic synthesis was carried out in a batch reactor using several Au/TiO_2 samples. The results of photocatalytic experiments showed that gold play a positive role in the efficiency of the process, enhancing the final yield of phenol compared to that obtained with bare TiO_2. The major drawback of the process is still the low selectivity of the process and the formation of secondary oxidation products such as benzoquinone, for all the used photocatalysts.

The research study conducted during the PhD course evidences the positive role of gold nanoparticles supported on titania or ceria at low loadings in photocatalytic processes and suggest the possibility to use solar light to carry out environmentally sustainable processes.

References

[1] Fujishima, K. Honda, Nature 238 (1972) 37.

[2] A. Strini, Schiavi L., Applied Catalysis B: Environmental, 103 (2011).

[3] Q. Geng , Chen N., Chemical Engineering and Technology, 34 (2011) 400.

[4] Q.L. Yu, M.M. Ballari, H.J.H. Brouwers, Applied Catalysis B: Environmental, 99 (2010) 58.

[5] D. Gumy, C. Morais, P. Bowen, C. Pulgarin, S. Giraldo, R. Hajdu, J. Kiwi, Applied Catalysis B: Environmental, 63 (2006) 76.

[6] D.M. Blake, Maness P., Huang Z., Wolfrum E.J., Huang, J., Separation and Purification Technology, 28 (1999) 1.

[7] G. Petriconi, H. M. Papee, Water, Air, & Soil Pollution, 20 (1983) 273.

[8] E. Kabachkov, E. Kurkin, V. Nadtochenko, A. Terentyev, Journal of Photochemistry and Photobiology A: Chemistry, 217 (2011) 425.

[9] T. Xuliu, X. Zhongli, A. Baili, Environmental Science and Technology, 42 (2008) 4540.

[10] Y. Y. Hsu , T.L. Hsiung, H. P. Wang, Y. Fukushima, Y.L. Wei, J.E. Chang, Marine Pollution Bulletin, 57 (2008) 873.

[11] R. A. Al-Rasheed, SWCC Acquired Experience Symposium held in Jeddah, 2005.

[12] D. Ravelli, D. Dondi, M. Fagnoni, A. Albini, Chemical Society Reviews, 38 (2009) 1999.

[13] L. Palmisano, A. Sclafani. Wiley & Sons, Chichester, (1997) 109.

[14] M. R. Hoffmann, S. T. Martin, W. Choi, D. W. Bahnemannt, Chemical Reviews, 95 (1995) 69.

[15] M. Litter, Applied Catalysis B: Environmental, 23 (1999) 89.

[16] G. Palmisano, V. Augugliaro, M. Pagliaro, L. Palmisano, Chemical Communication, 33 (2007) 3425.

[17] M. D. Ward, J. R. White, A. J. Bard, Journal of the American Chemical Society, 105 (1983) 27.

[18] M. Ni, M. K. H. Leung, D. Y. C. Leung, K. Sumathy, Renewable and Sustainable Energy Reviews.

[19] K. Kabra, R. Chaudhary, R. L. SawhneyInd., Industrial & Engineering Chemical Research, 43 (2004), 7683.
[20] S. J. Teichner, Journal of Porous Materials, 15 (2008) 311.
[21] T. E. Agustina, H. M. Ang, V. K. Pareek, Chemical Engineering Journal 135 (2008) 151.
[22] S. Bekkouche, M. Bouhelassa, N. Hadj Salah, F.Z. Meghlaoui, Desalination, 166 (2004) 355.
[23] V. Subramanian,V.G. Pangarkar, A.A. Beenackers, Clean Product and Processes 2 (2000) 149.
[24] T. Y. Wei, C.C. Wan, Industrial & Engineering Chemical Research, 30 (1991) 1293.
[25] G. A. Parks, Chemical Reviews 65 (1965) 177.
[26] Colloidal Dynamics Inc., ZetaProbe Application, Determining the Isoelectric Point (IEP), Warwick, Rhode Island, USA, (2002).
[27] T. Sreethawong, T. Puangpetch, S. Chavadej, S. Yoshikawa, Journal of Power Sources, 165 (2007) 861.
[28] D.S. Bhatkhande, V.G. Pangarkar, A.A.M.C. Beenackers, Journal of Chemical Technology and Biotechnololy, 77 (2001) 102.
[29] E. Evgenidou, K. Fytianos, I. Poulios, Journal of Photochemistry and Photobiology A: Chemistry, 175 (2005) 29.
[30] K. Schoumacker, C. Geantet, M. Lacroix, E. Puzenat, C. Guillard, J. M. Hermann, Journal of Photochemistry and Photobiololgy, 152 (2002) 147.
[31] M. Nikazar, K. Gholivand, K. Mahanpoo, Desalination, 219 (2008) 293.
[32] M. A. Behnajady, N. Modirshahla, H. Fathi, Journal of Hazardous Materials, 136(2006) 816.
[33] H. M. Coleman, M. I. Abdullah, B. R. Eggins, F.L. Palmer, Applied Catalysis B: Environmental, 55 (2005) 23.
[34] L. Zhang, C. Xu, Z. Chen, X. Li, Advanced Materials Research 233 (2011) 466.
[35] J. Herrmann, P. Pichat, Journal of the Chemical Society, Faraday Transsactions, 76 (1980) 1138.
[36] I. K. Konstantinou, T.A. Albanis, Applied Catalysis, B 49 (2004) 1.
[37] R. Molinari, A. Caruso, T. Poerio, Catalysis Today, 144 (2009) 81.
[38] X. Wu, Q. Wei, J. Zhaohua, Thin Solid Films, 496 (2006) 288.

[39] G. R. Bamwenda, T. Uesigi, Y. Abe, K. Sayama, H. Arakawa, Applied Catalysis A: General, 205 (2001) 117.
[40] M. S. Seyed-Dorraji, N. Daneshvar, S. Aber, Global Nest Journal, 11 (2009) 535.
[41] S. Chen, G. Cao, Desalination, 194 (2006) 127.
[42] G. R. Bamwenda, K. Sayama, H. Arakawa, Journal of Photochemistry and Photobiology A: Chemistry, 122 (1999) 175.
[43] S. F. Chen, X. L. Cheng, Chinese Journal of Chemistry, 17 (1999) 419.
[44] N. San, A. Hatipoglu, G. Kocturk, Z. Cinar, Journal of Photochemistry and Photobiology: A, 146 (2002) 189.
[45] Y. Mu, H. Q. Yu, J. C. Zheng, S. J. Zhang, Journal of Photochemistry and Photobiology A: Chemistry, 163 (2004) 311.
[46] A. Koca, M. Sahin, International Journal of Hydrogen Energy, 27 (2002) 363.
[47] G. R. Bamwenda, H. Arakawa, Solar Energy Materials and Solar Cells, 70 (2001) 1.
[48] R. Abe, K. Sayama, K. Domen, H. Arakawa, Chemical Physics Letters, 344 (2001) 339.
[49] K. Sayama, K. Mukasa, R. Abe, Y. Abe, H. Arakawa, Journal of Photochemistry and Photobiology A: Chemistry, 148 (2002) 71.
[50] K. Lee, W. S. Nam, G. Y. Han, International Journal of Hydrogen Energy 29 (2004) 1343.
[51] Y. Sasaki, A. Iwase, H. Kato, A. Kudo, Journal of Catalysis, 259 (2008) 133.
[52] E. Niehues, I.S. Scarmínio, K. Takashima, Journal of the Chilean Chemical Society, 55 (2010) 320.
[53] R. F. Howe, Developments in Chemical Engineering and Mineral Processing, 6 (1998) 55.
[54] C. H. Fischer, J. Lillie, H. Weller, L. Katsikas, A. Henglein, Berichte der Bunsen Physical Chemistry, 93 (1989) 61.
[55] D. Beydoun, R. amal, G. low, S. mcevoy, Jounal of Nanoparticle Research, 1 (1999) 439.
[56] M. A. Fox, M. T. Dulay, Chemical Reviews, 93 (1993) 341.
[57] M. Trillas, M. Pujol and X. Domenech, Journal of Chemical Technology & Biotechnology, 55 (1992) 85.
[58] S. Navaladian, C.M. Janet, B. Viswanathan, R. P.Viswanath, Photo/electrochemistry & photobiology in the environment, energy and fuel. Research signpost, 37 (2007) 1.

[59] C. H. Wu, Chemos-phere, 57 (2004) 601.
[60] D. Monllor-Satokca, L. Borja, A. Rods, R. Gomez, P. Salvador, A European Journal of Chemical Physics and Physical Chemistry, 7(2006) 2540.
[61] C. Santato, M. Odziemkowski, M. Ulmann, J. Augustynski, Journal of the American Chemical Society, 123 (2001) 10639.
[62] U. A. Joshi, R. J. Darwent, H. H. P. Yiu, M. J. Rosseinsky, Journal of Chemical Technology and Biotechnology, (2011).
[63] N. M. Zholobak, V. K. Ivanov, A. B. Shcherbakov, A. S. Shaporev, O.S. Polezhaeva, A.Ye. Baranchikov, N.Ya. Spivak, Yu.D. Tretyakov, Journal of Photochemistry and Photobiology B: Biology, 102 (2011) 32.
[64] X. D. Zhou, W. Huebner, H. U. Anderson, Applied Physical Letters, 80 (2002) 3814.
[65] X. D. Zhou,W. Huebner, H.U. Anderson, Chemical Materials 15 (2003) 378.
[66] U. Diebold, Surface Science Reports, 48 (2003) 53.
[67] A. Di Paola, G. Cufalo, M. Addamo, M. Bellardita, R. Campostrini, M. Ischia, R. Ceccato, L. Palmisano, Colloids and Surfaces A, 317 (2008) 366.
[68] K. Pan, Q. Zhang, Q. Wang, Z. Liu, D. Wang, J. Li, Y. Bai, Thin Solid Films, 515 (2007) 4085.
[69] Y. X. zhang, G. H. Li, Y. X. Jin, Y. Zhang, J. Zhang, L. D. Zhang, Chemical Physics Letters, 365 (2002) 300.
[70] J. M. Macak, H. Tsuchiya, A. Ghicov, K. Yasuda, R. Hahn, S. Bauer, P. Schmuki, Current Opinion in Solid State & Materials Science, 11 (2007) 3.
[71] Y. C. Zhu, C. X. Ding, Nanostructured Materials, 11 (1999) 427.
[72] H. Sun, C. Wang, S. Pang, X. Li, Y. Tao, H. Tang, M. Liu, Journal of Non-Crystalline Solids 354 (2008) 1440.
[73] C. Giolli, F. Borgioli, A. Credi, A. D. Fabio, A. Fossati, M. M. Miranda, S.Parmeggiani, G. Rizzi, A. Scrivani, S. Troglio, A. Tolstoguzov, A. Zoppi, U. Bardi, Surface and Coating Technology, 202 (2007) 13.
[74] I. Oja, A. Mere, M. Krunks, R. Nisumaa, C. H. Solterbeck, M. Es-Souni, Thin Solid Films, 515 (2006) 674.
[75] M. Andersson, A. Kiselev, L. Osterlund, A. E. C. Palmqvist, Journal of Physical Chemistry, 111 (2007) 6789.
[76] J. H. Lee, Y. S. Yang, Materials Chemistry and Physics, 93 (2005) 237.

[77] M. Bellardita, M. Addamo, A. Di Paola, L. Palmisano, Chemical Physics, 339 (2007) 94.
[78] M. C. Hidalgo, M. Aguilar, M. Maicu, J. A. Navío, G. Colón, Catalysis Today, 129 (2007) 50.
[79] R. C. Xie, J. K. Shang, Journal of Material Science, 42 (2007) 6583.
[80] M. Andersson, A. Kiselev, L. Osterlund, A. E. C. Palmqvist, Journal of Physical Chemistry C, 111 (2007) 6789.
[81] Lj. D. Arsov, C. Kormann, W. Plieth, Journal of Raman Spectroscopy, 22(1991) 573.
[82] B. R. Ssankapal, S. D. Sartale, M. C. Lux-Steiner, A. Ennaoui, CR Chim, 9 (2006) 702.
[83] Y. Wang, Y.Wang, J. Ren, Y. Mi, F. Zhang, C. Li, X. Liu, Y. Guo, Y. Guo, G. Lu, Journal of Solid State Chemistry, 183 (2010) 277.
[84] N. Zhang, X. Fu, Y. J. Xu, Journal of Materials Chemistry, 21 (2011).
[85] S.C. Laha, R. Ryoo, Chemical Communication (2003) 2138.
[86] A. Corma, P. Atienzar, H. Garcia, J.Y. Chane-Ching, Nature Materials, 3 (2004) 394.
[87] L. Qiana, J. Zhua, W. Dub, X. Qiana, Materials Chemistry and Physics 115 (2009) 835.
[88] S.W. Yang, L. Gao, Journal of American Chemical Society, 128 (2006) 9330.
[89] J. Zhang, S. Ohara, M. Umetsu, T. Naka, Y. Hatakeyama, T. Adschiri, Advanced Materials, 19 (2007) 203.
[90] R. Si, Y.W. Zhang, L.P. You, C.H. Yan, Angewandte Chemie International Edition, 44 (2005) 3256.
[91] S. Sathyamurthy, K. J Leonard, R. T. Dabestani, M. P. Paranthaman, Nanotechnology, 16 (2005) 1960.
[92] I. Turkevych, Y. Pihosh, M. Goto, A. Kasahara, M. Tosa, S. Kato, K. Takehana, T. Takamasu, G. Kido, N. Koguchi, Thin Solid Films, 516 (2008) 2387.
[93] J. Liu, G. Liu, M. Li, W. Shen, Z. Liu, J. Wang, J. Zhao, L. Jiang, Y. Song, Energy & Environmental Science, 3 (2010) 1503.
[94] Z. Xiong, J. Ma, W. J. Ng, T. D. Waite, X.S. Zhao, Water Research, 45 (2010) 209.
[95] M. A. Lim, Y. W. Lee, S. W. Han, I. Park, Nanotechnology, 22 (2011).

[96] C. Periasamy, P. Chakrabarti, Journal of Applied Physics, 109 (2011).
[97] M. Hara, G. Hitoki, T. Takata, J. N. Kondo, H. Kobayashi, K. Domen. Catalysis Today, 78 (2003) 555.
[98] H. Mizoguchi, K. Ueda, M. Orita, S. C. Moonc, K. Kajiharaa, M. Hirano, H. Hosono, Materials Research Bulletin, 37 (2002) 2401.
[99] A. Iwase, H. Kato, A. Kudo, Catalysis Letters, 108 (2006) 7.
[100] Wu, T. Chen, G. Zhou, X. Zong, C. Li, Science in China Series B, 51 (2008) 97.
[101] Gurunathan K., International Journal of Hydrogen Energy, 29 (2004) 933.
[102] Y. Mizukoshi, K. Sato, T. J. Konno, N. Masahashi, Applied Catalysis B, 94 (2010) 248.
[103] G. C. Bond, P. A. Sermon, G. Webb, D. A. Buchanan, P. B. Wells, Chemical Communication, (1973) 444.
[104] M. Haruta, T. Kobayashi, H. Sano, N. Yamada, Chemical Letters, 16 (1987) 405.
[105] M. Haruta, A. Ueda, R. M. Torres Sanchez, K. Tanaka, Prp. Pet. Div. ACS Symp., New Orleans, 1996.
[106] L. Prati, M. Rossi, Journal of Catalysis, 176 (1998) 552.
[107] P. Landon, P. J. Collier, A. J. Papworth, C. J. Kiely, G. J. Hutchings, Chemical Communication, (2002) 2058.
[108] G. C. Bond, D. Thompson, Catalysis Reviews, Science and Engineering, 41 (1999) 319.
[109] M. Haruta, Gold Bullettin, 37 (2004) 27.
[110] G. J. Hutchings, Gold Bullettin, 37 (2004) 3.
[111] R. Meyer, C. Lemire, Sh. K. Shaikhutdinov, H. J. Freund, Gold Bullettin, 37 (2004) 72.
[112] J. Turkevich, Gold Bullettin, 18 (1985) 86.
[113] V. Ponec, G. C. Bond, Catalysis by Metals and Alloys, Elsevier, Amsterdam, 1996.
[114] R. Zanella, S. Giorgio, C. H. Shin, C. R. Henry, C. Louis, Journal of Catalysis, 222 (2004) 357.
[115] S. J. Lee, A. Gavriilidis, Journal of Catalysis, 206 (2002) 305.
[116] H. Sakurai, M. Haruta, Applied Catalysis A: General, 127 (1995) 93.
[117] Y. Inoue, On Solar Hydrogen and Nanotechnology, Lionel Vayssieres, Chapter 18 (2010).
[118] T. Ikeda, T. Nomoto, K. Eda, Y. Mizutani, H. Kato, A. Kudo, H. Onishi, Journal of Physycal Chemistry C, 112 (2008) 1167.

[119] Q. Kang, Q. Z. Lu, S. H. Liu, L. X. Yang, L. F. Wen, S. L. Luo, Q. Y. Cai, Biomaterials, 31 (2010) 3317.
[120] R. Abe, K. Sayama, H. Sugihara, Journal of Physical Chemistry B, 109 (2005) 16052.
[121] S. Shet, K. S. Ahn, T. Deutsch, H. L. Wang, R. Nuggehalli, Y. F. Yan, J. Turner, M. Al-Jassim, Journal of Power Sources, 195 (2010) 5801.
[122] A. Kudo, M. Sekizawa, Chemical Communication, 15 (2000) 1371.
[123] W. Y. Choi, A. Termin, M. R. Hoffmann, Journal of Physical Chemistry, 98 (1994)13669.
[124] S. Y. Chae, M. K. Park, S. K. Lee, T. K. Kim, S. K. Kim, W. I. Lee, Chemical Materials, 15 (2003) 3326.
[125] D. Jing, Y. Zhang, L. Guo, Chemical Physics Letters, 415 (2005) 74.
[126] A. Kudo, H. Kato, Chemical Physics Letters, 331 (2000) 373.
[127] B. O'Regan, M. Graetzel, Nature, 353 (1991) 737.
[128] K. Y. Law, Chemical Reviews, 93 (1993) 449.
[129] S. Das, K.G. Thomas, M.V. George, in: V. Ramamurthy, K.S. Schanze (Eds.), Molecular and Supramolecular Photochemistry: Organic Photochemistry, 1 (1997), 467.
[130] J. Moon, C. Y. Yun, K. W. Chung, M. S. Kang, J. Yi, Catalalysis Today, 87 (2003) 77.
[131] K. B. Dhanalakshmi, S. Latha, S. Anandan, P. Maruthamuthu, International Journal of Hydrogen Energy, 26 (2001) 669.
[132] E. Borgarello, J. Kiwi, E. Pelizzetti, M. Visca, M. Gratzel, Nature, 289 (1981) 158.
[133] A. A. Nada, H. A. Hamed, M. H. Barakat, N. R. Mohamed, T. N. Veziroglu, International Journal of Hydrogen Energy, 33 (2008) 3264.
[134] C. F. Lin, C. H. Wu, Z. N. Onn, Journal of Hazardous Materials, 154 (2008) 1033.
[135] X. Chen, S. Shaohua, L. Guo, S. S. Mao, Chemical Reviews, 110 (2010) 6503.
[136] X. Wang, G. Liu, Z. G. Chen, F. Li, Journal of Materials Research, 25 (2010) 39.
[137] X. W. Wang, G. Liu, Z. G. Chen, F. Li, L. Z. Wang, G. Q. Lu, H. M. Cheng, Chemical Communication, 3452 (2009).
[138] C. A. Grimes, O. K. Varghese, S. Ranjan, Light, Water, Hydrogen, Edit. springer-Verlag New York Inc., 7 (2008).

[139] M. E. Rincon, M. W. Martinez, M. M. Harnandez, Thin Solid Films, 425 (2003) 137.
[140] K. Domen, S. Naito, T. Onishi, K. Tamaru, Journal of Physical Chemistry, 86 (1982) 3657.
[141] D. L. Trimm, Z. I. Onsan, Catalysis Reviews Science Engineering, 43 (2001) 31.
[142] J. D. Holladay, J. Hu, D. L. King, Y. Wang, Catalysis Today 139 (2009) 44.
[143] K. Sayama, K. Mukasa, R. Abe, Y. Abe, H. Arakawa, Chemical Communication, (2001) 24169.
[144] K. Sayama, R. Yoshida, H. Kusama, K. Okabe, Y. Abe, H. Arakawa, Chemical Physics Letters, 277 (1997) 387.
[145] A. E. Kozlova, P. Tatyana, P. Korobkina, V. A. Vorontsov, International Journal of Hydrogen Energy, 34 (2009) 138.
[146] K. Fujihara, T. Ohno, M. Matsumura, Journal of Chemical Society, Faraday Transaction, 94 (1998) 3705.
[147] N. Bao, L. Shen, T. Takata, Chemical Materials, 20 (2008) 110.
[148] G. L. Chiarello, E. Selli, L. Forni, Applied Catalysis B, 84 (2008) 332.
[149] R. Konta, T. Ishii, H. Kato, A. Kudo, Journal of Physical Chemistry B, 108 (2004) 8992.
[150] K. Maeda, T. Takata, M. Hara, N. Saito, Y. Inoue, H. Kobayashi, K. Domen, Journal of the American Chemical Society, 127 (2005) 8286.
[151] K. Maeda, K. Teramura, D. Lu, T. Takata, N. Saito, Y. Inoue, K. Domen, Nature, 440 (2006) 295.
[152] Z. Zou, J. Ye, K. Sayama, H. Arakawa, Nature, 414 (2001) 625.
[153] H. Liu, J. Yuan, W. Shangguan, Y. Teraoka, Journal of Physical Chemistry C, 112 (2008) 8521.
[154] O. S. Mohamed, A. A. M. Gaber, A. A. Abdel-Wahab, Journal of Photochemistry and Photobiology A, 148 (2002) 205.
[155] S. M. Bonesi, E. Carbonell, H. Garcia, M. Fagnoni, A. Albini, Applied Catalysis B, 79 (2008) 368.
[156] P. Du, J.A. Moulijin, G. Mul, Journal of Catalysis, 238 (2006) 342.
[157] G. Palmisano, M. Addamo, V. Augug liaro, T. Caronna, A. Di Paola, E. Garcia Lopez, V. Loddo, G. Marcì, L. Palmisano, M. Schiavello, Catalysis Today, 122 (2007) 118.
[158] H. Park, W. Choi, Catalysis Today, 101 (2005) 291.
[159] K. Shimizu, H. Akahane, T. Kodama, Y. Kitayama, Applied Catalysis A: General, 269 (2004) 75.

[160] C. E. Taylor, Topics in Catalysis, 32 (2005) 179.
[161] T. Shishido, K. Teramura, T. Tanaka, Catalysis Science & Technology, 1 (2011) 541.
[162] G. Palmisano, S. Yurdakal, V. Augugliaro, V. Loddo, L. Palmisano, Advanced Synthesis andCatalysis, 349 (2007) 964.
[163] J. C. Colmenares, M.A. Aramendìa, A. Marinas, J.M. MArinas, F.J. Urbano, Applied Catalysis A, 306 (2006) 120.
[164] W. Y. Ahn, S.A. Sheeley, T. Rajh, D.M. Cropek, Applied Catalysis B, 74 (2007) 103.
[165] N. Sasirekha, S. J. Sardhar Basha, K. Shanthi, Applied Catalysis B, 62 (2006) 169.
[166] D. Ravelli, D. Dondi, M. Fagnonia, A. Albini, Chemical Society Reviews, 38 (2009) 1999.
[167] M. N. Chong, B. Jin, C. W. K. Chow, C. Saint, Water Research, 44 (2010) 1997.
[168] O. Carp, C. L. Huisman, A. Reller, Progress in Solid State Chemistry, 32 (2004) 33.
[169] L. Ge, Journal of Molecular Catalysis A: Chemistry, 282 (2008) 62.
[170] L. Lhomme, S. Brosillon, D. Wolbert, Journal of Photochemistry and Photobiology A, 188 (2007) 34.
[171] R. Molinari, F. Pirillo, V. Loddo, L. Palmisano, Catalysis Today, 118 (2006) 205.
[172] Y. Zhang, J. L. Zhou, B. Ning, Water Research, 41 (2007) 19.
[173] Y. C. Oh, W. S. Jenks, Journal of Photochemistry and Photobiology A, 162 (2004) 323.
[174] M. M. Haque, M. Muneer, Dyes and Pigments, 75 (2007) 443.
[175] L.L.P. Lim, R.J. Lynch, Applied Catalysis A: General, 394 (2011) 52.
[176] X. Zeng, J. Wu, D. Zhang, G. Li, S. Zhang, H. Zhao, T. An, X. Wang, J. Fu, G. Sheng, Research on Chemical Intermediates, 35 (2009) 827.
[177] X. Yang, L. Zhu, L. M. Yang, W. Y. Zhou, Y. H. Xu, Transactions of Nonferrous Metals Society of China, 21 (2011) 335.
[178] Y. Hu, D. Li, Y. Zheng, W. Chen, Y. He, Y. Shao, X. Fu, G. Xiao, Applied Catalysis B: Environmental, 104 (2011) 30.
[179] H. Fu, G. Lu, S. Li, Journal of Photochemistry and Photobiology A: Chemistry, 114 (1998) 81.
[180] N. Serpone, Y. K. Ah-You, T. P. Tran, R. Harris, E. Pelizzetti, H. Hidaka, Solar Energy, 39 (1987) 491.

[181] A. Troupis, A. Hiskia, E. Papaconstantinou, Applied Catalysis B: Environmental, 52 (2004) 41.
[182] K. M. Joshi, B. N. Patil, D. S. Shirsath, V. S. Shrivastava, Advances in Applied Science Research, 2 (2011) 445.
[183] K. Tennakone, K. G. U. Wijayantha, Journal of Photochemistry and Photobiology A: Chemistry, 113 (1998) 89.
[184] D. Zhang, G. Li, J. C. Yu, Journal of Materials Chemistry, 20 (2010) 4529.
[185] R. A. Damodar, S. J. Y, H. H. Chou, Journal of Hazardous Materials, 172 (2009) 1321.
[186] R. A. Damodar, S. J. Y, Separation and Purification Technology, 71 (2010) 44.
[187] E. Erdim, E. Soyer, S. Tasiyici, I. Koyuncu, Desalination Water Treatment, 9 (2009) 165.
[188] S. Mozia, A. W. Morawski, M. Toyoda, T. Tsumura, Desalination, 250 (2010) 666.
[189] J. Grzechulska-Damszel, M. Tomaskewska, A. W. Morawski, Desalination, 241 (2009) 118.
[190] S. A. Lee, K. H. Choo, C. H. Lee, H. I. Lee, T. Hyeon, W. Choi, H. H. Known, Industrial and Engineering Chemical Research, 40 (2001) 1712.
[191] B. Mounir, M. N. Pons, O. Zahraa, A. Yaacoubi, A. Benhammou, 148 (2007) 513.
[192] K. H. Choo, D. I. Chang, K. W. Park, M. H. Kim, Journal of Hazardous Materilas, 152 (2008) 183.
[193] D.J. Connolly, W.F. Gresham, Fluorocarbon Vinyl Ether Polymers, US Patent 3, 282, 875 (1 November 1966).
[194] A. W. H. Mau, C. B. Huang, N. Kakuta, A. J. Bard, A. Campion, M. A. Fox, J. M. White, S. E. Webber, Journal of the American Chemical Society, 106 (1984) 6537.
[195] N. Kakuta, J. M.White, A. Campion, A. J. Bard, M. A. Fox, S. E. Webber, Journal of Physical Chemistry, 89 (1985) 48.
[196] I. Willner, B. Steinberger-Willner, International Journal of Hydrogen Energy, 13 (1988) 593.
[197] G. K. Mor, K. Shankar, M. Paulose, O. K. Varghese, C. A. Grimes, Nano Letters, 5 (2005) 191.
[198] J. H. Park, S. Kim, A. J. Bard, Nano Letters, 6 (2006) 24.
[199] G. Girishkumar, T. D. Hall, K. Vinodgopal, P. V. Kamat, Journal of Physical Chemistry B, 110 (2006) 107.
[200] S. S. Chin, K. Chiang, A. G. Fane, Journal of Membrane Science, 275 (2006) 202.

[201] T. Moritz, S. Benfer, P. Arki, G. Tomandl, Colloids and Surfaces A: Physicochemical and Engineering Aspects, 195 (2001) 25.
[202] A. Alem, H. Sarpoolaky, M. Keshmiri, Ceramic International, 35 (2009) 1837.
[203] R. Thiruvenkatachari, T. O. Kwon, I. S. Moon, Separation Science Technology, 40 (2005) 2871.
[204] R. Thiruvenkatachari, S. Vigneswaran, I. S. Moon, Korean Journal of Chemical Engineering, 25 (2008) 64.
[205] T. H. Lim, S. D. Kim, Chemosphere, 54 (2004) 305.
[206] A. Haarstrick, O. M. Kut, E. Heinzle, Environmental Science Technology, 30 (1996) 817.
[207] W. Y. Wang, A. Irawan, Y. Ku, Water Research, 42 (2008) 4725.
[208] G. Mascolo, R. Comparelli, M. L. Curri, G. Lovecchio, A. Lopez, A. Agostiano, Journal of Hazardous Materials, 142 (2007) 130.
[209] A. Primo, A. Corma, H. Garcia, Physycal Chemistry Chemical Physics, 13 (2011) 886.
[210] G. R. Bamwenda, S. Tsubota, T. Nakamura, M. Haruta, Journal of Photochemistry and Photobiology A, 89 (1995) 177.
[211] A. A. Ismail, D. W. Bahnemann, I. Bannat, M. Wark, Journal of Physical Chemistry C, 113 (2009) 7429.
[212] J. T. Carneiro, C. C. Yang, J. A.Moma, J. A. Moulijn, G. Mul, Catalysis Letters, 129 (2009) 12.
[213] S. Neatu, B. Cojocaru, V. I. Parvulescu, V. Somoghi, M. Alvaro, H. Garcia, Journal of Materials Chemistry, 20 (2010) 4050.
[214] A. Grirrane, A. Corma, H. Garcia, Nature Protocols, 5 (2010) 429.
[215] S. L. Murov, I. Carmichael, G. L.Hug, Handbook of Photochemistry, 2nd ed., Marcel Dekker: New York, 1993.
[216] A. Corma, H. Garcia, Chemical Society Reviews, 37 (2008) 2096.
[217] M. W. Kanan, Y. Surendranath, D. G. Nocera, Chemical Society Reviews, 38 (2009) 109.
[218] K. Maeda, K. Domen, Chemical Materials, 22 (2010) 612.
[219] C. G. Silva, Y. Bouizi, V. Fornes, H. Garcia, Journal of the American Chemical Society, 131 (2009) 13833.
[220] Z. G. Zou, J. H. Ye, K. Sayama, H. Arakawa, Nature, 414 (2001) 625.

[221] C. Y. Lin, D. Y. Lee, S. Y. Wang, C. C. Lin, T. Y Tseng, Surface and Coatings Technology, 203 (2008) 480.
[222] A. Corma, P. Atienzar, H. Garcia, J. Y. Chane-Ching, Nature Material, 3 (2004) 394.
[223] M. Chtchigrovsky, A. Primo,P. Gonzalez, K. Molvinger, M. Robitzer, F. Quignard, F. Taran, Angewandte Chemie International Editino, 48 (2009) 5916.
[224] V. Khatko, F. Guirado, J. Hubalek, E. Llobet, X. Correig, Physical Status Solid (a), 10 (2005) 1973.
[225] C. G. Silva, R. Juàrez, T. Marino, R. Molinari, H. Garcìa, Journal of the American Chemical Society, 133 (2011) 595.
[226] A. Primo, T. Marino, A. Corma, R. Molinari, H. Garcìa, Jornal of the American Chemical Society, 133 (2011) 6930.
[227] R. Abe, Journal of Photochemistry and Photobiology C: Photochemistry Review, 11 (2010) 179.
[228] B. Seger, K. Vinodgopal, P. V. Kamat, Langmuir, 23 (2007) 5471.
[229] J. Ramìrez, L. A. Godìnez, M. Mèndez, Y. Meas, F. J. Rodriguez, Journal of Apllied Electrochemistry, 40 (2010) 1729.
[230] J. Feng, X. Hu, P. Yue, Water Research, 39 (2005) 89.
[231] S. Sabhi, J. Kiwi, Water Research, 35 (2001) 1994.
[232] J. Kiwi, Proceedings of the Third Asia-Pacific Conference onSustainable Energy and Environmental technologies, 2000, pp. 562.
[233] N. Takeda, T. Torimoto, S. Sampath, S. Kuwabata, H. Yoneyama, Journal of Physical Chemistry, 99 (1995) 9986.
[234] J. Matos, J. Laine, J. M. Herrmann, Carbon, 37 (1999) 1870.
[235] J. Matos, J. Laine, J. M. Herrmann, Applied Catalysis B: Environmental, 18 (1998) 281.
[236] B. Tryba, A.W. Morawski, M. Inagaki, M. Toyoda, Applied Catalysis B: Environmental, 63 (2006) 215.
[237] A. Primo, A. Corma, H. García, Physical Chemistry Chemical Physics, 13 (2011) 886.
[238] F. Rodríguez-Reinoso, Carbon 36 (1998) 159.
[239] T. Cordero, C. Duchamp, J. M. Chovelon, C. Ferronato, J. Matos, Applied Catalysis B: Environmental, 73 (2007) 227.
[240] T. Cordero, C. Duchamp, J.M. Chovelon, C. Ferronato, J. Matos, Journal of Photochemistry and Photobiology A: Chemistry, 191 (2007) 122.

[241] S. Carretin, P. Concepción, A. Corma, J.M. López-Nieto, V.F. Puntes, Angewandte Chemie International Edition, 43 (2004) 2538.
[242] J. Matos, E. García-López, L. Palmisano, A. García, G. Marci, Applied Catalysis B: Environmental, 99 (2010) 170.
[243] S. Brunauer, P.H. Emmett, E. Teller, Journal of the American Chemical Society, 60 (1938) 309.
[244] M.V López, F. Stoeckli, C. Moreno-Castilla, F. Carrasco, Carbon, 37 (1999) 1215.
[245] J. Matos, A. García, L. Zhao, M.M. Titirici, Applied Catalalysis A: General, 390 (2010) 175.
[246] J. Matos, M. Labady, A. Albornoz, J. Laine, J.L. Brito, Journal of Material Science, 39 (2004) 3705.
[247] J. Laine, A. Calafat, M. Labady, Carbon, 27 (1989) 191.
[248] P. Andrew, M.A.P. Sherwood, Carbon, 21 (1983) 53.
[249] W. Shen, Z. Li, Y. Liu, Recent Patents on Chemical Engineering 1 (2008) 27.
[250] P. Behrens, H Beuthien, H.P Eickhoff, W Metz, W Niemann, Synthetic Metals 23 (1988) 95.
[251] J. Matos, J. Laine, J.M. Herrmann, D. Uzcategui, J.L. Brito, Applied Catalysis, B: Environmental, 70 (2007) 461.
[252] C. Lettmann, K. Hildenbrand, H. Kisch, W. Macyk, W.F. Maier, Applied Catalysis B: Environmental, 32 (2001) 215.
[253] G.S. Shao, F.Y. Wang, T.Z. Ren, Y. Liu and Z.Y. Yuan, Applied Catalysis B: Environmental, 92 (2009) 61.
[254] G. Colon, J.M. Sanchez-España, M.C. Hidalgo, J.A. Navío, Journal of Photochemistry and Photobiology A: Chemistry, 179 (2006) 20.
[255] L. Cermenati, C. Richter, A. Albini, Chemical Communications, 1998, 805.
[256] K. Weissermel, H. Harpe, Journal of Industrial Organic Chemistry, 4th edition, Wiley-VCH: Weinheim, 2003.
[257] Y. Shiraishi, N. Saito, T. Hirai, Journal of the American Chemical Society, 127 (2005) 12820.
[258] H. Park, W. Choi, Journal of Physical Chemistry: B, 107 (2003) 3885.
[259] H. Park, W. Choi, Catalysis Today, 101 (2005) 291.
[260] J. Chen, L. Eberlein, C. H. Langford, Journal of Photochemistry and Photobiology, A: Chemistry, 148 (2002) 183.
[261] A. Corma, H. Garcia, Chemical Review, 102 (2002) 3837.

[262] A. Primo, A. Corma, H. Garcia, Physical Chemistry Chemical Physics, 13 (2011) 886.
[263] D. Buso, J. Pacifico, A. Martucci, P. Mulvaney, Advanced Functional Materials, 17 (2007) 347.
[264] R. Martin, S. Navalon, M. Alvaro, H. Garcia, Applied Catalysis B: Environmental, 103 (2011) 246.

Appendix

Scientific Pubblications

1. "Influence of Excitation Wavelength (UV or Visible Light) on the Photocatalytic Activity of Titania Containing Gold Nanoparticles for the Generation of Hydrogen or Oxygen from Water", C. Gomes Silva, R. Juàrez, **T. Marino**, R. Molinari, and H. Garcìa, *The Journal of The American Chemical Society*, 2011, 133, 595.

2. "Efficient Visible-Light Photocatalytic Water Splitting by Minute Amounts of Gold Supported on Nanoparticulate CeO_2 Obtained by a Biopolymer Templating Method", A. Primo, **T. Marino**, A. Corma, R. Molinari, H. García, , *The Journal of The American Chemical Society*, 2011, 133, 6930.

3. "Membranes for photocatalysis in water and wastewater treatment" V. Loddo and L. Palmisano, Università di Palermo and **T. Marino** and R. Molinari, Università della Calabria, Italy. Edited by A. Basile, Italian National Research Council (ITM-CNR), Italy and S. Nunes, King Abdullah University of Science and Technology (KAUST), Saudi Arabia, Woodhead Publishing Series in Energy 2011, 23, 746.

4. "Hydrogen Photoproduction by Water Splitting under UV and Visible Irradiation of Au-TiO_2/Activated Carbon", **T. Marino**, J.Matos, A. García, Raffaele Molinari, H. García, *submitted to Applied Catalysis A: General*, 2011.

5. "Visible light photocatalytic overall water splitting by combining gold nanoparticles supported on TiO_2 and CeO_2", **T. Marino**, A. Primo, A. Corma, R. Molinari, H. Garcìa, *submitted to Chemical Communications*, 2011.

6. "Positive influence of gold nanoparticles on the photocatalytic activity of TiO_2 for hydroxylation of benzene by water", **T. Marino**, R. Molinari, H. Garcìa, *submitted to Catalysis Today*, 2011.

Partecipation in Scientific Congresses

1. "Photocatalytic overall water splitting by combining gold nanoparticles supported on TiO_2 and CeO_2", Marino T., Primo A., Corma A., Molinari R., Garcìa H., 2nd European Simposium on Photocatalysis, Bordeaux (France), 29th-30th September 2011, pp P1.6.

2. "Preparation of CeO_2 nanoparticles using biopolymers for the photocatalytic generation of O_2 from water", Primo A., **Marino T**., Garcia H., VII Simposio Investigadores Jovenes RSEQ-Sigma Aldrich, Valencia (Spain), 10st-12nd November 2010, pp. P40.

3. "Photoanode for hydrogen generation using a membrane photoreactor", **Marino T.**, Molinari R. , Atienzar P. , Garcia H., Atti del convegno "Summer School on Ceramic Membranes for Green Chemical Production and Clean Power Generation", Valencia (Spain), 8th-10th September 2010, pp. P19.

4. "Phenol production in a photocatalytic membrane contactor", **Marino T.**, Poerio T., Molinari R.. Atti del convegno "COST Action 543 - Second Training School", Rende (CS) - Università della Calabria, 26th-29th April 2010, A cura di Basile A., Calabro' V., Università della Calabria – Centro Editoriale e Librario, Rende (CS) - Italia, 2010, pp. 277-278.

5. "Performance of TiO_2, WO_3 and SnO_2 as photocatalysts in a membrane reactor to convert benzene to phenol", **Marino T.,** Molinari R., Poerio T., Atti del Convegno Congiunto delle Sezioni Calabria e Sicilia della Società Chimica Italiana, Aci Castello, 1st-2nd Dicember, 2009, pp. P24.

Teaching Activity

1. Ottobre 2009-Gennaio 2010: Supporto alle attività didattiche in qualità di Esercitatore, nell'ambito dell'insegnamento di Chimica, per i Corsi di Laurea della la Facoltà di Ingegneria dell'Università della Calabria.

2. Ottobre 2011-*sino ad ora*: Supporto alle attività didattiche in qualità di Esercitatore, nell'ambito dell'insegnamento di Chimica, per i Corsi di Laurea della la Facoltà di Ingegneria dell'Università della Calabria.

Acknowledgments

First of all, I would like to thank my Supervisors, Professor Raffaele Molinari and Hermenegildo Garcìa, for giving me the opportunity to work with them. Their professionality and enthusiasm for research was motivational and stimulating for me. I really appreciate all their contributions of ideas and time. Thanks to their support and suggestions, I have improved my way of doing research.

All the people of ITQ have contributed immensely to my personal and professional time at Valencia. I am thankful for the excellent examples Professors Corma, Fornes and Miranda have provided me as successful Chemists and Professors.

The Istitute has been a source of friendships as well as good advices and collaborations…

…Quiero dar mi más sincero agradecimiento a todos mi companeros y amigos de laboratorio y del ITQ, y en particular a Pedro, Amparo, Fran, Raquel, Marcos, Esther, Abdessamad, Çesc, Maykel, Nacio, Ana, Ivan...

...A Paula, Edurne, Sonia, Patri, Miguel, Tania, Olalla, Karen, Victoria por hacer de todos mis dias en Valencia, momentos expeciales.

A todos los investigadores, a todo el equipo de taller del ITQ por ayudarme en todo lo que he necesitado y a todos los técnicos de diferentes servicios.

Gracias también a todos los que han colaborado activamente al desarrollo de los trabajos que componen esta tesis especialmente al Profesor Juan Matos y a Claudia.
Quiero dar las gracias a mis amigos y companeros de piso, en particular a Helena y Diego, que han estado siempre conmigo y que han echo que el ano pasado en Valencia sea uno de los mejores de mi vida....
Y sobre todo, quiero dar mi más sincero agradecimiento a Fabrizio,
..senza il quale probabilmente in questo momento non avrei potuto parlare dell'esperienza vissuta a Valencia.

Ringrazio Teresa e Pietro per il supporto e la disponibilità che da sempre hanno mostrato nei miei confronti.

Grazie a Marzia, Diego e Giuseppe, miei amici da sempre.

Grazie a Ivan, per essermi sempre vicino come un fratello.

Un grazie speciale a papà e mamma, Nadia e Riccardo, ai quali dedico questa tesi. Senza il loro amore e la loro fiducia non avrei raggiunto questo obiettivo.

Infine grazie a Te, che sei in ogni mio respiro e dai un senso alla mia vita…Questo traguardo è anche tuo..GRAZIE Antonio.